Air Force Institute of Technology

AFIT Scholar

Theses and Dissertations   Student Graduate Works

3-16-2009

Finite Element Model Optimization of the FalconSAT-5 Structural Engineering Model

Cole C. Doupe

Follow this and additional works at: https://scholar.afit.edu/etd

Part of the Space Vehicles Commons

**Finite Element Model Optimization of the
FalconSAT-5 Structural Engineering Model**

THESIS

Cole C. Doupe, Captain, USAF

AFIT/GA/ENY/09-M04

**DEPARTMENT OF THE AIR FORCE
AIR UNIVERSITY**

AIR FORCE INSTITUTE OF TECHNOLOGY

Wright-Patterson Air Force Base, Ohio

AFIT/GA/ENY/09-M04

FINITE ELEMENT MODEL OPTIMIZATION OF THE
FALCONSAT-5 STRUCTURAL ENGINEERING MODEL

THESIS

Presented to the Faculty

Department of Aeronautics and Astronautics

Graduate School of Engineering and Management

Air Force Institute of Technology

Air University

Air Education and Training Command

In Partial Fulfillment of the Requirements for the

Degree of Master of Science in Astronautical Engineering

Cole C. Doupe, BS

Captain, USAF

March 2009

FINITE ELEMENT MODEL OPTIMIZATION OF THE
FALCONSAT-5 STRUCTURAL ENGINEERING MODEL

Cole C. Doupe, BS

Captain, USAF

Approved:

_____
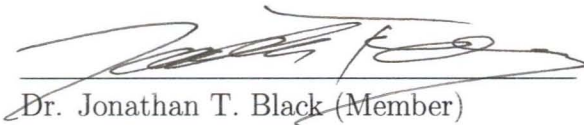Lt Col Eric D. Swenson (Chairman)

13 Mar 09
_____
Date

_____
Dr. Jonathan T. Black (Member)

16 MAR 09
_____
Date

_____
Dr. Richard G. Cobb (Member)

11 MAR 09
_____
Date

AFIT/GA/ENY/09-M04

Abstract

Space launch vehicles produce tremendously harsh environments for their payloads. One of the worst contributors to this harsh environment is vibration. Launch vehicle contractors require accurate dynamic models in order to perform coupled loads analyses with each payload to mitigate risks. Accurate predictions of the dynamic response of the payload are not achieved easily. The Finite Element (FE) method has proven to be the best approach in creating accurate dynamic models of complex structures. To improve the agreement between an FE model and the structure it represents, a common practice is to 'tune' or adjust parameters of the FE model to match experimentally measured data. In order to collect spatially dense and accurate dynamic responses from a satellite, a Polytec laser vibrometer is used which measures the Doppler shift to determine the frequency response from an excitation. To illustrate the benefits of employing this approach, a process is developed to measure dense modal data and tune an FE model of the US Air Force Academy's FalconSAT-5 Structural Engineering Model.

The first step in the process developed in this research involves measuring and tuning models of the satellite structure panels individually. In tuning the structural panels, material stiffness is the major design variable. The tuned FE models of the panels are integrated into the full satellite model which is then tuned based on the spring constant of the connections between the panels. The first eight modes of each side panel, six modes of the top panel, and five modes of the base panel were tuned with eigenvalues matching measured natural frequencies within 2%. Next, the first five modes ranging through 154 Hz were tuned on the full satellite FE model. Predicted natural frequencies were within 3% of measured values for most cases and modes. Modal assurance criterion values comparing tuned FE model eigenvectors and measured mode shapes decreased with increasing numbers of modes tuned, but remained above 0.75 through tuning five modes.

Acknowledgements

My wife and kids have endured the extra time away from home. My thesis advisor Lt Col Swenson has been steadfast in his leadership and devotion to this project. Dr Black has provided expert knowledge and guidance in the subject area. Jay Anderson, John Hixenbaugh, Chris Zickefoose, Wilbur Lacy, and Barry Page provided top-notch lab support. And Lt Col Lynnane George, Don Waite, SSgt Mike Wickersheim, and Lt Col Rick Adams have been gracious in allowing me to babysit their satellite for so long. Thank you to all.

Cole C. Doupe

Table of Contents

List of Figures

List of Tables

List of Abbreviations

Finite Element Model Optimization of the FalconSAT-5 Structural Engineering Model

I. Problem Statement

Satellites are geometrically complex structures comprised of thousands of components made from a wide variety of materials. Creating accurate dynamic models of these complex structures is a challenging process. The goal of this research effort is to create a process for developing accurate finite element (FE) models using geometrically dense modal analysis data to tune the FE model. This process is demonstrated by creating an accurate FE model of a structural engineering model (SEM) of the US Air Force Academy FalconSAT-5. Typically, the first of three physical models in the spacecraft production process is an SEM. The SEM is a full-size structure with mass simulators in place of all internal components (Figure 1.1).

The FE method has proven to be the best approach for creating accurate dynamic models of complex structures. A model created using the FE method will typically have tens to hundreds of thousands of degrees of freedom (DOF). This large number of DOF is required to obtain accurate predictions of the satellite's response to harmonic excitations spanning frequencies up to several hundred Hertz (Hz). However, accurate predictions of the dynamic response to harmonic excitations are not achieved easily. Small details in a structure are often neglected in FE models but nonetheless affect the dynamic response.

FE models need to be adjusted, or tuned, to match measured data in order to attain higher levels of accuracy. The process developed in this research involves first tuning FE models of the spacecraft structural panels individually where the material stiffness is the major design variable. The tuned FE models of the panels are integrated into the full spacecraft FE model which is then tuned where the spring constants that connect the panels are adjusted. The tuning process adjusts the design parameters within their predefined constraints in order to minimize a cost function based on differences of measured natural frequencies and mode shapes with corresponding analytical eigenvalues

and eigenvectors computed from the satellite FE model. The resulting deliverable from this process is a tuned FE model of the spacecraft which may be used by launch vehicle integration engineers for coupled loads analyses.

To develop the FE tuning process, this research focuses on the United States Air Force Academy (USAFA) FalconSAT-5 SEM II. The section that follows explains the history of the FalconSAT program. Research goals and thesis organization are discussed last in this chapter.
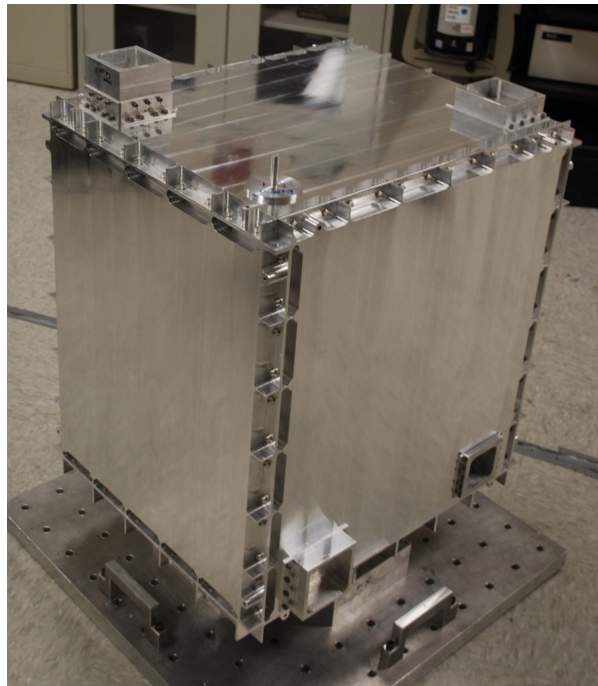
Figure 1.1:   FalconSAT-5 Structural Engineering Model II

1.1   The FalconSAT Program

USAFA has designed and built several FalconSAT (FS) satellites as a capstone program where cadets "Learn Space by Doing Space". The cadets and staff design, test, and fabricate FS satellites in the Space Systems Research Center (SSRC) at USAFA. The SSRC is comprised of officer, contractor, and cadet members. The officers and contractors working at USAFA provide the continuity needed to maintain the FS program. While working in the FS program, cadets take on responsibilities such as Program Manager, Chief Engineer, System Engineer, and Director of Operations.

Cadets at USAFA gain real-world hands-on experience in the FS program. Initiated in the mid 1990's, the FS founders established the paradigm of evolution rather than revolution - meaning the FS program is focused on achievable, adaptable objectives. Disciplined documentation of design procedures allows future FS generations to build upon past experience. The SSRC follows a design and test process involving three models of any one FS spacecraft. The SEM is the first model built in the process. An integration of the full-size structure and mass simulators for other components allows the SSRC to get measurements on mass properties, moments of inertia, and vibration modes. The second model in the process is the qualification model (QM) [*Visser*, 2006]. QMs integrate full-size structures with flight quality components, but usually use mass simulators for the payloads. Thermal-vacuum and vibration tests of the QM give cadets and faculty greater confidence in the design. A flight model (FM) is the final iteration of the SSRC design process and is the actual spacecraft that will fly [*Tavelli and Holland*, 2006]. Acceptance testing of the FM is the final validation before launch vehicle integration and involves measuring mass properties, testing avionics in a thermal vacuum, and subjecting the FM to vibration testing.

FalconGOLD, the first cadet developed satellite, launched as a secondary payload on an Atlas-Centaur in 1997. The mission of FalconGOLD (Figure 1.2) was to characterize Global Positioning System (GPS) signals at altitudes beyond that of the GPS constellation. Designing, building, and operating this first satellite resulted in a wealth of process knowledge.

Although ultimately suffering electrical power system failure, FalconSAT-1 (Figure 1.2) was launched in 2000 on a converted Minuteman II missile. Its mission was to collect data on spacecraft charging hazards. During the one month commissioning period, cadets and staff at the SSRC gained invaluable academic knowledge and refined operating procedures.

With FalconSAT-2, the SSRC began to significantly improve ground operation procedures. FalconSAT-2 (Figure 1.3) was originally scheduled to launch from the Space Shuttle Atlantis in 2003. Following the Space Shuttle Columbia accident, the launch of FalconSAT-2 was delayed. The SSRC used the FalconSAT-2 flight model to develop space
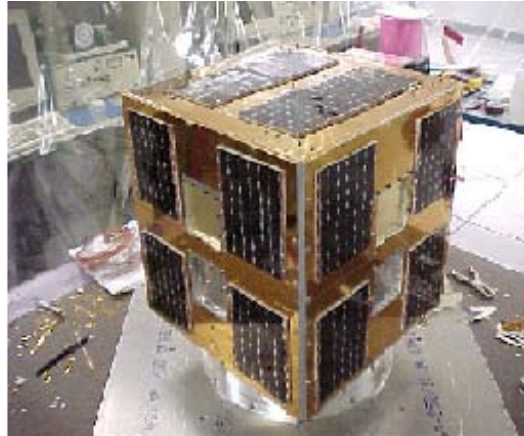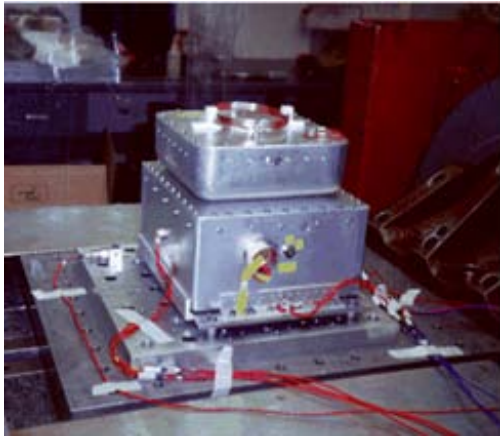
Figure 1.2:   FalconGOLD (left), and FalconSAT-1 (right) ([*O'Reilly*, 2004])
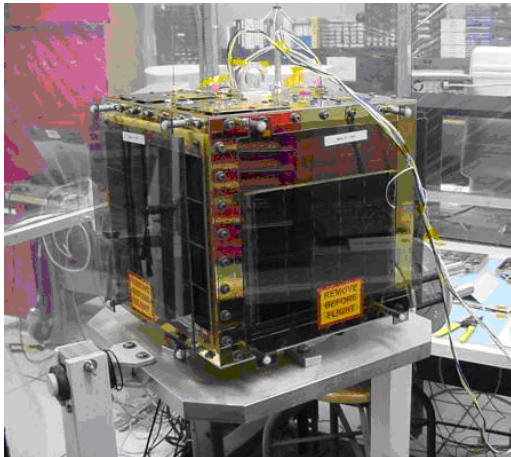
Figure 1.3:   FalconSAT-2 flight model before launch (left)([*O'Reilly*, 2004]), and FalconSAT-2 flight model after launch and recovery (right) ([*France and Lawrence*, 2006])

operations procedures and training for cadet operators until a new launch vehicle could be scheduled. USAFA performs all space operations in house. Cadets and faculty adopted operating procedures from nearby GPS squadrons at Schriever Air Force Base to apply in their own ground station at USAFA shown in Figure 1.4. The mission of FalconSAT-2

Figure 1.4: Cadets operating telemetry, tracking, payload, and support equipment stations at the SSRC ground station ([*Deal et al.*, 2007])

was to measure ionospheric plasma bubbles. These bubbles cause scintillations in the ionosphere and disrupt GPS signals. However, the failed maiden launch of the Space-X Falcon 1 in March 2006 doomed the FalconSAT-2 flight model to take up residence in the SSRC museum before any on-orbit data could be collected [*France and Lawrence*, 2006].

FalconSAT-3, Figure 1.5, took a large technological step forward from FalconSAT-2 by including the following five DoD Space Experiments Review Board (SERB) ranked experiments:

- Gravity gradient boom

- Shock ring launch adapter

- Micro Propulsion Attitude Control System

- Flat Plasma Spectrometer (FLAPS)

- Plasma Local Anomalous Noise Experiment

5

The SSRC partnered with the Air Force Space Test Squadron to manifest FalconSAT-3 on an Atlas V as rocket using the Evolved Expendable Launch Vehicle (EELV) Secondary Payload Adapter (ESPA). FalconSAT-3 was successfully launched and inserted into orbit in March 2007. Teams of space operations cadets at USAFA run sorties on the satellite and plan to convert it for amateur radio use at the conclusion of its mission.
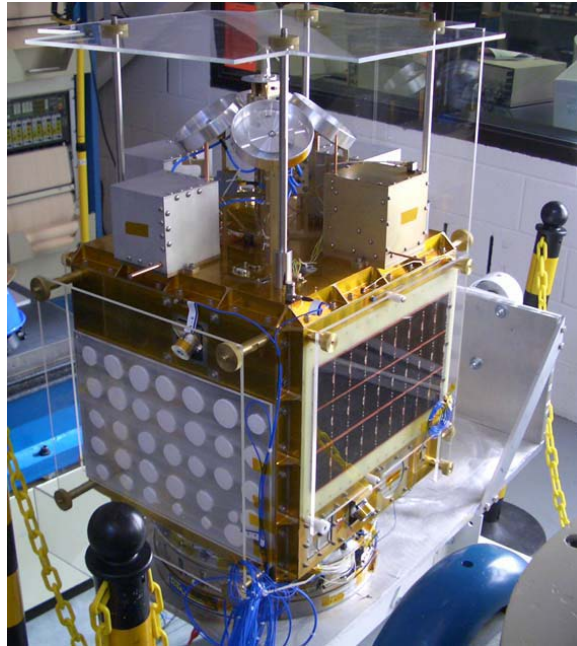
Figure 1.5:   FalconSAT-3 flight model courtesy of *Tavelli and Holland* [2006]

During the process of designing the next generation of FS, the SSRC combined payloads of the proposed FalconSAT-4 and FalconSAT-5 satellites into one FalconSAT-5 version. FalconSAT-5 (FS-5) (Figure 1.6) missions include:

- The FalconSAT-2 plasma bubble sensor

- A follow-on to FLAPS which detects proximity operations by measuring thruster ion plumes

- A Xenon ion source

- Ammonia cold gas thrusters

- A radio frequency measurement device
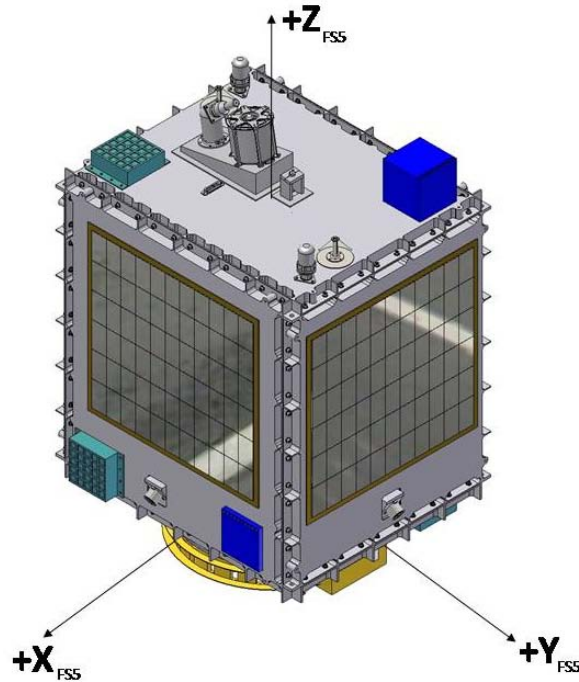
Figure 1.6:   FalconSAT-5 ([*Deal et al.*, 2007])

FalconSAT-5 is scheduled for launch as a secondary payload on a Minotaur IV
in Fall 2009. The launch vehicle is also host to three other secondary payloads, all of
which are similar in size to FS-5. Orbital Express, the launch vehicle contractor, wants
to perform a coupled loads analysis with the four secondary payloads as part of their
risk mitigation plan. Vibration analysis data for each satellite is needed for such an
analysis. For the previous versions of FS, cadet run shaker table vibration tests at the
Air Force Research Laboratory (AFRL) facilities at Kirtland Air Force Base (KAFB)
were sufficient for design engineers to ensure compliance with launch loads. However, for
the coupled loads analysis, Orbital Sciences requires each spacecraft manufacturer to go
a step further and provide an accurate FE model of their respective spacecraft. Orbital
Sciences integration engineers attach FE models of each payload to the rocket FE model
in order to perform coupled loads analyses.

Having successfully completed critical design review (CDR) for FS-5 in December
2007, the cadets and technicians built an SEM. The SEM is a valuable tool for structural
analysis, verification of mass, verification of mass moments of inertia, and simulation of
launch vehicle integration. Put to one more use, the SEM provides a means to collect ex-

7

perimental vibration data. To produce the required FE model for the launch contractor, this research effort will tune the FS-5 SEM II FE model using modal analysis data.

1.2   Research Goals

FalconSAT FE model generation has been a recent topic of collaboration between USAFA and the Air Force Institute of Technology (AFIT). Researchers at AFIT generated an FE model for the FS-5 SEM I and tuned the FE model using modal analysis data from a scanning laser vibrometer. The tuning process for the SEM I model used only a small portion of the data collected with the vibrometer and produced a model that was accurate for the first three modes (See Section 2.8). However, given the capability to collect dense vibration data over thousands of grid points using a scanning laser vibrometer presents an opportunity to strive for a more accurate FE model.

USAFA initiated major design changes which combined payload experiments from FalconSAT-4 with FS-5. The SSRC fabricated a new FS-5 SEM II to validate these design changes. Following shaker table vibration testing in May 2008 and fit checks with the other manifested payloads in July 2008, the SSRC shipped the SEM II to AFIT for detailed modal testing. Over a period of several months the work started by *Black et al.* [2008] in developing a spacecraft FE model tuning process was expanded. The modal tuning process followed is highlighted in Figure 1.7. Each block in Figure 1.7 is further detailed in Chapter 3.

The process begins with generating an untuned FE model of the satellite. Matching major structural element FE mesh representations to CAD drawings yields models with accurate mass. Fine-tuning the component masses is accomplished by manually adjusting element thicknesses of small simplified components such as rib junction fillets. Manually iterating FE model parameters such as element thickness or spring constants is often referred to as hand tuning in the remainder of this document. Vibration data is collected on each panel individually. The respective FE models for each panel are tuned where the modulii of elasticity are tuned for various sections of the panels. Finally, vibration data on the entire satellite was collected in order to tune the six DOF (6DOF) connection springs between tuned panels and adapter ring stiffness.

8
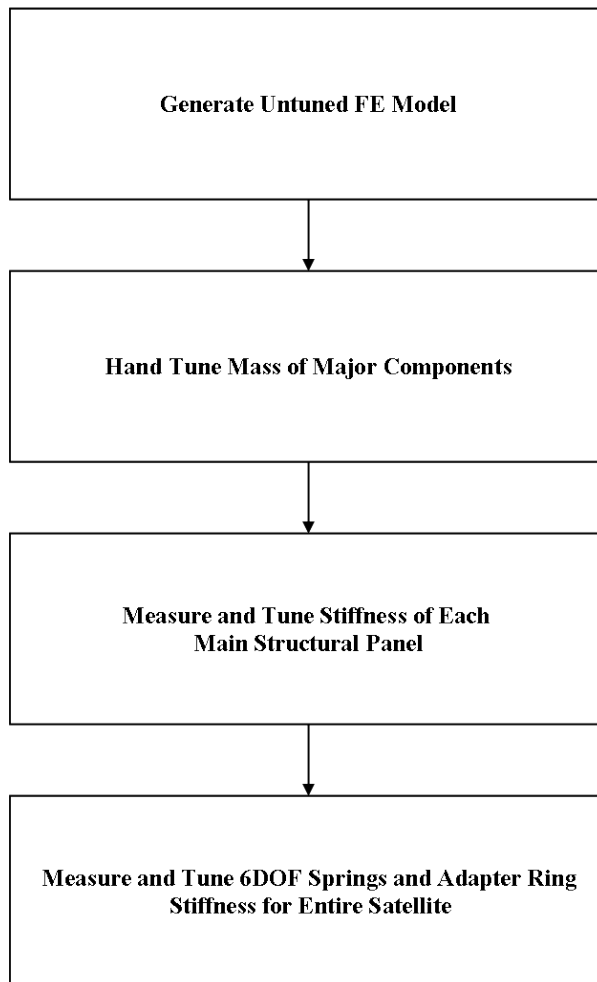
Figure 1.7:   Overall tuning process for FS-5 FE model tuning

1.3 Thesis Organization

Chapter 2 provides technical background on FE analysis, the data gathering, and optimization process. Chapter 3 details the specific test methods used in developing the FE model, gathering data, and tuning the results. Chapter 4 presents the results of the modal analysis, untuned, and tuned models. Chapter 5 highlights problems encountered, lessons learned, and recommends future work in the area of tuning satellite FE models.

II. Background

THIS chapter provides a background on the theory of FE and modal analysis as well discussing previous work in the topic area. First, a description of FE analysis is given including major steps and assumptions. Next, discussion is given which takes the reader from the initial equations of motion (EOM) for complex structures, through the eigenvalue problem (EVP), and concludes with the modal frequency response problem. An overview of the FE model tuning process is discussed next. This is followed by a recommended list of relevant references in the technical areas of modal analysis and FE model tuning. Then, a project which used many of the same FE model tuning approaches as used in this project to develop an accurate model of an antenna truss is highlighted. Next, the FalconSAT-3 FE model development approach is discussed. The FS-5 SEM I FE model tuning project, which was the direct predecessor to this research project, is discussed next. Finally, an overview of the FS-5 SEM II shaker table vibration tests is given.

2.1 Finite Element Analysis

FE analysis is a numerical process involving solution of field problems [*Cook et al.*, 2002]. The field values are any dependent variables described by differential or integral equations. FE analysis codes solve algebraic equations at discrete points called nodes, then interpolate the results between those nodes. Each node is connected to other nodes with elements. Elements can be any geometric shape from a two-node line element to a three-dimensional solid element. An arrangement of elements creates a mesh which represents the structure. The analyst models or meshes the structure using elements connected by the nodes. It is important to note that FE analysis is applied to a model problem which is typically thought of as two steps away from reality. Complex features of a structure's geometry are often simplified—meaning only essential features are modeled. For example, modeling a small bolt hole in a large panel only adds complexity and increases computation requirements if one is trying to predict the global behavior of the entire panel. Assumptions used in the FE analysis for this project include

- Homogeneous materials - same properties throughout material

- Isotropic materials - same properties in every direction

- Constant material properties - no material fatigue

- Small displacements and rotations

- Fixed loads and boundary conditions

- Linear material properties, geometry, and loads

The FE analysis process generally involves three steps: preprocessing, numerical analysis, and post-processing. Preprocessing involves selecting element types, material properties, loads, boundary conditions, and mesh density. Once an FE model has been built, the next step in the FE analysis process is to compute solutions - numerical analysis. For a modal analysis, which is the focus of discussion in this paper, the EVP is solved for either a desired number of eigenpairs or a set of eigenpairs whose natural frequencies are between requested cutoff frequencies. In the third step - post-processing - a graphical interface is typically used to view mode shapes and natural frequencies. More detailed discussion of the specific methods used in this project are in Section 3.2.

2.2 Modal Analysis

Modal analysis is the process of predicting, measuring, and documenting three dynamic characteristics of structures: natural frequencies, damping ratios, and mode shapes. Natural or resonant frequencies of a structure are those frequencies at which the structure resonates. When a structure is excited at one of its natural frequencies, the response is an uncontrolled increase in deflection unless this vibrational energy is removed - typically by damping mechanisms. Damping involves any mechanism which removes energy from a structure and is present in all real structures. Shock absorbers on an automobile is a classic example of a viscous damper. A mode shape is the magnitude-independent shape of a structure when the structure is resonating at a natural frequency.

The FE discretized EOM for complex structures can be written in the time domain as

$$M\ddot{\bar{x}}(t) + (1 + i\gamma)K\bar{x}(t) = F(t). \tag{2.1}$$

The mass matrix $M \in \mathbb{R}^{n \times n}$ and stiffness matrix $K \in \mathbb{R}^{n \times n}$ are symmetric and very sparse. The dimension of M and K is n, the number of FE DOF, which is typically more than ten thousand for accurate FE models of complex structures. The load or force matrix $F(t) \in \mathbb{R}^{n \times m}$ has m load cases which is typically between ten and several hundred. Because all components in the FS-5 SEM II are made entirely of aluminum, only one structural damping coefficient γ is required. Viscous damping terms are typically present in equations like Equation (2.1), but viscous damping terms are not required because the FS-5 SEM II does not have any components that require viscous damper representation. From the modal analysis performed in this research, modal damping will be estimated and included in the final modal representation of the structure along with the structural damping representation. The displacement vector $\bar{x} \in \mathbb{R}^{n \times 1}$ and the acceleration vector $\ddot{\bar{x}}(t) \in \mathbb{R}^{n \times 1}$ contain the response to loads $F(t)$ as a function of time. For the undamped free vibration case, Equation (2.1) reduces to

$$M\ddot{\bar{x}}(t) + K\bar{x}(t) = 0. \tag{2.2}$$

A synchronous motion solution can be considered - one in which all coordinates execute the same motion in time - as

$$\bar{x}(t) = \bar{\phi}e^{i\omega t} \tag{2.3}$$

where ω is the radian frequency and $\bar{\phi}$ is a constant real-valued vector of dimension n. Substituting Equation (2.3) into Equation (2.2) yields the real-valued EVP

$$K\bar{\phi} = \lambda M\bar{\phi} \tag{2.4}$$

where $\lambda = \omega^2$. Equation (2.4) possesses nontrivial orthogonal solutions $\bar{\phi}$ referred to as eigenvectors for n typically distinct values of λ called eigenvalues. However, typically only a subset of the total number of eigenpairs, or sets of eigenvalues along with the associated eigenvectors, are of interest. Combining the l computed eigenvectors $\bar{\phi}$ into a matrix of eigenvectors Φ yields

$$\Phi = [\bar{\phi}_1, \bar{\phi}_2, \ldots \bar{\phi}_l]. \tag{2.5}$$

13

Equation (2.4) has nontrivial solutions if

$$\det[K - \lambda M] = 0 \qquad (2.6)$$

where $\det[K - \lambda M]$ is the characteristic determinant. Mass normalizing each eigenvector in $\bar{\Phi}$, the mass and stiffness matrices may be diagonalized with

$$I = \Phi^T M \Phi \qquad (2.7)$$

and

$$\Lambda = \Phi^T K \Phi \qquad (2.8)$$

where I and Λ are of dimension l. The diagonalized modal mass matrix is the identity matrix I, and the modal stiffness matrix is a diagonal matrix with the eigenvalues on the diagonal. The modal mass and stiffness matrices can be used in calculating the modal frequency response of the structure to an input force $F(\omega)$

$$X(i\omega) = \Phi(-\omega^2 I + (1 + i\gamma)\Lambda)^{-1}\Phi^T F(\omega). \qquad (2.9)$$

The magnitude $|X(i\omega)|$ and phase angle $\rho(\omega)$ of $X(i\omega)$ is computed from

$$|X(i\omega)| = \sqrt{[ReX(i\omega)]^2 + ImX(i\omega)^2} \qquad (2.10)$$

and

$$\rho(\omega) = tan^{-1}\frac{-ImX(i\omega)}{ReX(i\omega)} \qquad (2.11)$$

where Re are the real values and Im are the imaginary values.

Plots of magnitude $|X(i\omega)|$ and phase $\rho(\omega)$ versus ω are valuable tools in modal analysis. Peaks in the magnitude plot occur at natural frequencies. Damping affects the slopes and widths of the peaks. Additionally, mode shapes may be calculated by combining magnitude and phase information. The goal of this research effort is to tune the FE model so as to produce accurate eigenvalues, λ and eigenvectors $\bar{\phi}$ through an

14

optimization process. Before the FE model may tuned, measured data is collected with a Polytec scanning laser vibrometer.

2.3   Scanning Laser Vibrometer Data Collection Fundamentals

Many methods are available to collect such data. Early modal analyses used strobe lights timed to flash at the desired frequency so that mode shapes could be seen visually. But this technique only works for structures which undergo large deflections and does not allow recording data beyond photographs. Another method of data collection common today is shake table testing. The structure is placed on a hydraulically activated table and shook at a range of frequencies. Several accelerometers attached to the spacecraft's surfaces measure accelerations at that location. The accelerations are used to create FRFs. Quality results and data can be achieved using the shake table method of modal analysis, but for the purposes of tuning an FE model, measurements in more locations than could practically be achieved using accelerometers are sought. Therefore the choice of excitation methods turns to laser vibrometry.

Laser vibrometry provides the capability to measure and store vast amounts of data for a modal analysis. A laser vibrometer, shown in Figure 2.1, is a highly specialized piece of hardware which uses three laser heads to measure modal data by means of the Doppler effect. The Doppler effect states that an object in motion and emitting a periodic signal is perceived to have a higher frequency when traveling toward an observer than when traveling away from the observer. A classic example of this principle is the high pitched sound of an ambulance traveling toward an observer versus the lower pitched sound once it has passed. Using the Doppler equations, the vibrometer emits laser energy at a known frequency and measures the frequency of the reflected light to determine the velocity of a particular scan point on the test article. The Doppler equation, adopted from *Rees* [2001] is

$$\frac{\lambda_d}{\lambda_t} = \frac{\sqrt{1 - \frac{v^2}{c^2}}}{1 - \frac{v \cos \theta}{c}} \tag{2.12}$$

where λ_t is the transmitted frequency, λ_d is the detected frequency, c is the speed of light, θ is the angle of the detector in relation to the source, and v is the velocity of the
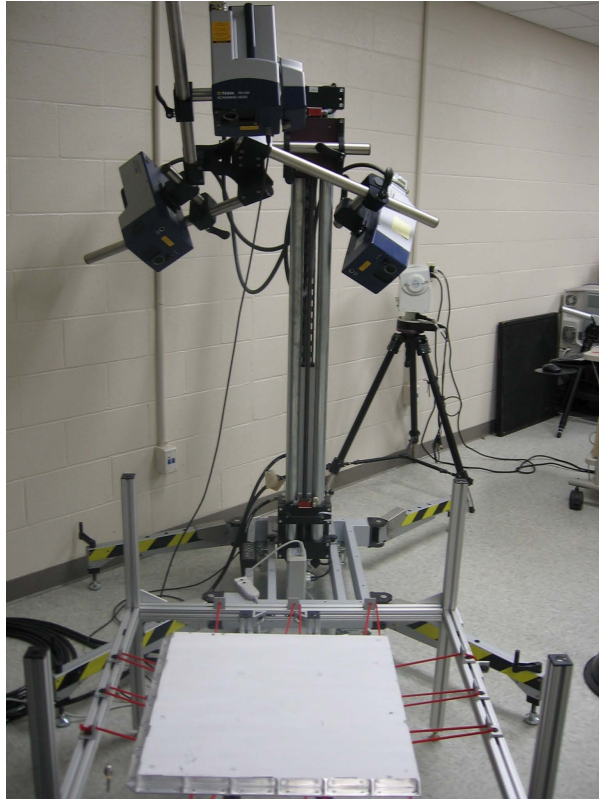
Figure 2.1:   Scanning laser vibrometer

scan point. Note that the angle dependence θ means that the precise location of each scan point with respect to each detector as well as the position of each detector with respect to the laser source must be known.

In order to ensure these detection angles are correct, the vibrometer system requires the user to perform both a two-dimensional and three-dimensional alignment prior to testing. From the two-dimensional alignment process, the Polytec software determines the location of each laser head with respect to the other heads. The user performs this alignment head-by-head, assigning multiple laser positions on the test article in a random pattern. The three-dimensional alignment instructs the vibrometer software on the location of the test article with respect to the laser vibrometer. This step requires that all three laser beams are coincident on nodes of known coordinates in three dimensions. Once the vibrometer has been aligned, the set of scan points generated from the FE model may be entered into the analysis program and testing may begin. More information on vibrometer setup can be found in *Polytec* [2007a] and *Polytec* [2007c].

16

Solving the equations of motion of Section 2.2 in the time domain is computationally inefficient (See Chapter 3.1 of *Meirovitch* [2001]). The Polytec scanning laser vibrometer software thus converts the time domain signals into the complex frequency domain via a fast Fourier transform (FFT). Derivation of the FFT is found in several engineering math texts, but the general process starts with the ordinary Fourier transform

$$F(\omega) = \int_{-\infty}^{\infty} f(t)e^{-i\omega t}\mathrm{d}t \tag{2.13}$$

with $F(\omega)$ as the frequency domain signal, $f(t)$ as the time domain signal, and ω as the frequency. Since sampling generates the signals as a set of finite points, however, the discrete Fourier transform (DFT) converts discretized data to the frequency domain

$$F_n = \sum_{k=0}^{N-1} f(t_k)e^{-int_k}, \qquad n = 0, \cdots, N-1 \tag{2.14}$$

where N is the number of samples. However, the DFT involves a function on the order of $\Theta(N^2)$ operations. Considering the large amount of data collected to avoid aliasing, the number of operations required when using the DFT method is extremely large. The FFT method therefore, breaks down the DFT equation into a sum of several smaller equations and ultimately reduces the number of operations to a function on the order of $log_2 N$.

From the FFT, the vibrometer software calculates the FRF using the general equation

$$\frac{outputFFT}{inputFFT}. \tag{2.15}$$

In practice, for numerical stability, the calculation of this fraction is not as straightforward as it appears. The FRFs calculated are actually estimates based on spectral densities. Spectral densities are the FFTs of the correlation functions. From Chapter 3 of *Friswell and Mottershead* [1995], the four spectral densities as related to the input

(hammer impulse) FFT, $R(\omega)$ and the output (Doppler velocity) FFT, $C(\omega)$ are

$$S_{CC}(\omega) = C(\omega)\bar{C}(\omega),$$

$$S_{RR}(\omega) = R(\omega)\bar{R}(\omega),$$

$$S_{CR}(\omega) = C(\omega)\bar{R}(\omega), \text{ and}$$

$$S_{RC}(\omega) = R(\omega)\bar{C}(\omega). \tag{2.16}$$

where $C(\omega)$ and $R(\omega)$ are the FFTs of the response and input respectively and the overbar denotes complex conjugate. Two estimates of the FRF are made with these spectral densities, the $H1$ and the $H2$ are

$$H1(\omega) = \frac{S_{CR}(\omega)}{S_{RR}(\omega)} \quad \text{and} \quad H2(\omega) = \frac{S_{CC}(\omega)}{S_{RC}(\omega)}. \tag{2.17}$$

Each of these estimates results in an FRF with the general value of output divided by input, but the $H1$ estimator is primarily affected by noise on the input while the $H2$ estimator is primarily affected by noise on the output. For scanning measurements, output noise is generally greater than input noise. Hence the $H1$ estimator is a better choice for viewing the FRF in this application because it is less sensitive to output noise. In order to minimize the effect of noise in the data, averaging is used. Specifically, since impact excitation is used and animation of mode shapes with the collected data is desirable, complex averaging is the best choice out of the averaging techniques available (See Section 6 and Table 12.2 of *Polytec* [2007b]).

Related to the $H1$ and $H2$ estimates, coherence is a test parameter which must be monitored to ensure quality data is recorded. Coherence is defined as $H1/H2$ and is a measure of consistency in the measured data. It relates how much of the output signal is directly caused by the input. A coherence of 1 means all of the output is due to the input and is favorable, while a coherence of 0 indicates none of the output is a result of the input. Good coherence is much easier to achieve using impact testing than shaking the structure with white noise and is a large part of the reason hammer excitation is

18

used in this research. Figure 2.2 shows a relatively good coherence achieved during panel testing.
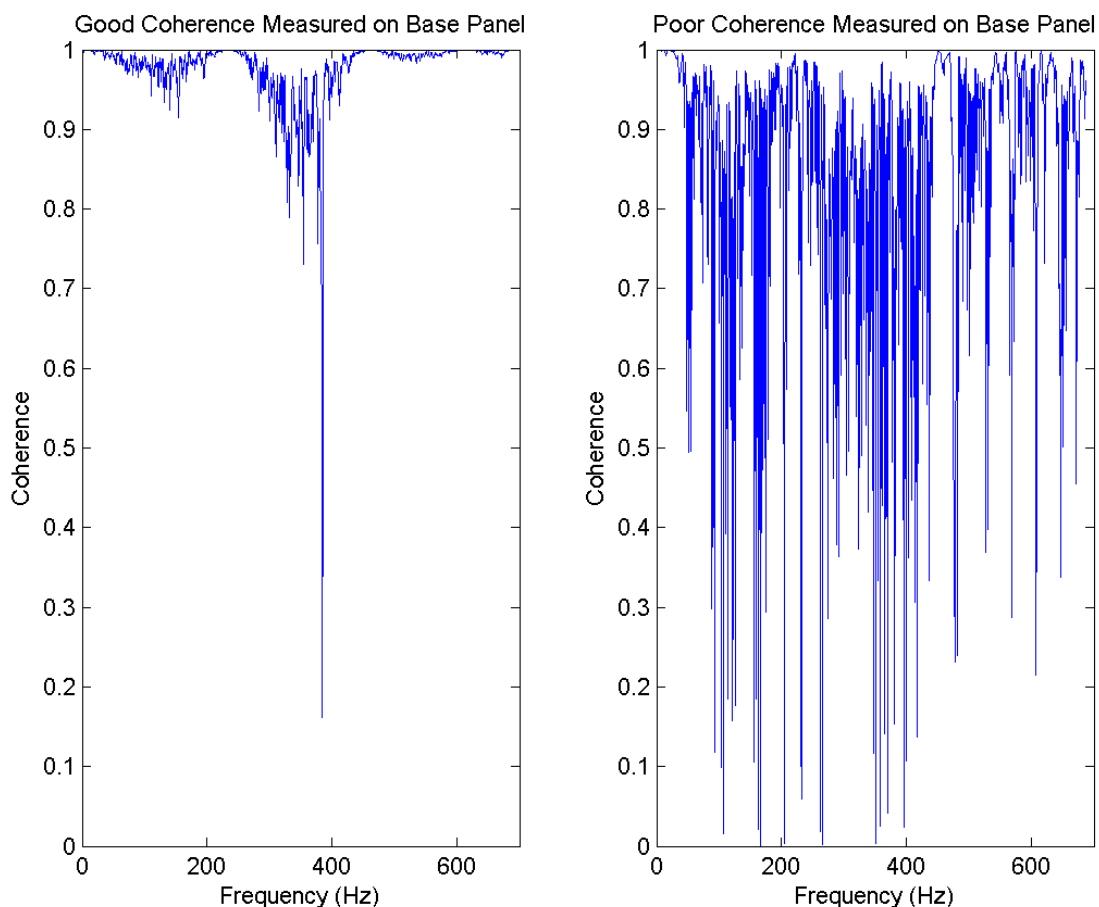
Figure 2.2:   Coherence value as a function of frequency for panel testing

Another common problem in collecting experimental data is leakage. Since the measured signals are not necessarily periodic at all times, the Fourier transform equations output a signal with some power from the expected frequency showing up in adjacent frequencies. A typical method of mitigating leakage is multiplying the suspect signals by a window function. The window functions for most excitation methods force the signal magnitude to be zero at the start and end of the sample, therefore making it as close to periodic as possible. For impact testing, an exponential window is commonly used on the response and a rectangular window is used on the input signal. This function allows the magnitude at the beginning of the sample to be high, but significantly tapers

19

off towards the end of the sample. For more information on common sources of error in data collection see *Friswell and Mottershead* [1995] and *Agilent* [2000].

With the signals characterized and settings established, the vibrometer is started in scan mode. The vibrometer records a number of FFTs at each scan point equal to the number assigned in the average command. After the FFTs have been collected at the current scan point, the lasers automatically shift to the next point and restart data collection. If the velocity of the scan point is of a greater magnitude than the selected laser sensitivity, the scan point is recorded as overrange. Scan settings allow the user to force the system to re-test these overrange points after finishing the entire scan. The sensitivity of the lasers to external noise sources is a great concern for the tester. When a scan is complete, the data can be processed and used for tuning the FE model.

2.4   Finite Element Model Tuning

An FE model can be tuned to closely predict a structure's harmonic response over a wide range of excitation frequencies. Creating an accurate model of a satellite is very challenging because there are typically hundreds to thousands of components with potentially complex interfaces. In order to improve the accuracy of an FE model, a common practice is to 'tune' or adjust model parameters like the modulus of elasticity or material density of the FE model to match the experimentally measured data. Acquiring experimental modal data from a structure can be accomplished in several ways. An overview of the process is stated here with specific details left until Chapter 3. The first step in experimentally extracting the modes of a structure is to determine or enforce boundary conditions - typically supporting or constraining it. For a single component of a structure, analysts may choose to simulate the article floating in space. In this way, the external loads placed on the object are minimal and the dynamic properties of the structure are largely unaffected by the boundary conditions. Other times, an analyst wishes to simulate a structure integrated with another relatively immobile structure by applying fixed constraints. In this case, the structure must be secured such that no vibrations propagate from or through fixed locations of the test article. Typically, this

is done by attaching the test structure to a much larger structure. In either case, the structure must also be excited.

Common mechanisms used to excite a structure for vibration analyses include shaker tables, electromagnetic generators, and impact hammers. The excited structure will vibrate with a combination of all natural mode shapes. An important note is that real structures have an infinite number of modes, however, the predominant response is dominated by those modes near the frequency of excitation. In terms of an FE model, it will have a finite number of modes - the same number as the number of FE DOF. However, for practical purposes, dynamic behavior of interest for most applications involves only the lowest set of natural frequencies and their associated mode shapes. With the structure excited, the tester must ensure that both the input and the structure's response are measured. Common devices which measure input are transducers for shaker tables and force cells for generators and hammers. Devices which measure response are typically accelerometers and lasers. Knowing both output and input, software can be used to calculate frequency response functions (FRF). An FRF is a plot of output divided by input in the frequency domain (See Figure 2.3). The plot shows the response of the structure over the frequency range of interest. Peaks in the FRF indicate natural frequencies. Damping can also be calculated from an FRF. By taking measurements at multiple locations, operational deflection shapes (ODS) can also be measured. Specialized software is used by analysts to extract mode shapes, natural frequencies, and damping factors from the FRF and ODS data using curve fitting processes (See Section 3.4.4).

Once the experimental modal analysis parameters have been measured and extracted, the process of tuning the FE model may begin. The overall goal is to modify the eigenvalues and eigenvectors of the FE model to closely match the measured data. Selected parameters in the FE model are adjusted to match analytical natural frequencies and mode shapes with the measured. The parameters which are allowed to vary in this process must be chosen carefully as to not invalidate mass, moments of inertia, or other well known quantities. An FE model with tens to hundreds of thousands of FE DOF is too difficult to precisely tune by hand. Therefore, a common practice is to minimize
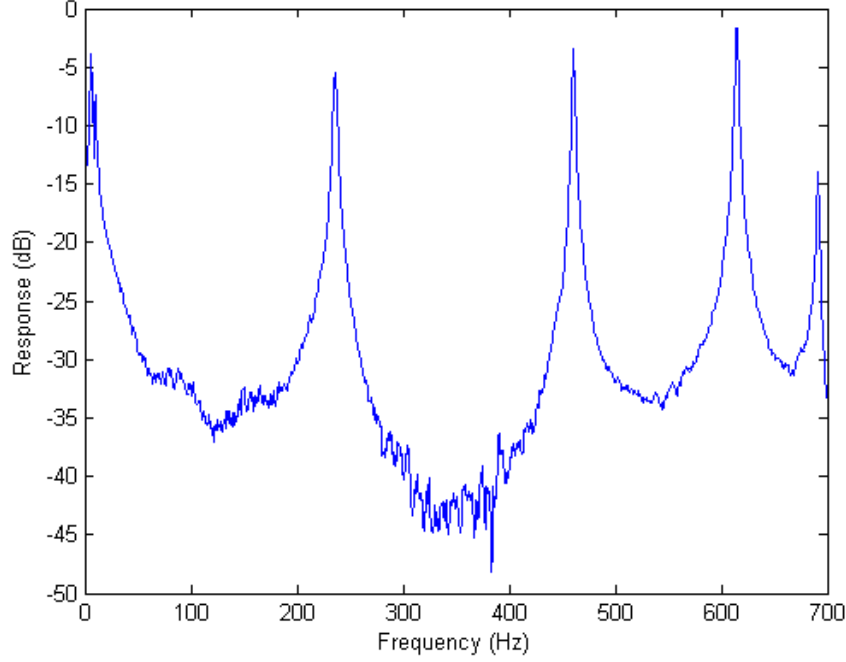
Figure 2.3: This FRF was measured on the base panel of FS-5 using a laser vibrometer. Natural frequencies occur at 237, 460, 615, and 691 Hz. Rigid body motion generates the peaks near zero Hz.

a cost or objective function in an optimization routine. A common cost function is a measure of the difference between measured and analytical eigenvalues and eigenvectors given as

$$J = \sum_{i=1}^{p} a_i [1 - \frac{\lambda_{iA}}{\lambda_{iM}}]^2 + \sum_{i=1}^{p} \sum_{j=1}^{r} b_i [1 - |\frac{\phi_{ij_A}}{\phi_{ij_M} \phi_{iN}}|]^2. \tag{2.18}$$

Here a_i and b_i are weighting factors, λ_{iA} and λ_{iM} are the ith analytical and measured natural frequencies, respectively, and ϕ_{ij_A} and ϕ_{ij_M} are the ith analytical and measured eigenvectors or mode shapes, respectively. The analytical eigenvectors are normalized with the same DOF that the measured modes are normalized with ϕ_{iN}. The summation limits are the number of modes desired p and the number of measurement locations r. The optimization routine minimizes the non-dimensional value J by iteratively varying the chosen parameters in the FE model within a specified set of constraints. The difference between the analytical and measured natural frequencies and mode shapes are minimized. Matching natural frequencies alone is fairly common and simple to perform since they are scalar values. However, matching mode shapes, a vector quantity, requires

the use of a cross-orthogonality check [*Agilent*, 2000]. Cross-orthogonality checks are basically a check to ensure the measured and analytical modes are matched. Specific details are provided later in Section 3.4.5. Using the above described technique, the FE model is tuned to experimental data resulting in an FE model that can be used to closely predict the dynamic response of the real structure within a certain frequency range.

2.5 *Modal Analysis and FE Model Tuning References*

A significant amount of research has been accomplished in the field of modal analysis and FE model tuning. Though some specific examples relevant to the FalconSAT project are given in the following sections, here a short background on some of the more general references is provided. The documents highlighted in this section provide the reader with a review of the entire process from modal testing through FE model tuning and gives an example of the process used in another application.

The first step in performing modal analysis is collecting data. Data collection for modal analysis can be accomplished using any one of a large number of techniques. *Agilent* [2000] presents a practical discussion on the experimental modal technique of FRF testing. The document begins with an introduction to the theory and assumptions involved with structural dynamics, specifically those relevant to FRF measurements. Next, the document shows typical experiment set-up schematics for supporting the structure, exciting the structure, measuring vibration data, and interpreting the the data. Techniques which can improve the accuracy of data collection follow with explanations of averaging, windowing, and finding the correct data resolution. Data reduction techniques are introduced including curve fitting and calculation of complex-valued versus real-valued mode vectors. The document finishes with listing several applications for modal data. Structural modification, FE correlation, and forced response simulation are few of the examples introduced.

Once the data has been collected, the next step in the general FE tuning process is to extract the modal data. Extracting modal data involves determining natural frequencies, mode shapes, and damping coefficients from measured FRFs - resulting in estimated transfer functions. Typically, a curve fitting method is used to determine these

parameters from the measured data. A good summary of the modal extraction process is explained in *Richardson and Schwarz* [2003]. The article presents theory and examples on two popular curve fitting techniques - Rational Fraction Polynomial (RFP) and Complex Exponential (CE). The RFP method is used in the modal extraction software for this thesis. The RFP method solves a set of linear equations to find unknown coefficients in the complex-valued transfer function

$$H(\omega) = \left. \frac{\displaystyle\sum_{k=0}^{2m-1} a_k s^k}{\displaystyle\sum_{k=0}^{2m-1} b_k s^k} \right|_{s=j\omega} \tag{2.19}$$

where m is the number of modes and a and b are the unknown coefficients [*Richardson and Schwarz*, 2003]. The method examines a small band of frequencies at a time in order to accurately fit a polynomial expression to the measured data. Natural frequencies occur at peaks in the FRFs and are solved to determine the poles of the transfer function. To determine the coefficients of the transfer function denominator, partial fraction expansion is applied to the poles resulting in residues. The residues show the strength of a mode with respect to all other modes. A second application of the RFP curve fitting method determines the coefficients of the numerator. A complete transfer function equation predicts the structure's response at any frequency and yields complex-valued orthogonal mode shape vectors.

After complex-valued modes have been extracted from the measurement data they must be converted to real-valued modes in order to compare with the real-valued analytical eigenvectors in the FE model. A very good reference on updating FE models with experimental data is *Friswell and Mottershead* [1995]. This book covers the entire modal tuning process from FE model generation through vibration measurement and model updating. Sections of the book involving comparisons of FE data with measured and extracted modal data are very insightful. The modal assurance criterion (MAC), which is central to this research project, is discussed in detail. Also of great importance to this thesis is the selection of tuning parameters or design variables with which to iterate dur-

ing the optimization of the objective function. *Friswell and Mottershead* [1995] devotes several chapters to design parameter and optimization method selection. Examples are displayed in the text which helps the reader understand the process.

Putting the entire modal analysis and FE model updating process together has been the topic of numerous research projects. An example of a report on this process is *Coppotelli et al.* [2008]. This report highlights a procedure used to update a large FE model using experimentally measured modal data on the VEGA Launch Vehicle payload adapter. Sine sweep vibration testing was performed on the structures to collect modal data. An FE model of the payload adapter and connecting structures with was generated and contained 1,500,000 DOF and 250,000 elements. Instead of using an objective function to refine the values of design parameters, the authors use a sensitivity-based approach to increase the accuracy of the FE model. This approach directly places the estimated transfer functions from the vibration test into sensitivity matrices. Partial derivatives of the experimental transfer functions with respect to the analytical transfer functions allows the analyst to determine which design variable values (mass and stiffness matrix elements in this case) best affect model correlation. With such a large number of DOF and design variables, the authors developed a technique which uses singular value decomposition to reduce the rank of the sensitivity matrix used in tuning the model. Results of the project show a successful use of the "rank control enhancement" technique in reducing the computational size of the tuning problem. The authors achieved a converged optimization in which the tuned FE model better matched natural frequencies with the measured data.

2.6   Early Development of the Tuning Objective Function

Development of the tuning algorithm used in this research can be traced back to use by *Cobb et al.* [1996]. In an experiment testing a six meter antenna truss, the authors first developed an untuned FE model of the structure. The truss FE model consisted of 100 elements including various diameter tubular beams for the main structure and concentrated masses for brackets. Excitation was achieved with two reaction mass actuators at the top of the structure. Activating both actuators in phase excited bending

modes while activating them 180 ° out-of-phase excited torsional modes. The response of the structure was measured using eight single-axis accelerometers spaced evenly along a single vertical corner of the antenna.

The mass, cross-sectional area, and moment data for each major structural element of the truss were measured in order to establish the FE model baseline. When the untuned FE model's analytical FRF showed significant deviance from the measured FRF, the tuning process was begun. Design variables for the tuning process included mass and stiffness of the beam elements and mass of the concentrated elements. Each similar element was assigned the same design variables in order to keep the properties symmetrical. The tuning algorithm for the truss project used an objective function very similar to the objective function used this FS-5 SEM II project. This objective function was

$$J = \sum_{i=1}^{p} a_i [\frac{\lambda_{iA}}{\lambda_{iM}} - 1]^2 + \sum_{i=1}^{q} \sum_{j=1}^{r} b_i j [\phi_{ijA} - \phi_{ijM}]^2. \tag{2.20}$$

Each variable in this equation is consistent with those of (2.18) in Section 2.4. Though not specified in the equation, normalization of eigenvectors occurred via the same point-normalization approach used in this project. *Cobb et al.* [1996] also added another term to this objective function which compared tuned values of the mass design variables to the initial baseline masses in order to minimize the deviance from the known values.

Since the actuators could only excite bending and torsion modes, the breathing modes predicted with the FE model of the truss had to be eliminated from the tuning process. The tuning algorithm used a mode tracking system which performed cross-orthogonality checks between iterations. This is the same process used in the FalconSAT project. Care was taken to ensure the measured modes were in the same order as those predicted with the untuned FE model in the truss project.

For the first tuning case of the truss antenna, the a_i weighting coefficients were all set to 100 and the b_{ij} coefficients were all set to one. This meant the researchers suspected all modes were excited and measured with equal quality, but a greater emphasis on tuning eigenvalues was desired rather than on eigenvectors. The resulting tuned FE model of

the truss posted analytical modes with natural frequencies very closely matching the measured values through 60 Hz - the frequency range of tuning.

Next, the researchers examined the capability of the tuned FE model to predict the structure's frequency response when damaged. Specifically, one strut was removed from both the structure and the tuned FE model. However, with the damaged structure breathing modes were captured with the accelerometers. The tuned FE model predictions for the breathing modes were poor since those mode shapes were not part of the first tuning case. Therefore, the untuned FE model was tuned a second time to match the damaged truss measured data. Results of the tuning yielded an FE model which very closely matched the second, more robust data set.

Overall, the project displayed the same tuning process used in this FalconSAT project. The findings highlight the importance of verifying that as many modes are excited as possible during measurements. Also stressed was the importance of comparing measured modes to analytical modes before tuning to ensure the optimization has reduced the chance for mode switching errors. The truss project also demonstrates the benefits of testing FE models with off-nominal conditions.

2.7 FalconSAT-3 FE Model Results

Transitioning now to FE models generated for the FalconSAT program, FalconSAT-3 (FS-3) is discussed. FS-3 was the first USAFA satellite to fly on the ESPA ring. At the time, the ESPA ring was a new technology, and as such, much emphasis was placed on risk reduction for each of its payloads. FS-3 was the most structurally complex of the payloads on this first ESPA flight and so accurate modeling became paramount. The FS-3 report, *Sarafin* [2003], details multiple studies performed using a 450 node FE model of the satellite. One major concern for integration engineers was ensuring FS-3 axial modes did not occur in the same frequency range as predicted spikes in the power spectral density induced by the ESPA ring. Another concern was that the diameter of the gravity gradient boom on FS-3 was very close to the diameter of the corresponding hole in the ESPA ring through which it was inserted during launch. Analysts needed to ensure rocking frequencies for the boom did not coincide with launch vehicle environments which

would cause contact during launch. As a first step in mitigating these risks, USAFA chose to use a CSA Engineering Shock Ring between the Lightband separation device and the ESPA ring.

The FS-3 FE model, developed by *Sarafin* [2003] is shown in Figure 2.4. The

Antenna cluster

MPACS

Module stack

Adapter ring

Lightband

Shock Ring

- Approx. 450 grids, 2700 degrees of freedom
- 116 lb (52.7 kg)
- CG at
  - X = 0.19"
  - Y = 0.00"
  - Z = 5.69"
- MOI at CG:
  - I_{XX} = 37.2 lb-in-s^2
  - I_{YY} = 37.6 lb-in-s^2
  - I_{ZZ} = 13.5 lb-in-s^2

Boom (100-Hz bending mode)
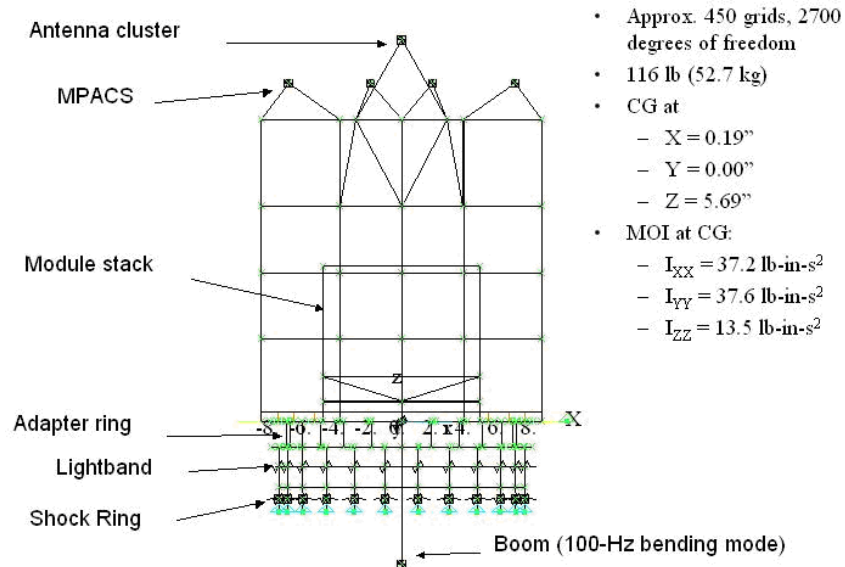
Figure 2.4:   FalconSAT-3 FEM version FS3FM-2LS displayed here with the permission of *Sarafin* [2003]

model was hand-tuned over a period of eight months based on measured vibration tests and structure modifications between the SEM, qualification model, and flight model. Tests were performed on the FS-3 flight model using several configurations. First the satellite was constrained directly from the adapter ring. Second, it was constrained from the Lightband interface. Finally, the satellite was constrained from the Shock Ring interface. This data allowed the FE model to be tuned at each configuration and significantly improved the accuracy. Element stiffnesses, thicknesses, and moments were adjusted to match the measured data in each case.

The vibration tests on the FS-3 flight model showed axial mode peaks close to the 110-120 Hz range, which directly matched the peaks in spectral density resulting from ESPA resonance. Therefore, FE analysts performed trade studies on such parameters as dimensions of the adapter ring, thickness of base panel ribs, boom stowed fundamental

frequency, and Shock Ring stiffness. Findings from the FS-3 FE model report state a correlation existed between the frequency of the first rocking mode and the first axial mode. Since the Shock Ring design allows relatively simple damping adjustments which affect the rocking modes of the spacecraft, the *Sarafin* [2003] report provides recommendations that the Shock Ring should be designed to force the first rocking mode of the satellite to occur at approximately 30 Hz. A first rocking mode frequency of 35 Hertz coincides with the first axial mode frequency in the range of peak spectral density. Recommendations on boom stiffness were also made which ensure the boom vibration modes do not couple with spacecraft modes. This report showcased the value which accurate FE models can provide to a spacecraft design team.

2.8   SEM I Vibrometer Test

The most recent FalconSAT FE model project and the predecessor to this project was that of *Black et al.* [2008]. Before USAFA made major design changes to FS-5, described in Section 3.2.2, they built the FS-5 SEM I, shown in Figure 2.5. Cadets
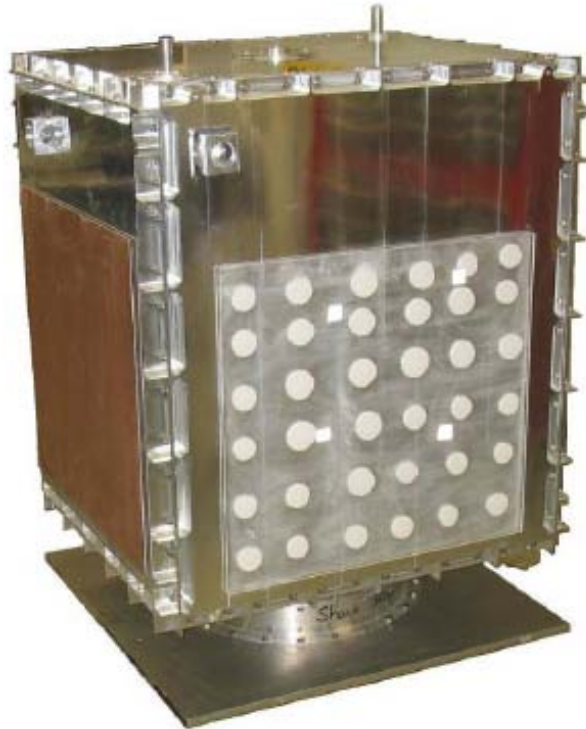
Figure 2.5:   FalconSAT-5 SEM I courtesy of *Black et al.* [2008]

and faculty performed vibration testing on the FS-5 SEM I using traditional shaker table actuation. Low-level sine sweeps at the base of the structure allowed data to be collected from 20 3-axis accelerometers. But since this data was not sufficient to extract mode shapes, *Black et al.* [2008] brought the SEM I to AFIT for modal tests using a laser vibrometer. Using this approach 6,495 FRFs were collected from a total of 2,165 measurement points over the surface of the structure.

An FE model of the SEM I was generated using the approach of matching node locations to midplanes on computer aided design (CAD) geometry files. The untuned SEM I FE model, shown in Figure 2.6 contained 11,000 elements and 10,000 nodes. Connections between panels included beam elements to simulate bolts and 6DOF spring elements to simulate contact surface interactions. Solid elements were used for thicker components and the internal mass simulators were meshed individually.

Figure 2.6:   FalconSAT-5 SEM I FE model courtesy of *Black et al.* [2008]

The initial untuned FE model of the SEM I predicted the first three natural frequencies within 8% of the measured values. To compare mode shapes, however, a MAC is used to estimate tuned FE model eigenvector correlation with measured mode shape

data. The MAC, adapted here from *Friswell and Mottershead* [1995], is defined as

$$MAC_{ij} = \frac{|\bar{\phi}_{Mi}^T \bar{\phi}_{Aj}|^2}{(\bar{\phi}_{Aj}^T \bar{\phi}_{Aj})(\bar{\phi}_{Mi}^T \bar{\phi}_{Mi})} \qquad (2.21)$$

where $\bar{\phi}_{Mi}$ is the ith measured eigenvector and $\bar{\phi}_A$ is the jth analytical eigenvector. For a set of n eigenvectors, the MAC is a n by n matrix. A model with analytical eigenvectors in close agreement with the measured data will have values approaching one along the diagonal of the MAC matrix and values near zero on the off-diagonals. This case indicates that the modes are nearly orthogonal. The off-diagonal values will never all be exactly zero because the MAC is an estimate. For instance, calculating a MAC of analytical eigenvector versus analytical eigenvectors will yield a 'best case' solution in which some of the off-diagonal values are not zero. Diagonal values significantly less than one and off diagonal values greater than zero in the MAC indicate that portions of one eigenvector are present in others. The untuned FS-5 SEM I FE model eigenvectors for the first three modes produced MAC values of 0.899, 0.921, and 0.905 respectively in the *Black et al.* [2008] report.

Using the objective function of Equation (2.18), the SEM I FE model was tuned using the bolt cross-sectional area, 6DOF spring constants, and panel modulii of elasticity as design variables. The first case tuned only the first three eigenvalues which resulted in those frequencies matching measured values to within 1%. The MAC values did not improve to the researchers' satisfaction using this relatively simple tuning case. Therefore, the second tuning case used a single measurement point on the positive X panel to tune the second eigenvector as well as the first three eigenvalues in the SEM I FE model. This case produced a tuned FE model which predicted the first three natural frequencies within 2% of the measured values and MAC values of 0.962, 0.988, and 0.970 - deemed successfully tuned.

Subsequent tuning cases performed by *Black et al.* [2008] included using two tuning points, five tuning points, and ten tuning points. These points were all chosen on either the positive or negative X panels. The resulting tuned FE models from these cases showed no improvement in correlation with the measured data for the first three modes.

An explanation given for this observation was that since the first two modes were rocking motions, the motion of data points on the positive and negative X panels had little motion with respect to each other. Using more data points in the tuning cases therefore did not add any new information to the objective function. However, higher modes were in fact affected by tuning a the greater number of data points, though a pattern or conclusions on tuning the higher modes could not be reached.

The work done by *Black et al.* [2008] suggests that tuning a spacecraft FE model accurately for the first three modes, generally the most important in terms of high translations during launch, can be done using the data collected from traditional shaker table vibration tests. But, the authors state that tuning an FE model beyond the first three modes requires the high-density data obtained with laser vibrometry. But with over 6,000 FRFs and several hundred design variables, tuning the satellite FE model for increasing numbers of data points begins to become very computationally challenging, even give today's processor cluster technologies. Therefore, the extension of the work by *Black et al.* [2008] is to develop a procedure for discretizing the tuning process into computationally manageable parts to allow tuning the spacecraft FE model at higher modes. In fact, the focus of this thesis is to use the FS-5 SEM II to develop this procedure. But first, one more piece of relevant background on the subject is discussed - the traditional shaker vibration test of the FS-5 SEM II.

2.9 SEM II Shaker Vibration Test

Following major design changes to FS-5, a new SEM II was fabricated at USAFA. In May 2008 the SEM II was subjected to the traditional shaker table test at the Aerospace Engineering Facility (AEF) at KAFB. A low-level sine sweep was performed to measure structural natural frequencies. Random vibration and sine burst tests were performed to validate the structural integrity and strength of the SEM II.

Results of the sine sweep test indicated the first modes as: rocking about the Y axis - 39.7 Hz; rocking about the X axis - 44.3 Hz; and first axial mode - 124 Hz [*Owen et al.*, 2008]. FRFs from relevant panels showing these modes are shown in Figure 2.6.
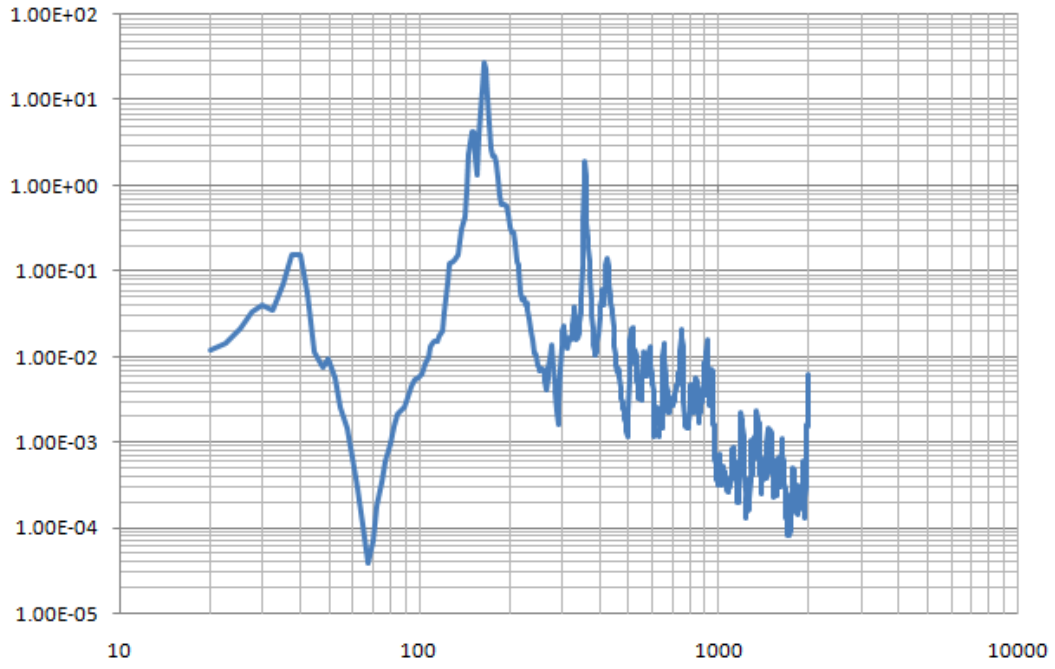
(a) FRF from negative Y panel
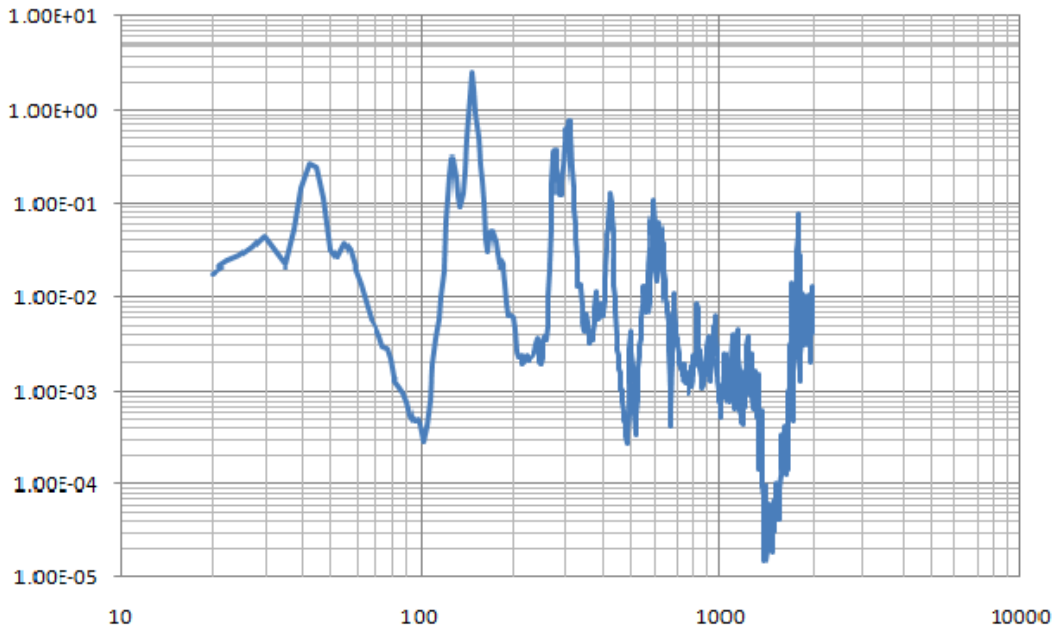
(b) FRF from positive X panel
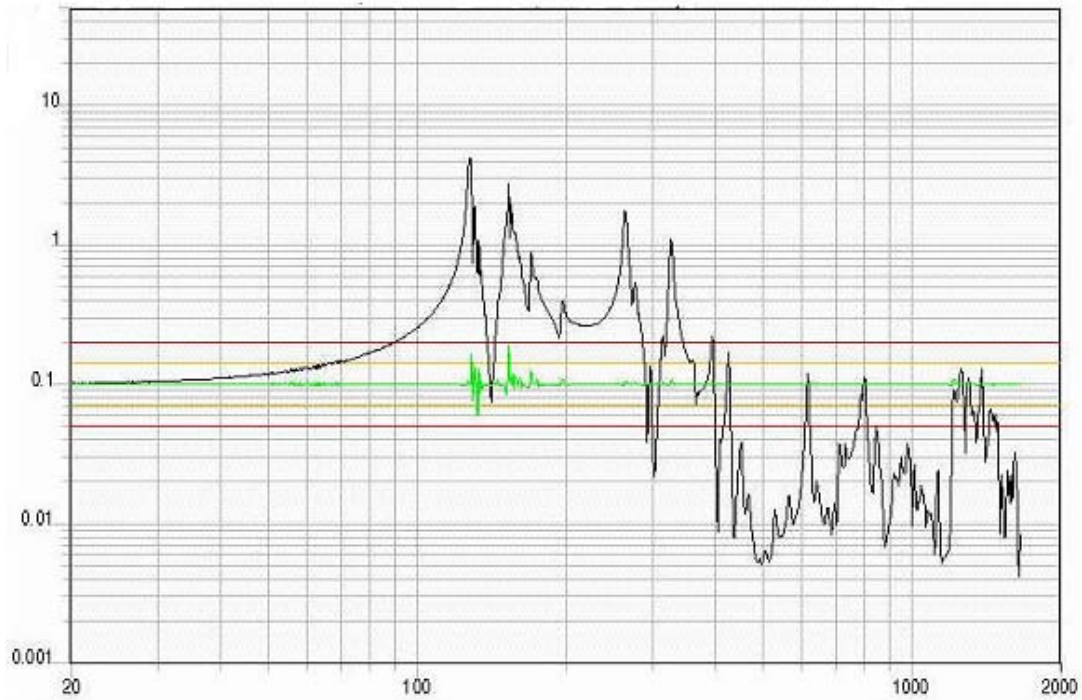
(c) FRF from top panel

Figure 2.6:   FRF plots from the May 2008 FS-5 SEM II vibration tests at Kirtland Air Force Base. Plot (a) is from an accelerometer on the -Y panel and shows the first rocking mode at 39.7 Hz. Plot (b) is from an accelerometer on the +X panel and shows the second rocking mode at 44.3 Hz. Plot (c) is from an accelerometer on the top panel and shows the first axial mode at 124 Hz. Plots courtesy of Poti Doukas, Instar Engineering.

Though the focus of this thesis is not a comparison of vibration test methods, the data collected during this shaker table test did provide some guidance for generating the early untuned FE model. Another important observation of the shaker table tests is that identifying mode shapes from the FRFs beyond the first three well-known modes is very difficult. Here laser vibrometry can enhance the shaker table results by assigning qualitative descriptions to each of the higher frequency peaks on the FRF plots.

III.   Method

I N this chapter, the detailed process of creating and tuning the FS-5 SEM II FE model is discussed. The process follows the flow described in Figure 1.7. After the entire process is summarized, the approaches used to generate an untuned FE model of the entire satellite are shown. Next, the major structural components are identified and the respective parts in the FE model are hand tuned. The process continues with measuring and tuning individual satellite panels. Measuring modal properties of the full satellite and tuning the integrated SEM II FE model is the final step in the process.

3.1   Method Overview

By weighing the mass of all major components of the FS-5 SEM, one can ensure that the mass of each of the FE discretized major components is the same as the measured. This approach is an improvement over previous efforts which modeled internal component as lumped masses. With the total mass of the FE model matching the actual mass of the SEM II to within two percent, any parameters in the FE model like element thickness are eliminated from the set of possible parameters that can be tuned.

Since the side panels, base panel, and top panel of the SEM II form the primary structure of the satellite, the process is focused on measuring and tuning the FE models of those individual panels. A test stand which allows the panels to vibrate freely is used to support the individual panels. Impact excitation is provided by an automated ping hammer. A three-dimensional laser vibrometer scans over grid points spaced approximately one inch apart over the surface of each panel. The laser vibrometer collect ODS data. Complex-valued mode shapes are extracted from the ODSs and converted to real values so that modal data can be extracted. This modal data is used in the objective function, Equation (2.18), in an optimization in which the modulii of elasticity of the panel ribs are allowed to vary within preset limits. In this way, each side panel FE model is tuned to match at least the first eight measured natural frequencies and ODS. Top and base panels, being heavier and stiffer, tuned to the first six and five natural frequencies and mode shapes respectively.

Once the FE models of each panel are tuned, they are assembled to form the full satellite model. The primary design variables for the full satellite FE model tuning process are the six DOF spring constants. Instead of modeling individual bolts, six DOF springs are used to represent component connections. Both connections between panels and connection of the base panel to the adapter ring were modeled in such a manner. Rigid link elements also connect the adapter ring to a lumped mass rocket simulator in order to constrain the FE model. The constraint allows calculation of FRFs without rigid body modes.

In order to tune the full satellite FE model, another set of measured data is required. To ensure that the SEM II has rigid boundary conditions, it is bolted to the floor. Laser vibrometer data is collected on the surface of each side panel and top panel of the assembled SEM II using the same one inch spacing as was used on the panels. Excitation is provided from the same automated ping hammer source, but instead of being perpendicular to a panel, it is actuated at a 45 degree angle on a top corner of the SEM II. In this manner, eleven ODS and their associated natural frequencies in the range of interest - under three hundred Hertz, are measured. The ODS are characterized using over two thousand measurement locations at which three translational velocities are measured. As with the individual plate data, the combined vibration data for the full SEM II tests is exported into mode extraction software then converted from complex values to real before passing the data into the optimizer. The overall goal of the research project is to develop the above FE model tuning procedure and document the precision of the results. The remainder of this chapter takes a closer look at each of the steps described above.

3.2   Generate Untuned Finite Element Model

The first step in the tuning process is generating or creating an untuned FE model. Figure 3.1 breaks down the first block of the overall process shown in flowchart Figure 1.7.
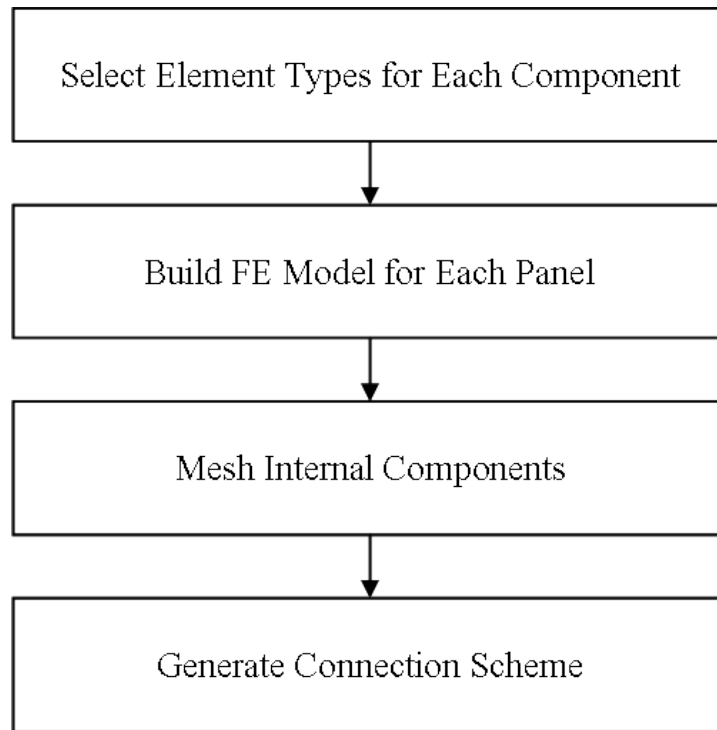
Figure 3.1: Flowchart of Step 1 of the tuning process - Generate Untuned FE Model

3.2.1 Plate Elements.   Since the primary structure of FS SEM II is comprised of panels with relatively thin thickness, bilinear plate elements are predominantly used in the FE modeling approach. There are numerous references that describe the behavior of individual FE elements, on good reference is *Cook et al.* [2002]. Each plate element in the FE model has a uniform thickness and has either three or four nodes. The shape of the bilinear quadrilateral plate elements need not be square nor line up with the model coordinate frame due to isoparametric element theory [*Cook et al.*, 2002] (though the rectangular shape of the satellite allows many elements to do just that; see Figure 3.2). Most of the SEM II internal components, represented by mass simulators, are modeled with plate elements due to their shape. For example, Figure 3.3 shows a drawing of one mass simulator which is a block of aluminum with the top interior and bottom interior hollowed out, leaving a middle plane. In only a small number of cases, solid elements are used. Solid elements are better to model items such as solid mass simulator blocks and panel stiffeners. Plate elements often produce erroneous results when subjected to shear forces. In locations where a hole in a panel structure supports a mass simulator,
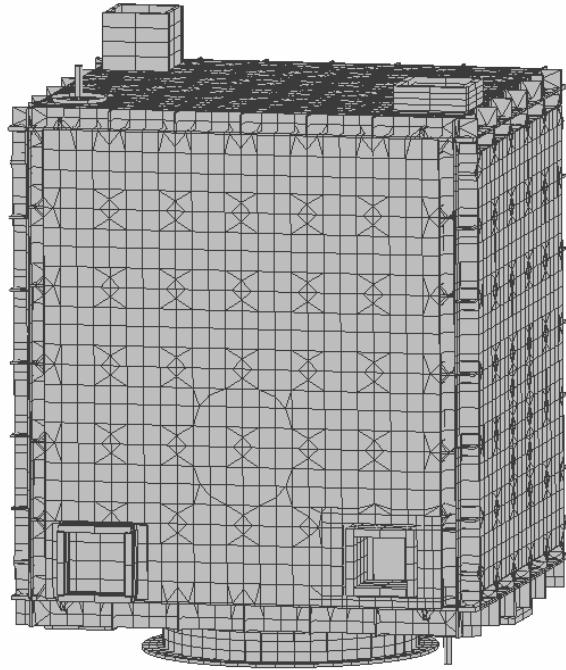
Figure 3.2:   FalconSAT-5 SEM II FE model
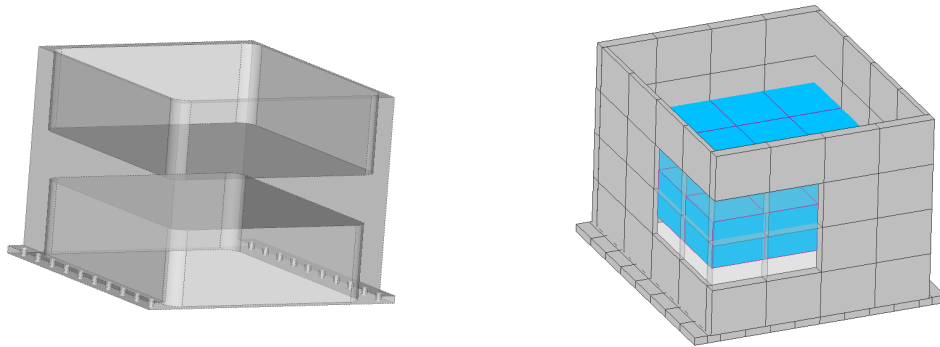
Figure 3.3:   FalconSAT-5 SEM II interior mass simulator structure (left) and plate FE model (right)

shear stress is likely to be relatively high. (See Section 3.2.2). Solid elements are used to model such features.

3.2.2   Panel Modeling.   When *Black et al.* [2008] created an FE model for the FS-5 SEM I, all panels are ribbed with four inch grids. The side and top panels of the SEM I were similar in build and are depicted in the drawing of Figure 3.4. The base
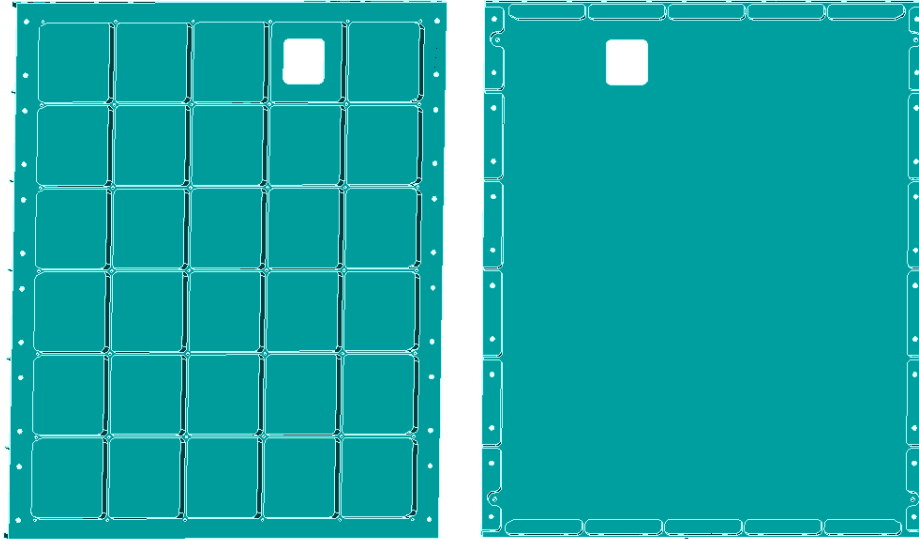
Figure 3.4:   FalconSAT-5 SEM I positive Y side panel interior (left) and exterior (right)

panel geometry of the SEM I contained stiffening around the adapter ring connection and rib edge connections as shown in Figure 3.5. Due to the significant design changes made by the SSRC, the FE models of SEM I had to be significantly modified. The most important change was adding the 32 kg Space Situational Awareness Source Module (SSASM) ion source experiment from FalconSAT-4 to the top panel of the satellite. Two ammonia tanks and a xenon tank were suspended from the interior of the top panel and the flow nozzle, fill/drain valve, and ion source secured to the exterior of the top panel. Consequently, the panels were stiffened to compensate for the additional mass. The SSRC added rib junction fillets and doubled the rib density on the top and base panel, adding significant mass and stiffness. The SEM II base panel drawings are shown in Figure 3.6. The side panels of the SEM II gained rib joint fillets and lobed fillets around the edge as shown in Figure 3.7. The predicted natural frequencies of the SEM I panel FE models from *Black et al.* [2008], do not closely match those of the SEM II (See Section
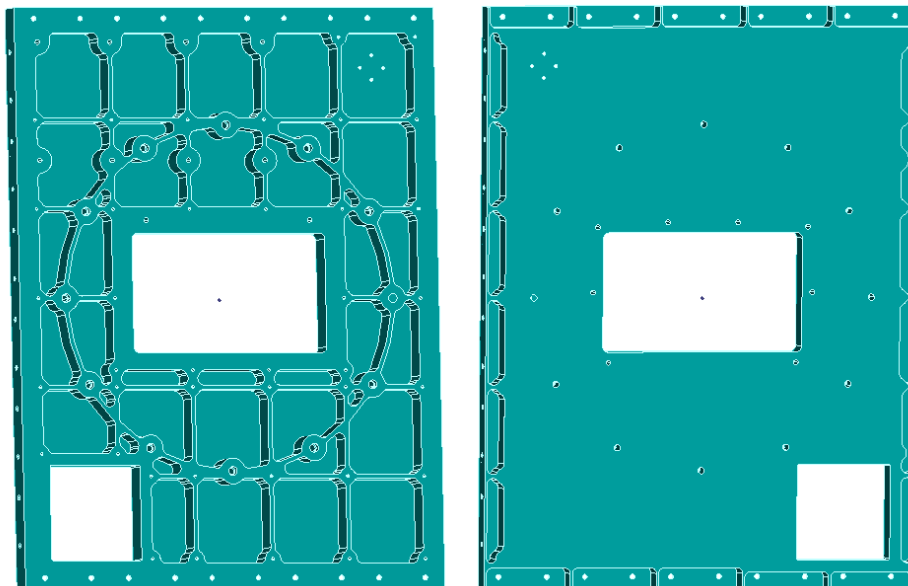
Figure 3.5:   FalconSAT-5 SEM I base panel interior (left) and exterior (right)
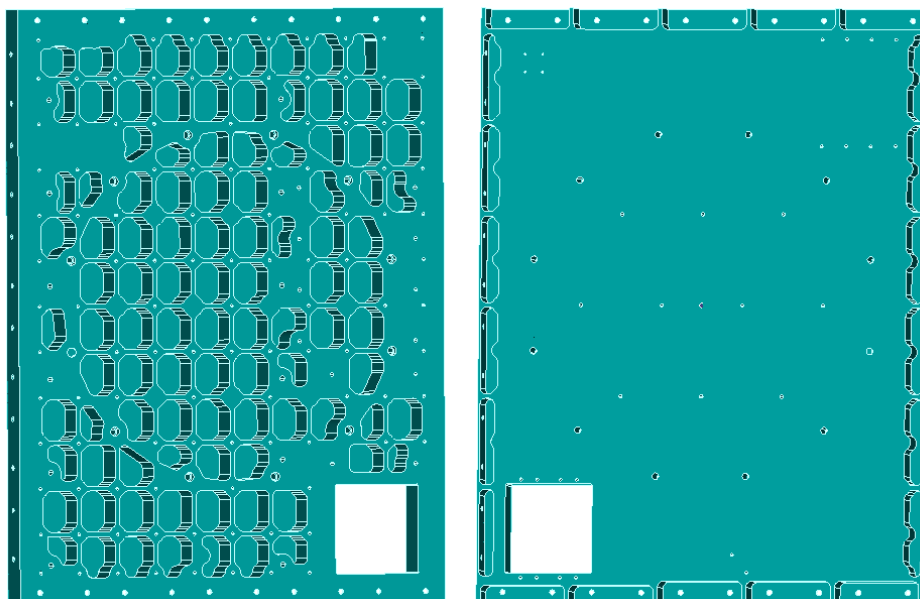
Figure 3.6:   FalconSAT-5 SEM II base panel interior (left) and exterior (right)
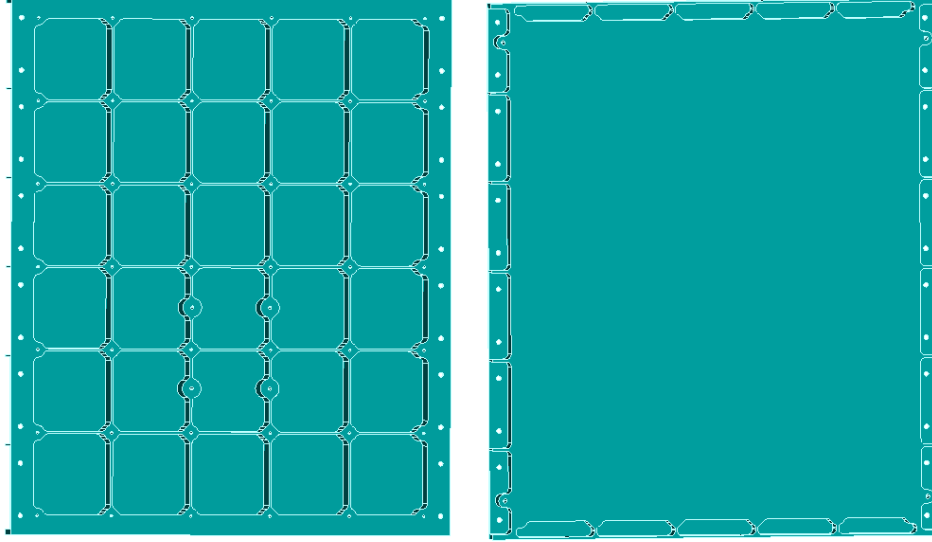
Figure 3.7: FalconSAT-5 SEM II positive Y side panel interior (left) and exterior (right)

4.1.1). Therefore, the SEM I panel FE models are modified to include plate elements representing the rib junction fillets and filled in mass blocks. The untuned FE panel models developed are accurate because the dimensions of each feature are determined from the CAD geometry files.

Discretization of elements forming the panels remained consistent with that of the SEM I model - approximately one element per square inch. Initial mesh refinement studies were conducted and further discretization or increases in interpolation order were deemed unnecessary. Figure 3.8 shows a side by side comparison of the SEM I positive X side panel FE model from *Black et al.* [2008] and the modified version for the SEM II. Also note in Figure 3.8 the difference in modeling for the WISPERS experiment hole. The SEM I model uses only plate elements for modeling the hole and has very little support around the edges. For the SEM II model, solid elements are used in order to more closely match the mass of the actual structure around the hole.

Another item of importance in generating the panel FE models is the practice of assigning materials. In Figure 3.9, material differences are shown in separate colors on the base panel model. During the tuning process, the Young's modulus of each material card is selected as a parameter in the plate tuning process. Assigning each rib of each
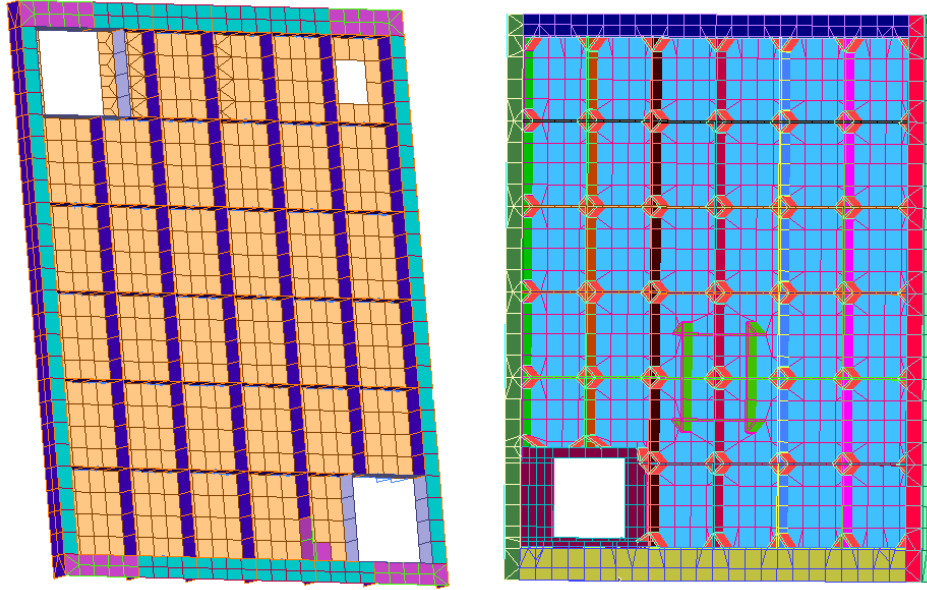
Figure 3.8:   FalconSAT-5 positive X side panel FE model, SEM I (left) and SEM II (right)

panel separate material properties results in a large number of design variables which can be tuned in the optimization process. To represent solid portions of the panels, a star pattern of plate elements is used as opposed to solid elements. More discussion on assigning material parameters is found later in Section 4.1.3.

3.2.3   Internal Component Modeling.   The panels of the SEM II make up the primary structure of the satellite. However, the internal components do add stiffness and are a significant contributor to the overall mass, which affects the dynamic behavior of the structure. One method of representing internal components is to use concentrated mass elements. Concentrated mass elements are spatially dimensionless and are usually connected to the structure with rigid links (See Figure 3.10).

In an initial untuned FE model of the FS-5 SEM II, the actual mass of several internal components were combined as concentrated mass elements. Placement of the concentrated mass within the satellite model can be such that moment of inertia properties of both model and structure are in close comparison. This method's main benefit to the analyst is ease of implementation. Concentrated mass elements are a quick way to model several components. The downfall of this approach is that internal components

43
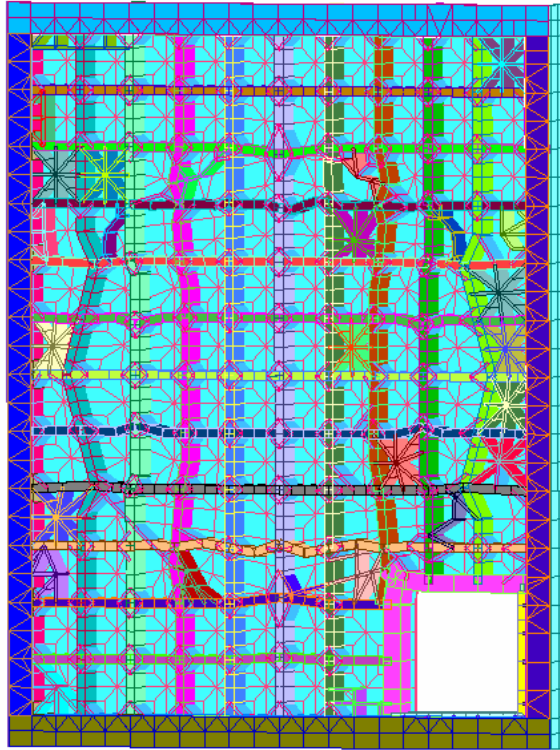
Figure 3.9:   FalconSAT-5 SEM II base panel FE model depicting assignment of material cards
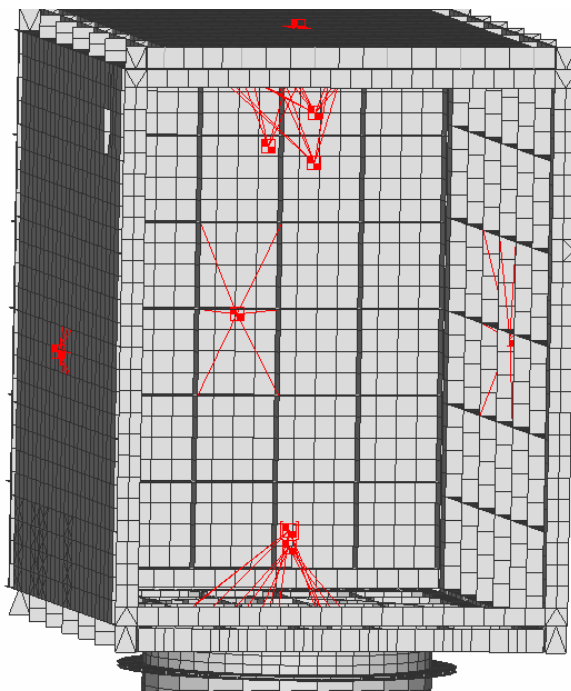
Figure 3.10:   Concentrated mass FS-5 SEM I model provided to Orbital Sciences for coupled loads analysis

not only affect mass and moment of inertia, but stiffness as well. While rigid links can simulate this stiffening for simple structures, the same cannot be accomplished effectively with complex structure such as the SEM II. The alternative to concentrated mass elements for internal components is to mesh components individually. This practice is more time-consuming, but more accurate (See Section 4.1.2). The mass of each component mesh is distributed more like it is in the real structure - making moment of inertia properties match closer. Furthermore, each component mesh may be discretized sufficiently to allow more detailed connections to panel elements. In this way, the stiffening that the internal components impart on the panels in the actual structure is also present in the model (See Figure 3.11).
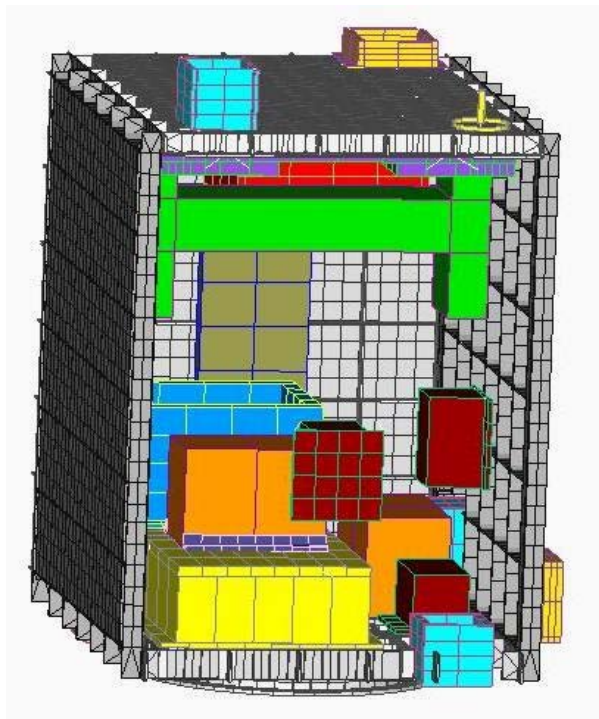
Figure 3.11:   Internal components meshed individually

3.2.4 Establish Component Connections.   Another important consideration for a researcher generating a satellite FE model is the approach taken to model connections between components. On the FS-5 SEM II, all components are bolted together. The panel contact edges are flat and approximately one inch wide. A single column of bolts connect each corner (See Figure 3.12). While it is possible to connect nodes on an
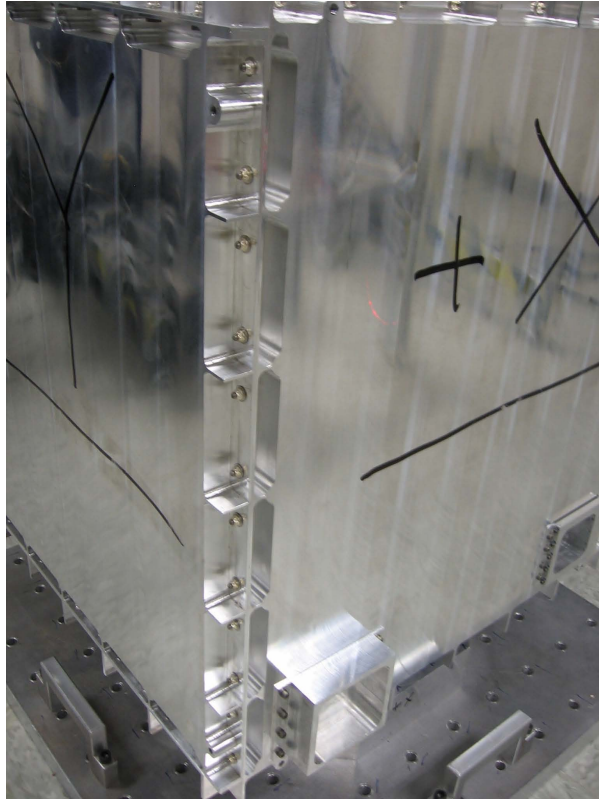
Figure 3.12:   Corner geometry for FS-5 SEM II

FE model using beam elements to simulate bolts, the faces of adjacent elements do not impinge on one another. The stiffening imparted across the face of one panel's connection surface from the perpendicular connection panel cannot accurately be modeled with a single column of beam elements connecting nodes on each panel. One approach to capture the stiffening effect of plate edges being in contact is to use 6DOF springs. 6DOF spring elements are massless springs having six degrees of freedom - three degrees of translation and three degrees of rotation. The approach taken to connect panel meshes in this research effort is to place three columns of 6DOF springs along each corner. The first column is attached down the center of the connection edge to represent the actual bolts. Then a column of springs is attached on either side of the center column giving the model the ability to account for the edge contact stiffness present in the actual structure (See Figure 3.13). 6DOF springs are used to connect the base panel to the adapter ring in three concentric circles of elements (See Figure 3.14). Each internal component mesh is connected to the panel meshes with rigid link elements. More rigid link elements for the

Figure 3.13:   6DOF spring elements connecting two panels on the FS-5 FE model

Figure 3.14:   6DOF spring elements connecting the base panel to the adapter ring on
the FS-5 FE model

FE component mesh connection are used than the number of bolts present in the actual structure in order to add the stiffness created by surface-on-surface effects (See Figure 3.15). Node-to-node connections between components add unrealistic degrees of stiffness to the model and do not account for surface-on-surface effects.
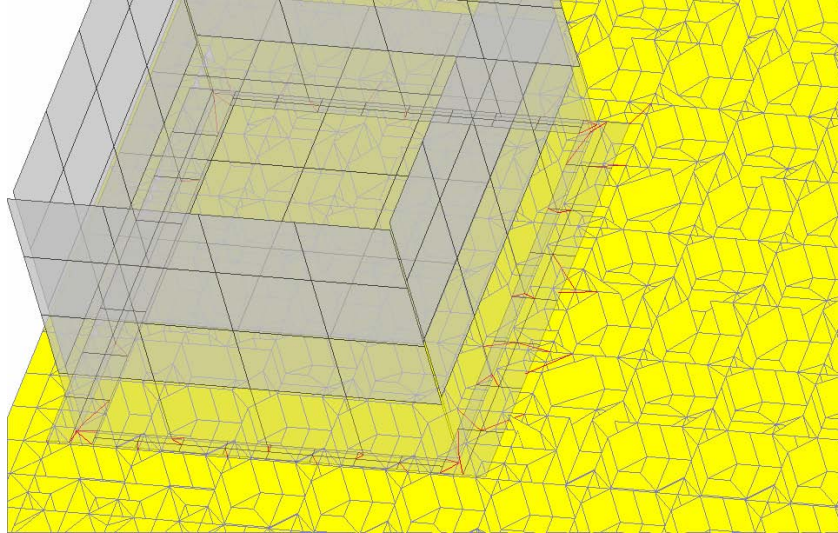
Figure 3.15:   Rigid links connecting a mass simulator to the top panel on the FS-5 FE model

3.3   *Hand Tune Mass of Every Component*

The second step in the tuning process (Figure 1.7) is hand tuning or adjusting the mass of each component of the FE model to match the measured mass. Measuring the mass of each structural component and carefully modeling the components results in very accurate mass matrices when solving the EVP for analytical modal analysis. Figure 3.16 breaks this step down into the topics to follow.

3.3.1   Major Components Identified.   In order to generate accurate mass matrices in the FE model, the major components of the satellite must be identified and weighed. Each of the four side panels, the top panel, and the base panel are each modeled and weighed. The SEM II has mass simulators inside the satellite to represent items on the flight model. Major concentrations of these internal mass simulators are bolted to the base panel and top panel (See Figure 3.17). The base panel mass simulators represent the battery stack, avionics stack, torque rods, communications electronics, and sensors.
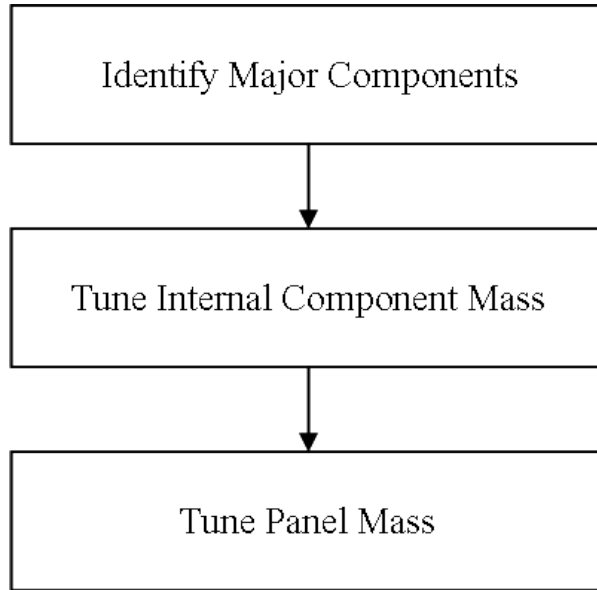
Figure 3.16:   Flowchart of Step 2 of the tuning process - Hand Tuning Mass of Major Components
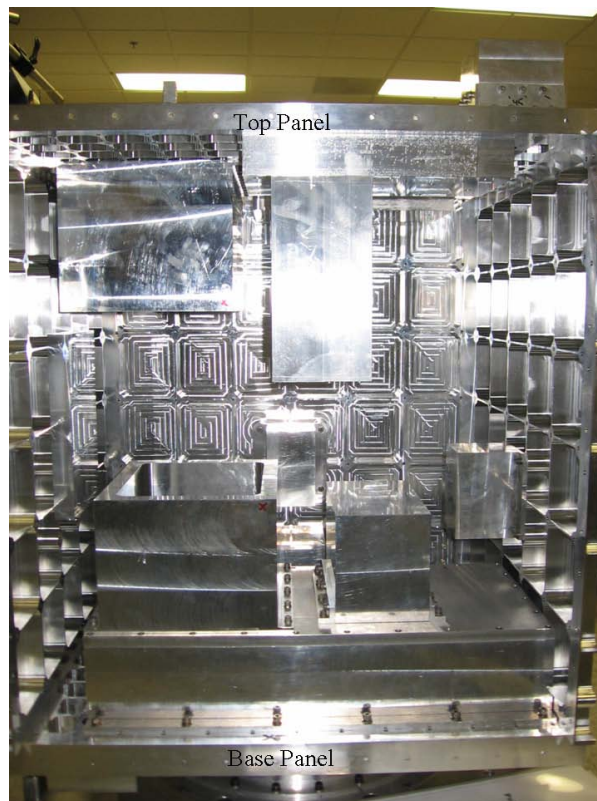
Figure 3.17:   Internal mass simulators of the SEM II

The mass simulators suspended from the top panel represent the ion source ammonia and xenon tanks. Three mass simulators are fastened on the external surface of the top panel - an s-band antenna, WISPERS sensor simulator, and IMESA sensor simulator (See Figure 3.18). Each side panel has smaller mass simulators bolted to the interior of the panel. These simulators were also weighed individually in order to tune the FE model.
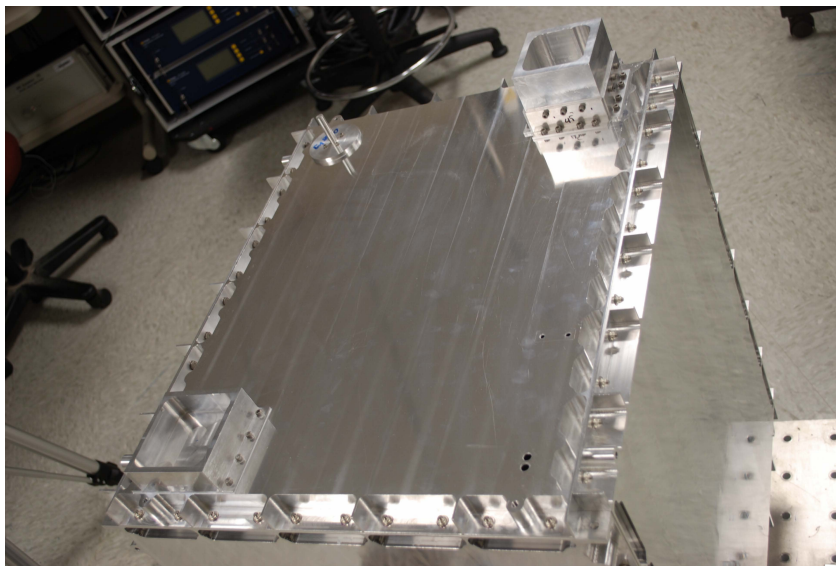
Figure 3.18:   Mass simulators on top panel exterior

3.3.2   Tune Internal Component Mass.   The components, including panels, of the SEM II FE model are meshed by generating nodes on the corresponding geometry files of the satellite structure. Meshed components then have accurate dimensions. Modeling some features on the structure, such as small fillets at the corners of hollowed-out mass simulators, is normally not necessary. In this procedure, bolt holes and bolts are also not modeled in each component or as separate components, respectively. For most cases, the approach of matching nodes to the computer aided design CAD geometry locations results in analytical mass matching very close to the actual structural component mass for the mass simulators. However, on the occasion that the extra features do add significant mass to the component and the FE mass is not within close proximity to the actual mass (typically <5% difference), an approach is needed to account for this in the component FE model mesh. The technique used here for tuning internal components' masses is

to adjust the thickness of plate elements composing the component until the FE model mass matches the structure mass. For large components such as the tank simulators suspended from the top panel (Figure 3.3), the thickness of all four sides is adjusted so there is little change to the component center of gravity. For smaller components, mass may be tuned by adjusting the thickness of fewer plate elements.

3.3.3 *Tune Panel Mass.* Tuning panel mass by hand is similar to tuning internal component mass. Discrepancies between the actual mass of the panel structure and analytical mass of the untuned FE model are caused by unmodeled features. One specific feature known to cause mass discrepancy with the FS-5 SEM II model is the junction of each rib on the interior of the panels. On the actual structure, these junctions are four fillets, one at each corner of the intersection. In the FE model, four plate elements connecting the intersected ribs in a diamond pattern represent these fillets (See Figure 3.19). This practice introduces some error in the analytical mass. In order to hand tune
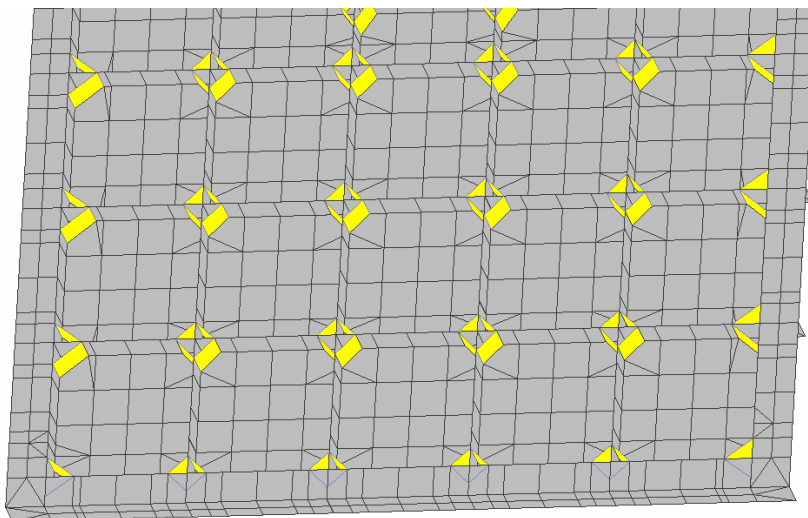
Figure 3.19:   Four plates are used to represent each rib junction on the FE model

the mass of each side panel, the thickness of these junction plates are adjusted to match the actual mass. Since all of the rib junction plates on a single panel of the FE model are assigned the same property and material cards, this adjustment is quite simple. In the case of the top and bottom panels, beside rib junction plates, mass error is also induced with the plate elements used to represent rib pockets filled-in with solid aluminum. Here,

two parameters with which to hand tune the mass of the model are available. The overall mass properties of the SEM II structure and corresponding mass of the hand-tuned FE model are summarized in Table 3.1.

Table 3.1:   FS-5 SEM II Mass

Component	Measured (kg)	Analytical (kg)	% Difference
Top Panel	7.285	7.281	0.1
Base Panel	14.040	14.108	0.5
Positive X Panel	4.950	4.946	0.1
Negative X Panel	4.535	4.521	0.3
Positive Y Panel	3.870	3.870	0.0
Negative Y Panel	3.870	3.870	0.0
Adapter Ring	2.512	2.53	0.8
Mass Simulators	114.799	112.734	1.8
Total	155.859	153.860	1.3

3.4   Measure and Tune Stiffness of Every Panel

The third step in the tuning process (Figure 1.7) is measuring and extracting modal data from each panel and tuning the corresponding panel FE models by adjusting the Young's modulus of the panel materials. This step results in a combined satellite model which has tuned stiffnesses, but untuned 6DOF connection springs. Figure 3.20 breaks this step down into the topics to follow.

3.4.1 Panel Preparation.   The first step in collecting data on a panel is to prepare it for test. A test harness which imparts the smallest amount of strain in the panel is desirable to simulate free vibration. The panel should be allowed to float freely in space. Many modal testers rest the test subjects on a bed of foam to provide this condition. In this case, allowance for multiple excitation locations in order to excite multiple modes is necessary. The first attempt to build such a harness can be seen in Figure 3.21. This harness suspends the panel vertically with springs attaching each corner of the panel to the harness. Pointed foam pads behind the panel press on rib connections in order to provide light damping and limit rigid body motion. Without this
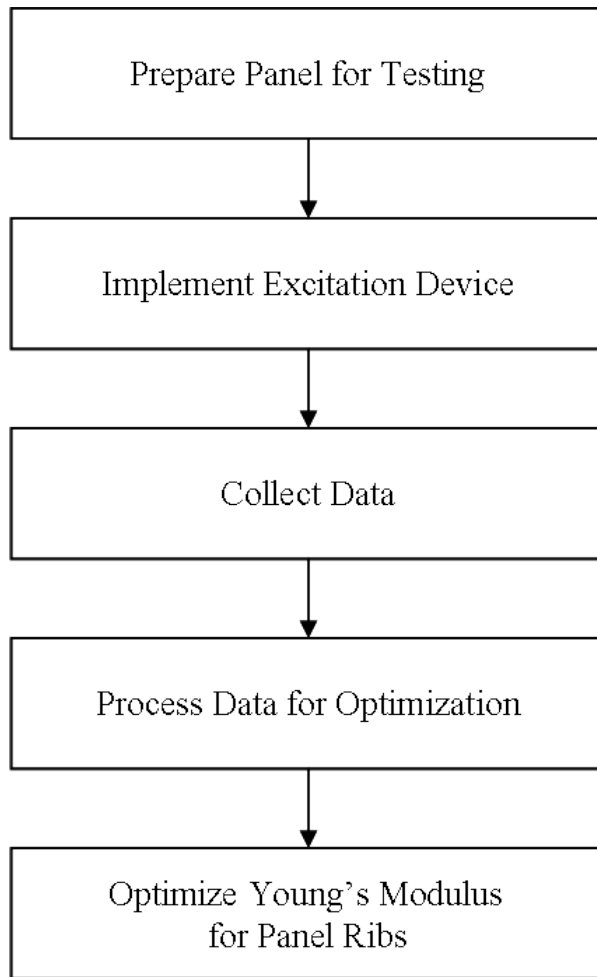
Figure 3.20:   Flowchart of Step 3 of the tuning process - Measure and Tune Stiffness of Each Main Structural Panel
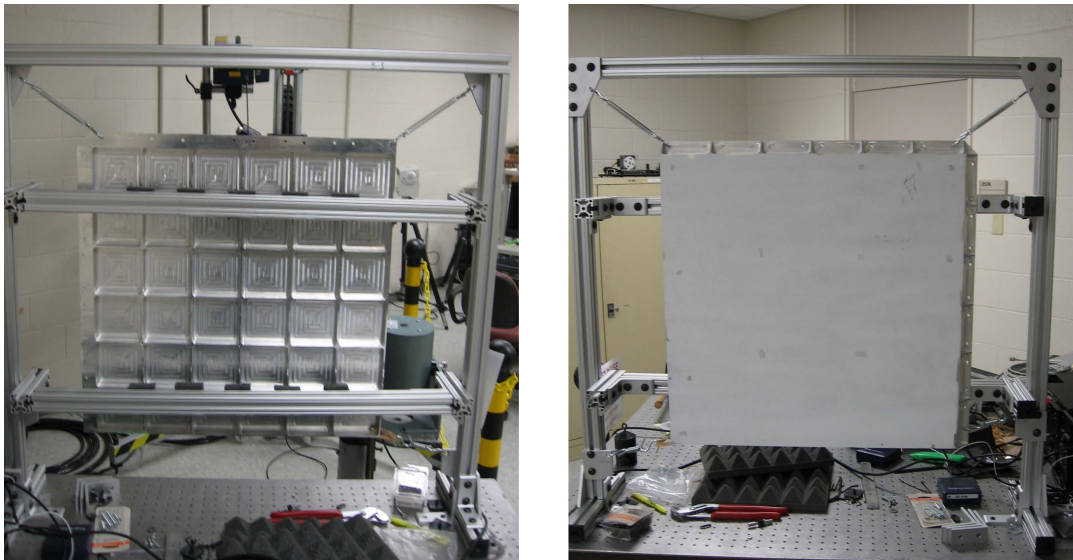
Figure 3.21:   Vertical harness for panel testing - back (left), front (right)

damping the panel vibrates for an extended period of time, inducing a long wait period between measurements while the motion comes to a rest. To characterize this vertical test stand, data on a test panel with the scanning laser vibrometer (See Section 3.4.3) is collected. Next, the test panel is removed from the harness, an accelerometer is attached to the face, and the panel is suspended with a string from one corner. A comparison of the first natural frequency of these two tests revealed a significant difference in value. Hence, the conclusion is that the springs suspending the panel in the vertical harness stiffen the structure so far as to change its dynamic properties. The vertical test harness discarded, the focus now turns to a horizontal test harness.

The horizontal test harness uses a mesh of bungee cords to suspend the panel above the floor (See Figure 3.22). The same pointed foam pads press up on the rib
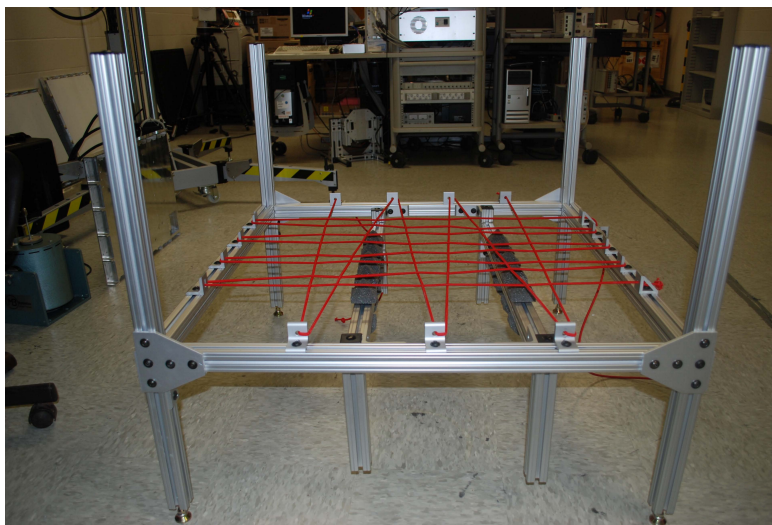
Figure 3.22:   Horizontal harness for panel testing

nodes from underneath the panel to provide light damping. The frame is adjustable in height to allow the excitation source to fit underneath. Comparisons of measured natural frequencies from the test panel revealed a much closer match in first natural frequency of the accelerometer test using this harness. Thus, this is the harness used for testing the SEM II.

Other actions required in preparing the panels for test include coating with light scattering material and coordinate frame development. Since a laser is used to measure vibrations of the panel (Section 3.4.3), a dispersive coating is applied to the shiny surface

of each panel. Without such a coating, the laser beam would reflect off the panel surface with very little of the signal returning to the detector in the vibrometer for measurement. A white spray-on powder called Spot Check suits this purpose. The powder provides diffuse scattering of the light and wipes away easily for clean-up. For a coordinate frame, one can turn to the FE model. The FE model of the panels contains nodes at approximately a one inch grid. Selecting a set of nodes on the surface of each panel, the three-dimensional coordinate set of these nodes is exported as a text file for input to the vibrometer. In order to perform alignment of the lasers, several points of known coordinates are required. For these, a precision caliper measures the two-dimensional location of selected nodes on the surface of the panel. Reflective tape and a pen point are used to mark the location of several nodes on the panel.

3.4.2 Panel Excitation. With the panel supported and prepared, the focus now shifts to the method of excitation. Many excitation devices can impart a wide variety of excitation functions. *Agilent* [2000] provides a good introduction to these options. For this research, however, an electromagnetic shaker acts like an automatic ping hammer which is programed to impart periodic impulses or impacts. Impact excitation produces an impulse in the structure which theoretically excites all frequencies, but in reality most of the energy is imparted to the lower frequencies. Impact excitation is chosen because the excitation device is not attached to the test article which could change the response of the structure. Impact excitation also provides a much better coherence than other methods. Coherence is a measure of the linear correlation between input and output or how much the response of a structure depends directly on the excitation input. The shaker is shown in Figure 3.23. An arbitrary waveform generator programed with a burst square wave function sends a signal through an amplifier to the shaker. Adjustment of pulse width, amplitude, and time between bursts is all controlled through the arbitrary waveform generator with great precision. A threaded rod, referred to as a stinger, connects the shaker's actuator to a force cell which has a flat plate at the other end as seen in Figure 3.23. Transducers inside the force cell vary an applied voltage corresponding to the impact force magnitude. Since the force cell calibration data is provided by the manufacturer, this voltage is easily converted into a force. The force
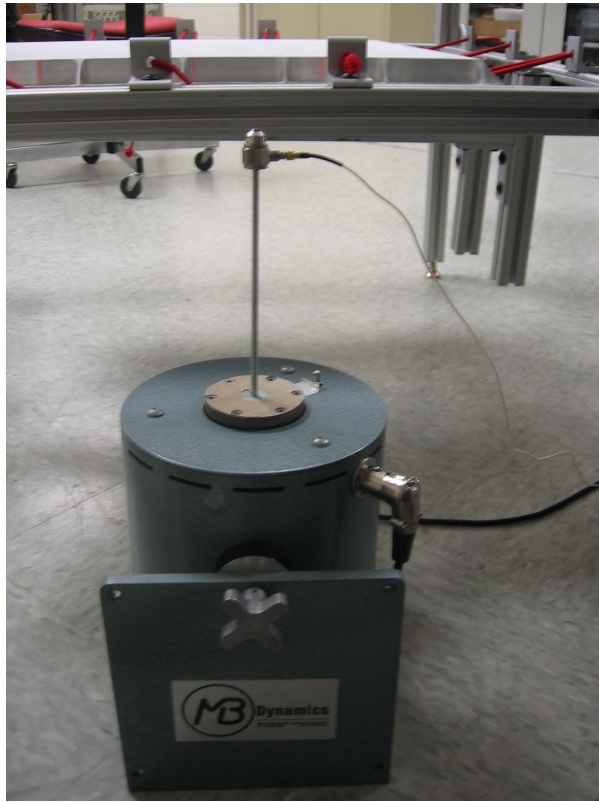
Figure 3.23:   Actuation device used to impart impact excitation

cell data is sent through a signal conditioner, which amplifies the signal, and then to the vibrometer as a reference input.

The shaker is placed underneath the test stand, oriented vertically, and adjusted so the strike plate on the force cell is directly below the desired excitation location. Choosing this desired location is a critical step in plate modal analysis. To figure out where to place the striker, the researcher can perform an eigenvalue/eigenvector analysis on the untuned FE model to aid in this decision. Displaying the eigenvectors as contour plots with total translation as the dependent variable shows the predicted mode shapes in a useful manner. Lines of very small displacement on these plots, referred to as nodal lines, show where not to place the impact hammer as exciting the structure in that location will not excite that particular mode very well (See Figure 3.24).

An important parameter to monitor on the input excitation signal is the spectral density. This is the amount of power imparted to the structure at each frequency. *Friswell and Mottershead* [1995] provides a good discussion on spectral density. For
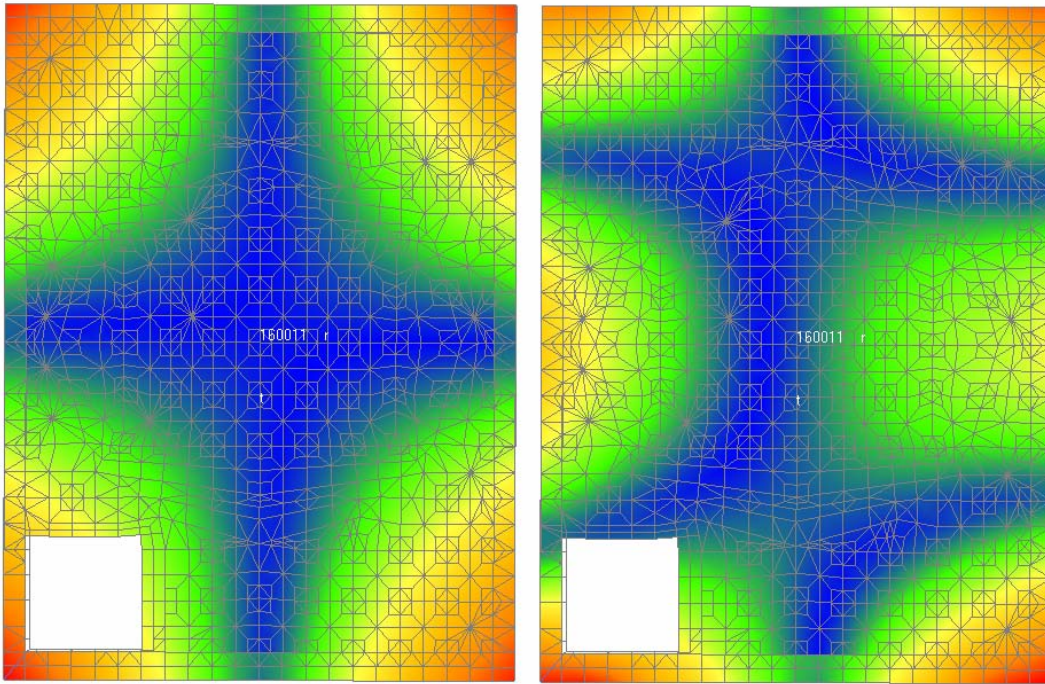
Figure 3.24:   Nodal lines on the untuned FE model contour plot are shown in blue. Red colors indicate portions of the structure which undergo a high degree of translation in that particular mode. In order to excite both of the mode shapes shown in the FE model images above, the analyst would orient the impact hammer to strike one of the top corners.

impact excitation, a typical spectral density plot is shown in Figure 3.25. A general rule of thumb is to keep the spectral density within 10dB to 20dB of the starting value throughout the frequency range of interest. If the spectral density drops off too quickly, sufficient energy will not be imparted into the structure at higher frequencies resulting in poor measurements at higher frequencies. Hardness of the impact plate connected to the force cell, magnitude and duration of the impulse from the shaker, and mass ratio of test article to impact device can all affect spectral density.
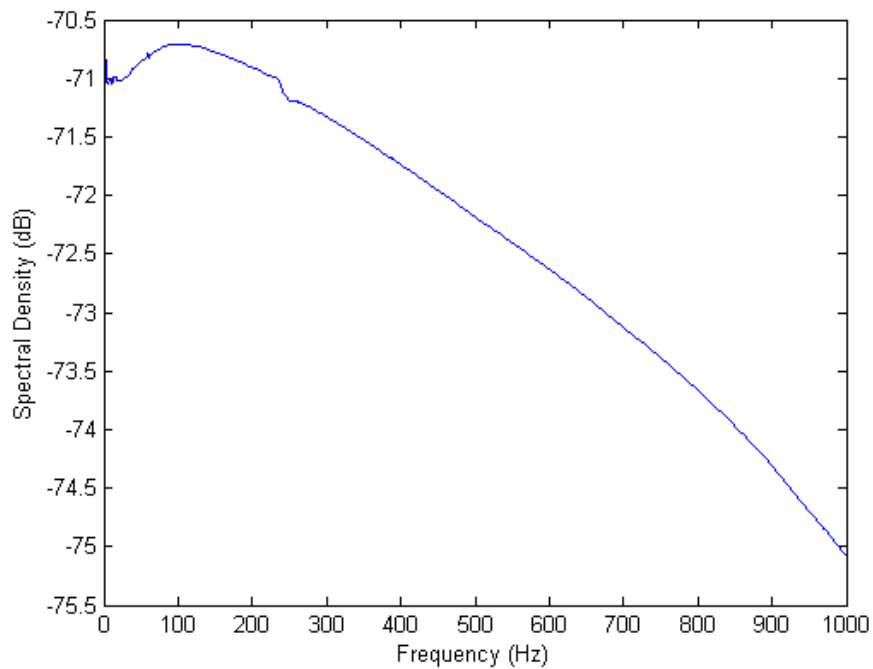
Figure 3.25: Spectral density of an impact excitation

Another important parameter to monitor during impact excitation is the time domain signal of the input. The time domain signal should look as close to a true impulse as possible. Realistically, force cells will record small voltages at the start and end of an impulse as the strike mass begins to accelerate and again as it recoils after the strike. These anomalies appear as side lobes to the main impulse in the time domain and must be minimized by adjusting the magnitude and frequency settings of the arbitrary waveform generator. Large side lobes on the time domain input signal have an adverse affect on coherence and reduce the quality of the data collected (See Figure 3.26). Minimizing side lobes is difficult in some circumstances. Adjustments which reduce side lobes can

cause the strike plate to impact the structure multiple times during one impulse if the pulse width is too wide.
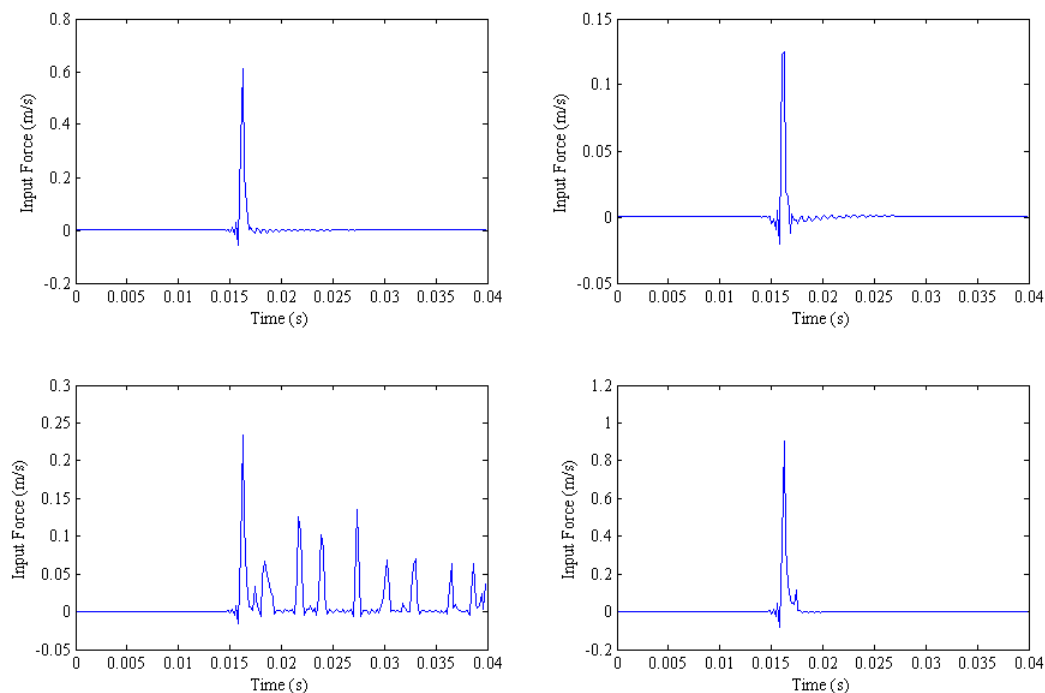
Figure 3.26: Top Left: A good impact excitation. Top Right: A squared-off peak on this impulse indicates that the hammer struck the test article too slowly. An adjustment of the arbitrary waveform generator frequency can correct this error. Bottom Left: The hammer tip strikes the test article multiple times in the same impulse indicating a magnitude and frequency adjustment is needed in the input function. Bottom Right: Side lobes on the main impulse indicate the magnitude of the impulse is too high.

3.4.3 Collect Panel Modal Data. With the panels supported and excited, data is now collected on the dynamic response over a wide range of frequencies. A grid of desired scan points approximately one inch apart is imported from the FE model to the Polytec scanning laser vibrometer for each panel surface. The three laser heads of the vibrometer focus on each point in succession and record velocity as a function of time as the panel is excited (See Figure 3.27). The excitation force for each impact is recorded as a function of time as well. Each impact of the ping hammer triggers the vibrometer to collect data for the programmed period of time and with the programed sampling rate. The sampling rate must be high enough to avoid the common anomaly of aliasing. Aliasing occurs when two signals of different frequency are sampled at such a rate as

59
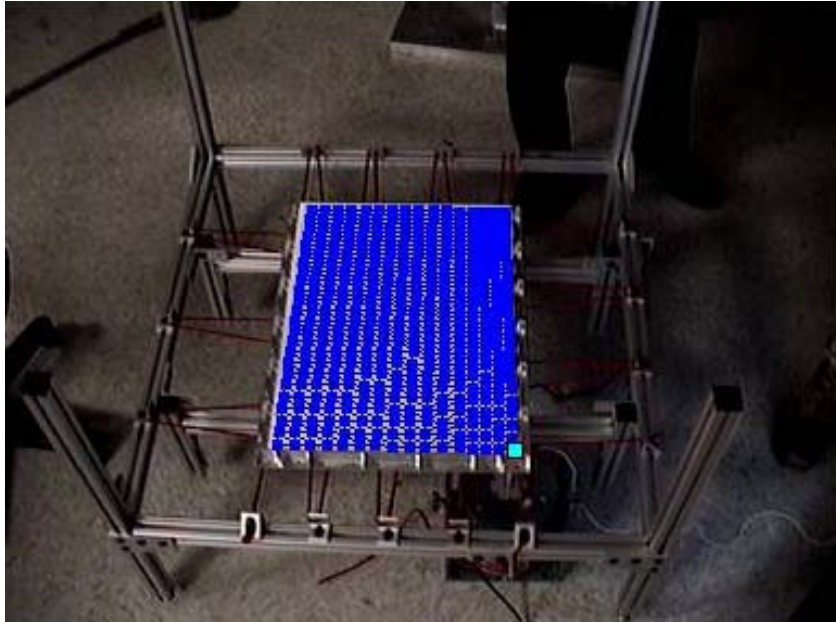
Figure 3.27:   Scan points over the surface of a panel. The Polytec vibrometer displays a color for each scanned point indicating the quality of the measurement.

they are recorded as the same signal. *Friswell and Mottershead* [1995] gives more details on this problem. The vibrometer software automatically sets the sampling rate at 2.56 times the maximum frequency of interest to prevent aliasing. In this way, each signal is characterized properly, but often at the cost of very large data sets.

Given the size of the SEM II panels, noise levels as low as those generated by people talking in the same room while data is collected can impart erroneous inputs or overrange the lasers. For this research project, all vibrometer data is collected at night while the fewest people are in the building. Signs are posted in the test area requesting low noise levels.

After a successful test, the Polytec vibrometer software applies all FFT data to the entire panel geometry, allowing animation of the ODS at any frequency. However, one is normally interested in looking at the resonant frequencies. The ODS represents the actual displacement shape of the structure at any particular frequency. If the location of the loading or magnitude of the forces on the panel change, the ODS changes. The ODS is a combination of all modes in the structure, but is normally dominated by a single mode shape in the same frequency range. The ODS contains both magnitude and phase information. Mode shapes and ODSs are erroneously interchanged quite often. In fact,

60

they are different as the mode shape does not depend on forces and loads, but on the properties of the structure [*Richardson*, 1997]. Mode shapes must be extracted from the measured data by a process such as curve fitting. It is these measured or extracted mode shapes that are used to tune FE model eigenvectors after they have been converted from complex-valued to real-valued mode shapes. Therefore, the FRF data is exported from the vibrometer software as a universal file. Only the translational displacement normal to the panel force is required for panel tuning. The H1 velocity FRF estimations are chosen along with the geometry file to pass into the next step of data processing.

3.4.4 Process Panel Modal Data for Optimization.   After collecting all of the FRF data, the next step in the process is complex mode extraction. Mode extraction software imports the FRF data from the vibrometer test. Curve fitting algorithms in this software essentially follow the process of analytically generating an FRF in Section 2.2, but in reverse. A transfer function is calculated by assigning poles and zeros to FRF corner frequencies. This transfer function fits a similar curve to the measured FRF. Natural frequencies, damping, and mode shapes are then estimated from the transfer function. These mode shapes are independent of the loads imparted on the structure during the test. Mode extraction software also animates the mode shapes by scaling the eigenvectors with a sinusoidal magnitude function in the time domain. From the animation, data points which are collected during noisy conditions, or otherwise corrupted, can easily be singled out visually. Viewing each extracted mode animation following a test allows the analyst to make a list of all 'bad nodes' for exclusion in later processing. Bad nodes are measurement locations in which the laser vibrometer recorded erroneous data. Typically, these bad points occur infrequently and are caused by an external noise source such as someone entering or leaving the test room while the laser was scanning that point. Another useful observation using animated modes is noting the quality of excitation. When a mode shape animation is very smooth then it is obvious that enough excitation energy was imparted to that mode during the test. If, however, the motion is not smooth (giving the impression of ocean water rippling) that particular mode may not have been excited to a level sufficient for accurate measurement (See Figure 3.28). Another vibrometer test with the ping hammer moved to a location that imparts more
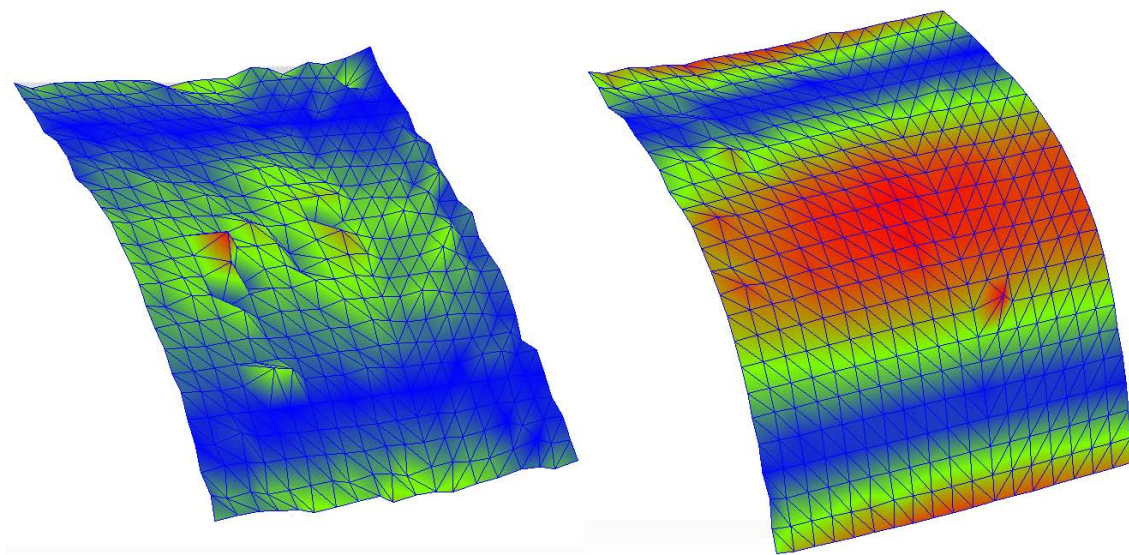
Figure 3.28:   Second bending mode (268 Hz) on the +Y panel - not well excited (left) versus well excited (right)

energy into that mode may be necessary to extract that mode properly. There is discretion involved with this step as the overall mode shape may be present, but with only a portion of the data appearing erroneous. This being the case, experimenters may choose to proceed to the next step before discarding a mode from their dataset as converting the data from the complex domain to the real domain can sometimes fix some problems with nodes being out of phase.

Once the complex-valued mode shapes have been extracted and reviewed, the next step in processing the data is to convert from the complex-valued to the real-valued domain. Since the analytical eigenvectors computed in this research are real-valued - a property of having M and K real-valued and symmetric - the optimization approach also requires the values to be real-valued. An equation developed by *Niedbal* [1984] which approximates the complex-valued mode shape matrix in the real domain is

$$\Phi_R = Re(\Phi_C) + Im(\Phi_C)[Re(\Phi_C)^T Re(\Phi_C)]^{-1} Re(\Phi_C)^T Im(\Phi_C) \tag{3.1}$$

After the modal data has been converted to the real domain, plotting the mode shapes again can reveal any DOF which were measured incorrectly. The conversion to the real-valued domain corrects some nodes which were 180 degrees out of phase with the bulk of

the data. All bad nodes remaining are removed at this point. With this set of spatially dense real-valued data, the analyst may move into the optimization step of panel tuning.

3.4.5   Panel Model Optimization.   The goal of optimization in the process of tuning FE models with experimental modal data is to adjust selected parameters in the FE model so that test results are closely approximated in a predetermined frequency range. A cost function (Equation (2.18)), is used to discern which parameter values best force the model to match the data. The optimization program used is Nastran (See *MSC.Software* [2003], and *Garmann*). Nastran uses a gradient-based optimization method to minimize the objective function. This method calculates partial derivatives of the objective function and constraints to find values of the design variables which cause the objective function to reduce at the fastest rate possible. In order to write an input file for a Nastran optimization, therefore, four basic elements must be characterized: measured values, design variables, constraints, and objective function.

Measured values, also referred to as target values, are those collected during testing. In the case of tuning panels, the target values are the real-valued modes and natural frequencies. Design variables are those parameters in the FE model that the analyst wishes to vary in order to tune the model. For panel tuning, the design variables are the Young's modulii of individual groups of ribs and major surfaces on the panel. The optimization input requires the user to link each design variable to its corresponding elements, typically through the elements' property card, in the model and also provide initial values and limits of each design variable.

In order to keep the model parameters from departing too far from the nominal values, constraints are specified in the optimization input which keep the design variables within desired bounds. Constraints also set the range for acceptable convergence. Specifically for tuning plates, the convergence constraint is an upper and lower bounds of the eigenvalues, typically input as a percentage of the measured eigenvalues. For example, a constraint of 20% would be written as

$$0.8\lambda_{iM} \leq \lambda_{iA} \leq 1.2\lambda_{iM}. \tag{3.2}$$

63

The eigenvectors must be handled with mode tracking functions built into the Nastran optimizer. Mode tracking requires a cross-orthogonality check between the mass normalized mode shapes of each design cycle via the equation

$$\Phi_i^T M_i \Phi_{i-1} = t_i \tag{3.3}$$

where i is the current design cycle and t_i is a n by n matrix. If there is no change in the mode shapes between design cycles, t_i is a diagonal matrix of ones. Changes in mode shape or mode order cause the values of the diagonal to drop below one and off diagonal terms to become non-zero. The default constraint on t_i diagonals is 0.9 but may be adjusted by the user. An important impact of this mode tracking algorithm in Nastran is that the analytical mode shapes must be in the same order as the measured when writing the optimizer input file in order to ensure corresponding mode shapes are being tuned. This is the case even if adjusting the order of the analytical mode shapes causes the eigenvalues to be out of order. The optimizer is not designed to swap mode shape order based on eigenvalues. If the analytical mode shapes are out of order, the optimizer may be able to force a small number of modes to match the measured data, but with each successive mode, tuning modes gets much harder and typically fails.

The objective functions serve several purposes. First, they link the individual measured values of eigenvectors and eigenvalues to their respective analytical values. The objective functions also link the measured value locations to the appropriate design variable locations. Second, the objective functions specify which portions of data are processed. For panel testing, a separate objective function is created for each mode. Third, the objective functions link the data to the design equation.

3.5   *Measure and Tune Full Satellite Springs and Adapter Ring Stiffness*

The fourth step in the tuning process is measuring modal data from the integrated satellite and tuning the corresponding FE model by adjusting 6DOF spring constants and Young's modulii of the adapter ring materials (See Figure 1.7 for the tuning flowchart). Data is collected using the same laser vibrometer system as displayed in Section 3.4.3.

This step results in a combined satellite FE model which is tuned to the experimental data. Figure 3.29 breaks this step down into the topics to follow.
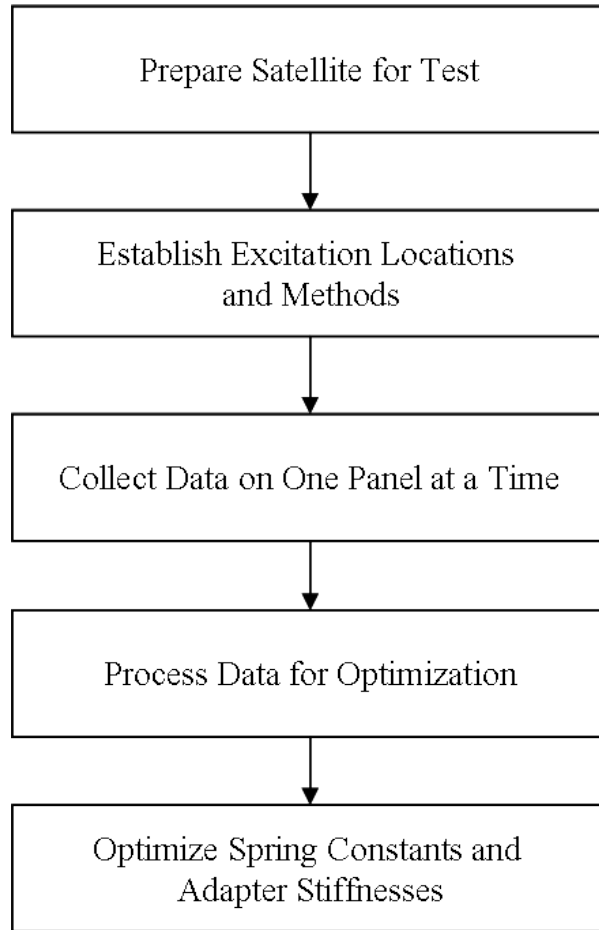
Figure 3.29:   Flowchart of Step 4 of the tuning process - Measure and Tune 6DOF Springs and Adapter Ring Stiffness for Entire Satellite

3.5.1 Test Preparation.   With each panel's vibration data collected, one other component requires measurement before the satellite is re-assembled, namely the adapter ring. Especially for the first two mode shapes, which are a rocking motion, the adapter ring plays a critical role in determining the satellite's forced response. Though not used in the optimization process, natural frequencies of the adapter ring are collected to ensure the FE model of the adapter ring is close to the measured. In order to measure modal data on the adapter ring, one surface is painted with the same light scattering powder as used on the panels. Next, a group of scan points is chosen from the FE model which forms a two-dimensional ring around the painted surface. Several of these points are

65

plotted on the adapter surface using a precision caliper and serve as known coordinates for vibrometer alignment . The adapter ring is placed on the horizontal test harness of Figure 3.22 and excited with the same automated ping hammer excitation. Laser vibrometer ODS and natural frequencies of the two-dimensional adapter ring representation allow the stiffness of the FE adapter ring model to be adjusted manually (See Figure 3.30).
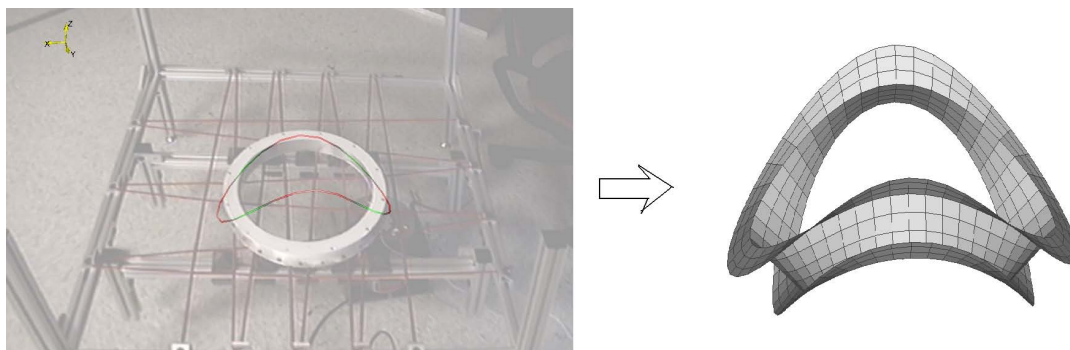
Figure 3.30:   Characterization of the adapter ring to manually tune the FE model

Following adapter ring characterization, the satellite is re-assembled. Care is taken during this task to leave the light scattering paint on the panels intact, saving tremendous time in moving the entire satellite to a painting facility and back before test. Bolting the satellite stand plate to the floor is an absolute necessity in order to provide rigid boundary conditions. Accelerometer tests show coupling occurs between the floor and the stand plate and significantly affects the vibration response.

The final preparation action for testing the satellite is generating a set of scan points. Though most of the same set of coordinates are used as in panel testing, the coordinate set for the integrated satellite requires modification. Replacing the mass simulators on the exterior of the panels causes some of the scan points to be shielded during test. Each panel is still tested separately during this integrated test, however, not every laser can reach all of the original coordinate locations. A new group of coordinates must be established from the FE model with holes around each external mass simulator. The tester must determine which measurement points are not obstructed with all lasers by trial and error.

3.5.2 Satellite Excitation. The same electromagnetic shaker that is used in panel testing provides excitation for the integrated satellite. Options include attaching the shaker to the satellite and shaking with white noise, or using the arbitrary waveform generator to create an automated ping hammer as done for panel testing. To characterize both options, a preliminary vibration test is performed with accelerometers and a hand-held ping hammer. The hand-held ping hammer, with a force cell embedded in the tip to measure the force of the impact, may excite the structure from any external location in almost any direction. Natural frequencies from measurements on all four side panels and the top panel are collected using these instruments in order to establish a baseline characterization. Now the decision of excitation methods for the full vibrometer test becomes one of accuracy and precision.

Tests showed that while directly attaching the shaker to the satellite puts more energy into the structure without adding enough mass to change the results, the data collected with the vibrometer has unacceptably low coherence. Using the shaker with a waveform generator to ping the satellite transfers less energy into the structure but significantly improves coherence. With the lower level of input energy, the location of the ping hammer strike is an important consideration. In order to excite the greatest number of modes using this technique, striking a corner at a 45° angle proves the best practice. This method of excitation - electromagnetic shaker programmed to burst with an impulse from an arbitrary waveform generator, striking the corner of the satellite at a 45° angle yields the best results in terms of coherence, excitation of low frequency modes, and modal extraction (See Figure 3.31). To create a strike location, a bolt is attached to the corner of the satellite. The bolt has a threaded rod bent at the 45 degree angle welded to the head. An inert force cell is screwed onto the rod with a flat strike surface screwed into the other end, creating a strike surface. As with panel testing, spectral density and the time domain signal of the input impulse are a concern during full satellite testing.

3.5.3 Satellite Collection Procedures. The process of collecting laser vibrometer data on the full satellite is very similar to the collection on the individual panels (See
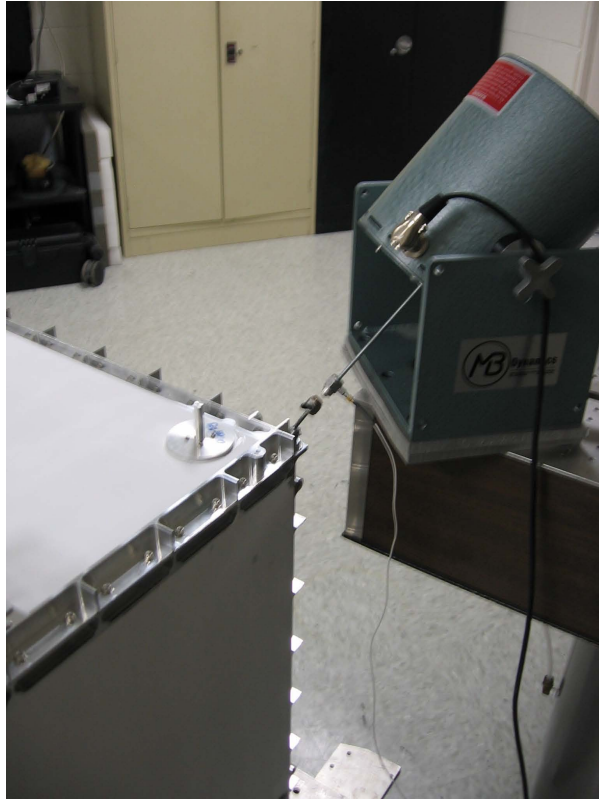
Figure 3.31:   Full satellite excitation

Section 3.4.3). Aliasing and leakage are issues which can be remedied with sampling rate and window functions. In this case, the same excitation method, same sampling rate, and an exponential window function are applied to the input signal. Unlike the panel data, three translational velocities are measured at each measurement point resulting in three FRFs for each measurement point.

Noise and disturbances in the test area are still a concern. Factors such as the full satellite being more massive than the panels and the fact that it is bolted to the floor reduce the effect of external noise on data collection. However, the sensitivity setting of the lasers is higher for testing the full satellite than it is for the panels because the full satellite displaces less than the panels. As a result, testing at night is still required to minimize signal perturbations. Since testing is limited to nights only, the number of averages per scan point is set to a value which will allow the test to finish before start of business the following day.

To ensure uniform measurements, each scan is performed on a single panel at a time (See Figure 3.32). Previous tests on the SEM I proved that taking data on multiple
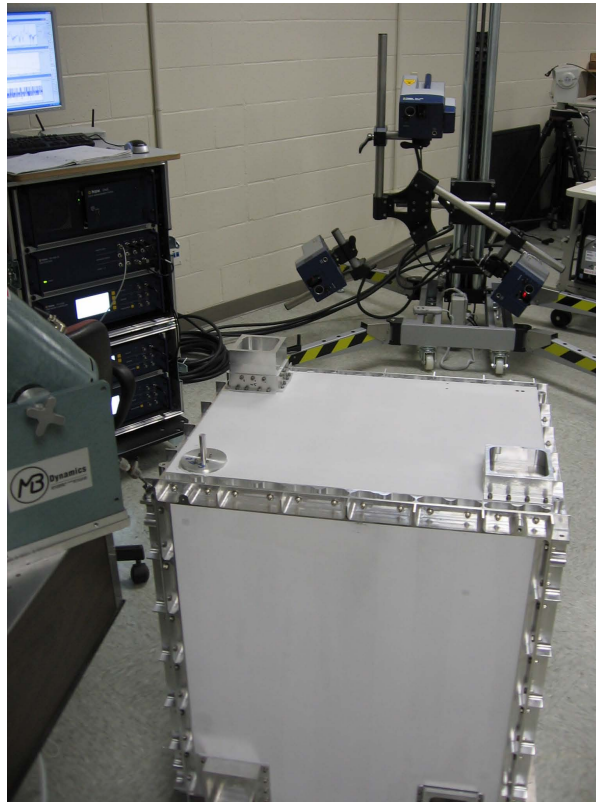
Figure 3.32:   Full satellite vibrometer test

panels at the same time causes data points to fall outside the scanning coverage or swath width area of one or several vibrometer heads. A best practice is to keep all scan points within 10 to 12 degrees of the field of vision for each head. In order to meet this restriction with the side panels, only one panel is tested at a time with the heads positioned directly facing the panel as shown in Figure 3.32. Meeting the swath width restrictions for the top panel is more difficult as the height of the tripod system limits the degree to which the heads may be extended above the top panel. Thus, the vibrometer heads are raised to the highest level and angled over the top panel to allow the best possible angle (See Figure 3.33). More scan points on the top panel are invalidated due to shielding from mass simulators than on the side panels due to this physicality as well.

Once all five panels have been tested, the FRF data must be prepared for export. The vibrometer software contains a function to stitch separate scans together into a
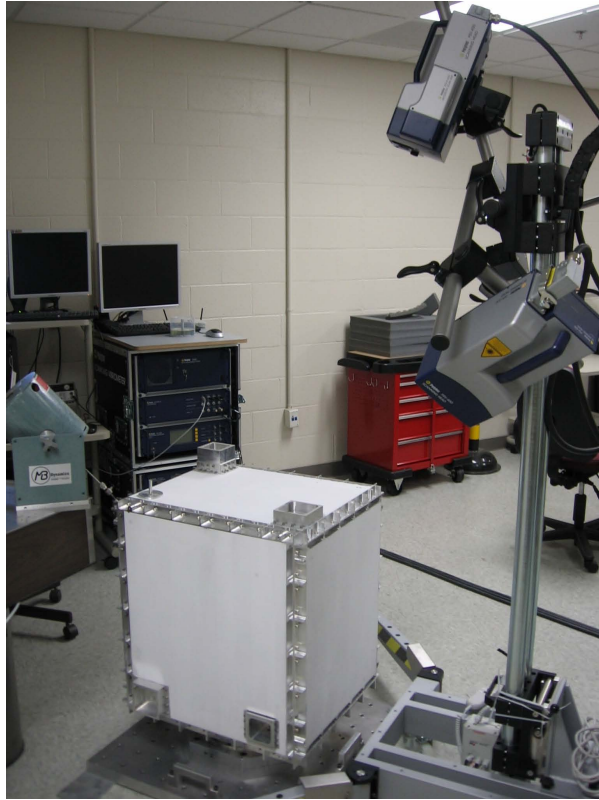
Figure 3.33:   Top panel vibrometer test configuration

single combined universal file following completion of the tests. When selecting data to export, the $H1$ FRF estimates for velocity are again selected, but this time all three degrees of freedom are required in the next post-processing step.

3.5.4   Process Satellite Data for Optimization.   Following data collection, the modal data must be extracted as described in Section 3.4.4, using curve fitting algorithms. When viewing extracted complex-valued mode shapes, any poorly measured nodes are noted. Since the relative input force to structure mass ratio is lower for the full satellite than for the individual panels as mentioned above, some panels may have a lower measured displacement in some modes than others. An example is shown in Figure 3.34. Witnessing a single panel with the 'ocean water' shaped complex mode shape does not necessarily mean the test is invalid when analyzing the full satellite. Converting the data to the real domain as described in Section 3.4.4 can correct phase problems. The suspect panel may simply have a low degree of deflection in that particular mode as compared to that of the other panels. Conversion to the real domain may cause the
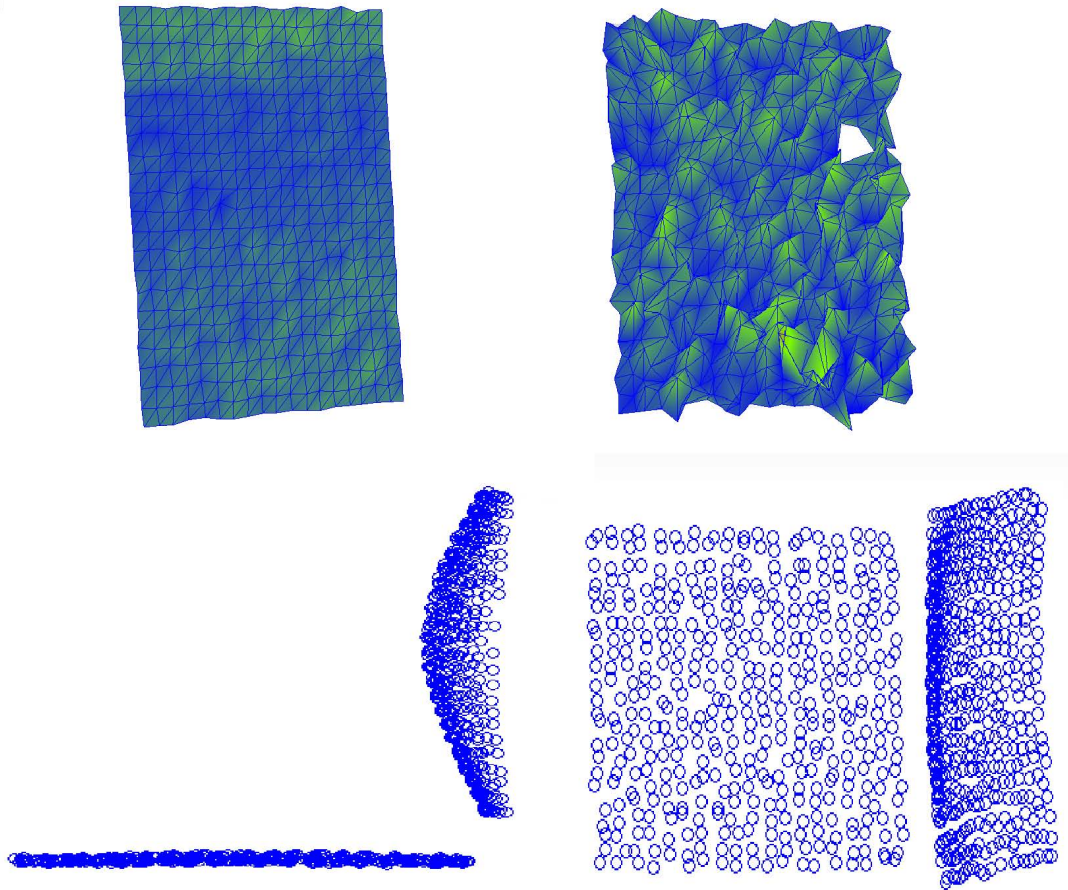
Figure 3.34: The positive Y panel has little deflection in the first axial complex-valued mode shape of the full satellite (top left). The negative X panel has a very suspect looking complex-valued first axial mode shape (top right). After converting the data to the real domain, the negative X panel has a clean shape and happens to displace much more than the positive Y panel for this mode. The real-valued first axial mode shape for these two panels is shown in top view (bottom left) and corner view(bottom right).

panel to exhibit a degree of ordered motion when the real-valued mode shape is animated as was the case for the negative X panel in Figure 3.34. All measured real-valued modes are plotted for such inspection.

Once all measured modes have been extracted, converted to be real-valued, and inspected for bad nodes, the next step in processing the data for optimization is to verify that the FE model analytical mode shapes match somewhat closely with the measured data. To accomplish this comparison, the FE model developed in Section 3.2 must be updated with the stiffness values from the panel panel optimization. If, upon entering the optimized stiffnesses and running an eigenvalue analysis, the natural frequencies of the FE model differ greatly from the measured values, the 6DOF spring constants may be hand-tuned to get a closer match between the first few predicted eigenvalues and the corresponding measured natural frequencies. While adjusting hundreds of spring constants by hand is certainly not recommended, all 6DOF springs are separated into two groups for this step: corner springs and adapter ring springs. Using trial and error with a data manipulation code to set all corner springs to the same value and all adapter ring springs to the same value, the model is manually tuned so that the first few analytical natural frequencies match the measured values. Now, with the model manually tuned, the analytical mode shapes may be compared with measured mode shapes to ensure that the order matches before starting the optimization.

3.5.5 Satellite Model Optimization. The process of optimizing the full satellite FE model is very similar to that of the panels. With full satellite optimization, the design variables are the 6DOF spring constants and adapter ring stiffnesses. The same cost function, Equation (2.18), provides the framework for the minimization. A major difference, however, is in the objective function. Nastran has a character limit for any component of the design equation of 32,000 characters. Due to the large amount of data collected for the full satellite, this limit is broken quite easily. A solution is to reduce the amount of data in the objective functions with two modifications to the input file. First, the number of objective functions is modified. Instead of having a different objective function for each mode, the data is further parsed by degree of freedom. Now there is a

72

separate objective function for each mode and each degree of freedom. The new adjusted
objective function is

$$J = \sqrt{\sum_{i=1}^{p} J_i^2}$$
(3.4)

where

$$J_i = a_i[1 - \frac{\lambda_{iA}}{\lambda_{iM}}]^2 + \sum_{k=1}^{3}\sum_{j=1}^{r} b_i[1 - |\frac{\phi_{((j-1)3+k)iA}}{\phi_{((j-1)3+k)iM}\phi_N}|]^2.$$
(3.5)

Here J_i is the cost function for the ith desired mode, a_i and b_i are weighting factors, and
λ_{iA} and λ_{iM} are analytical and measured natural frequencies, respectively. The number
of measurement locations is r. The measured real-valued mode shapes $\bar{\phi}_M$ are max
normalized after extraction by dividing every term in each mode by the largest DOF.
The analytical eigenvectors must be normalized by the value ϕ_N at the same DOF.
Normalization is achieved by dividing every term of $\bar{\phi}_N$ by the scalar ϕ_N. The objective
function, even parsed, at this point still exceeds Nastran's character limitation.

Second, the overall dataset of measured nodes is reduced by two thirds. The data
points kept are chosen pseudo-randomly so that each face is reduced by approximately
the same amount (See Figure 3.35). With this second reduction in data points each
objective function is kept below the 32,000 character limit.
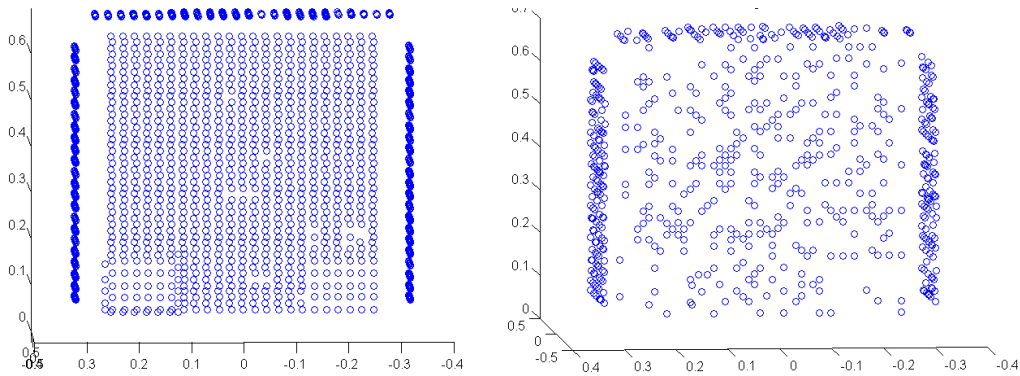
Figure 3.35:   Data reduction for optimization - $\frac{2}{3}$ of the points are removed

The end result of full satellite optimization is a tuned FE model. Natural frequen-
cies and mode shapes predicted by the model match those of the measured data up to the
degree achievable as determined by the constraints. Chapter 4 discusses specific results.

IV. Results and Discussion

T HIS chapter follows the flowchart, Figure 1.7, to explain results for each major step in the tuning process. First, a discussion on the decisions and results arrived at when generating the untuned FE model is given. Next, the results of measuring and tuning individual panels is presented. Finally, the results of measuring and tuning the full satellite are shown.

4.1   Untuned Finite Element Model Conclusions

The first step in the tuning process is generating an untuned FE model. Results for this step include examples of the stiffness effects due to the shift from SEM I geometry to SEM II geometry. Also, comparative results between the concentrated versus distributed mass approaches for the internal components are shown to portray the effect of mass modeling on the overall FE model stiffness. Next, a discussion is given on the practice of modifying the FE model panels based on measured results. Finally, specifications on the final untuned FE model are presented.

4.1.1   SEM II Modification Results.   When the SSRC modified FS-5 to include the FS-4 payloads, the major structural components gained more mass and significantly increased stiffness (See Section 3.2.2). Therefore, the predicted natural frequencies for the SEM II components are higher than those of the SEM I. Modifications are made to the SEM I FE model built by *Black et al.* [2008] to include the increased rib density on the top and base panel models, rib intersection fillets on side panels, and additional solid mass where necessary to support new components. Each of these modifications primarily increased stiffness to the structure. Analytical natural frequencies predicted with the SEM I and SEM II FE models for the top panel and positive X panel are shown in Table 4.1. Note that the first bending mode for the SEM II top panel resonates at more than double the natural frequency than that of the SEM I. The first bending mode for the positive X panel is also the most affected from the geometry modifications. Since the full satellite response is dominated by lower frequency modes, these changes to the geometry of the panels cause significant changes to the overall satellite response.

Table 4.1: SEM I versus SEM II Predicted Natural Frequencies

Component	Bending Mode Number	SEM I (Hz)	SEM II (Hz)	% Difference
Top Panel	1	32.0	80.3	151
	2	265	281	6.04
	3	323	343	6.19
	4	361	425	17.7
	5	462	486	5.19
	6	634	714	12.6
	7	659	755	14.6
	8	774	840	8.53
Positive X Panel	1	34.0	41.1	20.9
	2	210	219	4.29
	3	247	263	6.48
	4	259	277	6.95
	5	304	329	8.22
	6	478	508	6.28
	7	529	556	5.10
	8	588	641	9.01

4.1.2 Concentrated versus Distributed Mass Components. The next consideration when generating the untuned FE model is how to model internal components. In Section 3.2.3, the differences between using concentrated mass elements and modeling internal components individually was discussed. To illustrate the difference in predicted stiffness using these two approaches, a comparison of SEM I natural frequencies for the full satellite is shown in Table 4.2. The largest change in natural frequency between these two modeling approaches occurs on the third mode which is axial 'pogo'. Where the first two modes are rocking motions, the third mode involves the full satellite moving up and down harmonically in the Z direction with individual panels flexing in a 'breathing' motion. Attaching concentrated mass elements to single panels with rigid link elements in order to simulate internal components does little to stiffen the panels. On the other hand, meshing individual components and attaching them to the panels at multiple location does stiffen the panels.

4.1.3 Post-Test FEM Modifications. Following laser vibrometer testing, a visual comparison of animated complex-valued extracted mode shapes with animated FE

Table 4.2: SEM I Full Satellite Natural Frequencies Concentrated Versus Distributed Internal Components

Mode Number	Concentrated Mass (Hz)	Distributed Mass (Hz)	% Difference
1	33.7	42.9	27.3
2	35.7	44.2	23.8
3	50.5	121	140
4	73.0	137	87.7
5	117	156	33.3
6	129	172	33.3
7	134	195	45.5
8	146	206	41.1

model eigenvectors shows that the side panel models are in close agreement. The natural frequencies of each mode shape of the side panels are not in close agreement by a noticeable percentage, but the overall mode shapes match quite closely in the range of interest (See Section 4.2.3). The same is not true for the top and base panel, however. The original untuned FE models for the base panel and top panel predict eigenvectors which match the measured mode shapes closely for only the first five modes of each panel. Beyond this set, agreement between the measured and predicted mode shapes begins to diverge. Attempting to tune the base and top panel FE models for these divergent modes results in the optimization code suffering a mode tracking failure. The analytical eigenvectors do not meet the default 90% cross-orthogonality check limit. A solution to this problem is to adjust the FE models of the panels by hand using rigid link elements.

To illustrate this rigid link element approach, the case of the top panel is discussed. During the first attempt to tune the top panel, two problems arose. First, the predicted first bending mode's natural frequency for the top panel from the original untuned model is 80 Hz. The measured natural frequency for this mode is 104 Hz, a 30% difference. Second, the sixth analytical mode shape is noticeably different from the corresponding measured shape (See Figure 4.1). Attempts at tuning the top panel FE model for this mode and any modes beyond the sixth result in a mode tracking failure. In order to adjust the top panel untuned FE model to predict eigenpairs closer to the measured data, rigid link elements are added. First the natural frequency of the analytical first
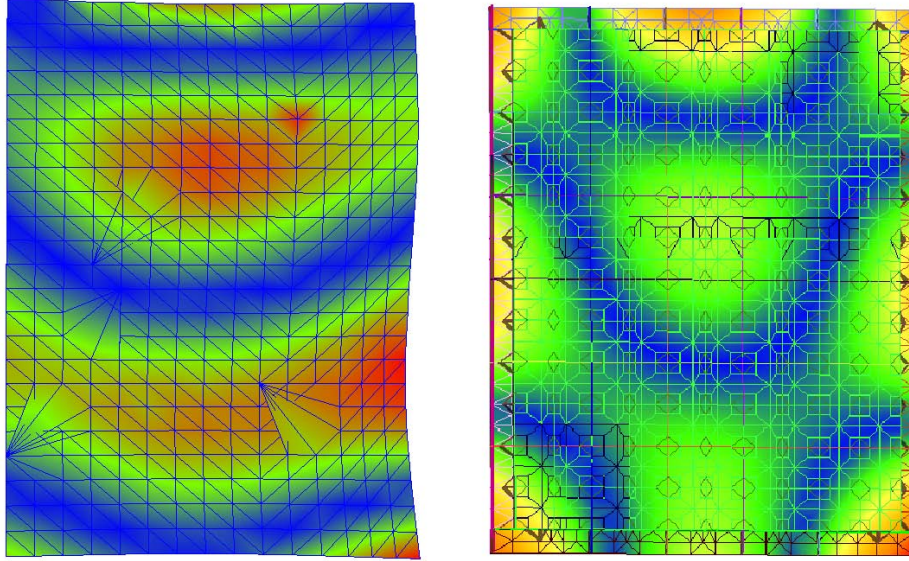
Figure 4.1:   Top panel measured sixth bending mode shape (left) and original untuned FE mode predicted sixth mode shape (right)

bending mode needs to be increased. Therefore, rigid link elements are added in an 'X' pattern diagonally from corner to corner on the interior face of the base FE model. To address the second problem of the divergent sixth analytical mode shape, rigid link elements are added horizontally near the top and bottom nodal lines in order to flatten them out. With these rigid elements added to the untuned FE model, the predicted mode shape is closer to the measured (See Figure 4.2). Rigid link elements should be used sparingly, and only in situations where the analytical mode shape is relatively close to the measured.

Another approach to potentially improve tuning results is to increase the number of design variables. For panel testing, this means increasing the number of material cards for each panel. Each material card stores the modulus of elasticity for the elements assigned to that card. In the original untuned FE model, a separate material card is assigned to each rib of each panel. However, since the original top panel FE model does not tune past the fifth mode, the number of material cards is doubled to two per rib by assigning a separate material card to each half rib. With the rigid link elements added as discussed above and the material cards doubled, tuning the adjusted FE model of the top panel allows convergence through the sixth mode.
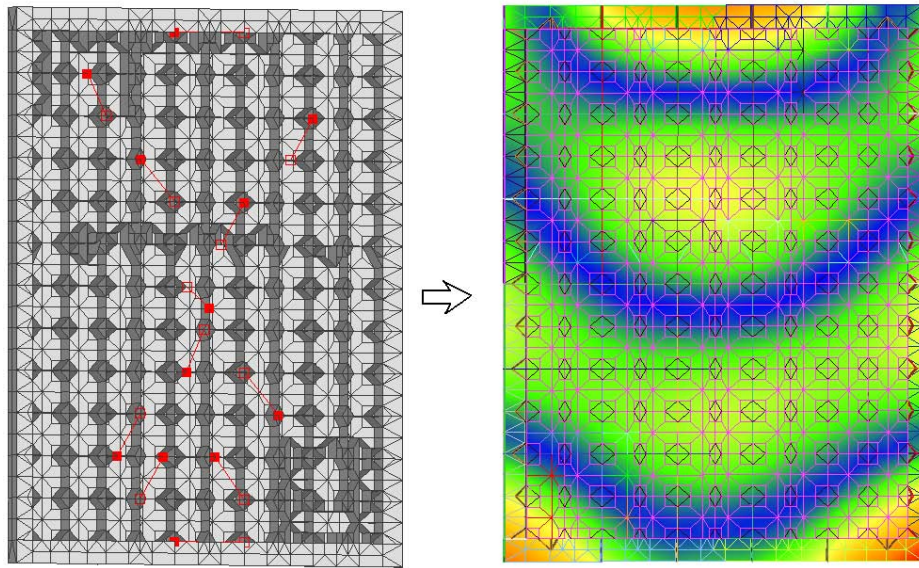
Figure 4.2:   Adding rigid link elements to the interior face of the top panel FE model in a pattern as shown on the left results in an a predicted natural frequency of 100 Hz for the first bending mode. This is much closer to the measured value of 104 Hz. The other affect of adding the rigid link elements is that the predicted mode shape for the sixth mode, shown on the right, is much closer to the measured shape.

Similarly, the number of design variables for tuning the full satellite can be increased by adding more property cards for the 6DOF spring elements. In the first version of the SEM II FE model, each corner, formed by adjacent panels, was attached with three rows of 6DOF spring elements running the entire length of the corner as shown in Figure 3.13. A single property card was assigned to each row of spring elements meaning each row must have the same stiffness constants. Also, the base panel was attached to the adapter ring with three concentric circles of 6DOF spring elements, each of which had a single property card (See Figure 3.14). After measurements were collected with the laser vibrometer the property cards for corner spring elements of the untuned FE model were doubled, giving each row two sets of stiffness constants. The adapter ring spring element property cards were quadrupled, giving four sets of stiffness constants per concentric circle.

4.1.4   Untuned FE Model Specifications.   The final untuned FE model has a total of 19,733 elements and 14,521 nodes. The primary material type in the model is aluminum 6061-T651 with the default mass density of 0.0975 lbf·s^2/in^4, Poisson's

78

ratio of 0.33, and reference temperature of 70 °F. The adapter ring of the FE model is constrained to an arbitrarily large concentrated mass element using rigid link elements. Specific numbers of properties, materials, and elements are displayed in Table 4.3. Of

Table 4.3:   Untuned FE Model Specifications

Parameter	Number
Elements	
—Bilinear Plate	17893
—Solid	146
—Beam	35
—6DOF Spring	958
—Rigid Link	700
—Concentrated Mass	1
Property Cards	374
Material Cards	254

the 254 material cards, 240 are assigned to the satellite panel elements. Specific numbers of tuning design variables (modulii of elasticity) for the panels are as follows

- Positive X Panel - 25 material cards

- Negative X Panel - 23 material cards

- Positive Y Panel - 23 material cards

- Negative Y Panel - 23 material cards

- Top Panel - 80 material cards

- Base Panel - 66 material cards

For tuning the full satellite, the number of design variables is equal to six times the number of 6DOF spring element property cards - 576, plus the number of material cards in the adapter ring - 12. Therefore, the full satellite FE model has 588 total design variables.

4.2   Panels Measured and Tuned

The results for the second step of the overall process - hand tuning the mass of major components are found in Section 3.3. In this section, results of the third step -

measuring and tuning the stiffness of each main structural panel are discussed. First, a characterization of using the automated ping hammer is discussed. Next, trends in minimizing the objective functions for panel tuning are shown. Trends in selected modulii of elasticity over each design cycle of the optimization follow. Next, tuning results of eigenvalues and eigenvectors for the base panel are shown. Finally, a summary table with the untuned, measured, and tuned eigenvalues for all panels is displayed.

4.2.1 Panel Excitation Results. Excitation locations for panel testing were determined by looking at nodal lines on the untuned FE model. For some panels, every mode of interest was sufficiently excited with a single ping location. Other modes of interest required multiple tests with the ping hammer moved in between. The number of tests required for each panel is shown in Table 4.4. The outlier in Table 4.4 - the

Table 4.4:   Number of Tests Required to Excite Modes of Interest in Each Panel

Panel	Number
Positive X	2
Negative X	2
Positive Y	3
Negative Y	1
Top	1
Base	2

positive Y panel - required three excitation locations because it was the first panel tested. Observations of the extracted modes during test allowed better placement of the automated ping hammer for subsequent tests.

4.2.2 Cost Function and Stiffness Trends - Panels. During the optimization of the modulii of elasticity for the FE panel models the objective function, Equation (2.18), minimized. All panel models, except for the negative X model, converged to an optimum in ten cycles or less. The negative X panel required 81 cycles to converge. Objective function values for each panel over the range of design cycles are shown in Figure 4.3 with a logarithmic vertical axis. Of note is that the objective function for the top panel model actually increased slightly between the initial value and final value. The optimization
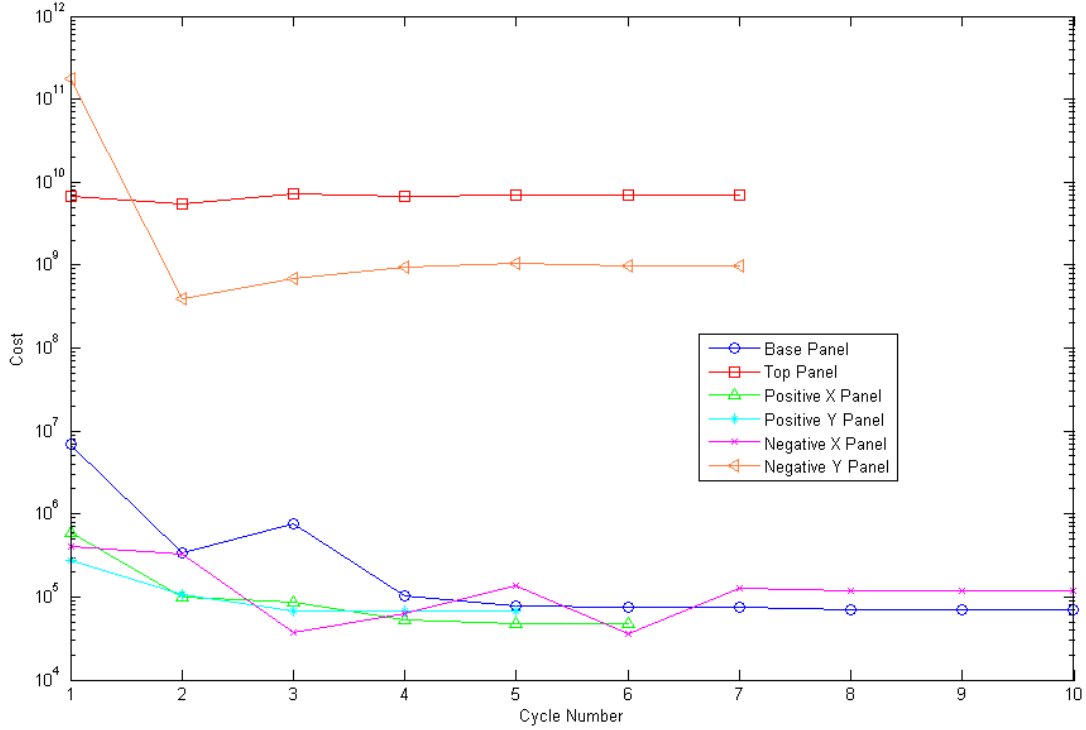
Figure 4.3: Objective function values for each panel across their respective range of design cycles. Values on the vertical axis are in log scale and are relatively large as result of the large number of measurement points and large number of modes tuned. The lines do not decrease monotonically because of the default step size in Nastran. When Nastran calculates the slope of the cost function using gradient-based methods, a large step size can skip peaks or troughs in the curve and create the case where the cost function slightly increases between two cycles. The step size must be large enough, however, to ensure the solution does not converge prematurely in a local trough and miss a lower trough for a better solution. Note: Negative X panel required 81 cycles to converge. Initial and final design cycles are only shown here for this panel. Also note for the negative X panel, that the final cost value is not the lowest cost achieved during the cycle of optimization iterations. An explanation for this is that the eigenvalue correlation constraint was not met for the lowest cost values and therefore Nastran was forced to make the eigenvector correlation slightly worse (raising the cost value) to meet that constraint.

81

for this top panel model did converge, and thus one could surmise that modeling the rib joint fillets and additional mass on the untuned top panel FE model discussed in Section 4.1.3 caused the analytical eigenpairs to be very close to the measured values before the tuning process started. For all other panels, the objective function decreased as a result of the tuning process.

During the panel optimizations the range of fluctuation for the modulii of elasticity is limited. The default Young's modulus for Aluminum 6061-T651 is 9.90 x 10^6 ksi. With the exception of the negative X panel, for which 25% deviation is allowed, the optimization routine is restricted to maintain stiffness within 20% of the default value for all rib and edge components of the FE model. For the base and top panel models,
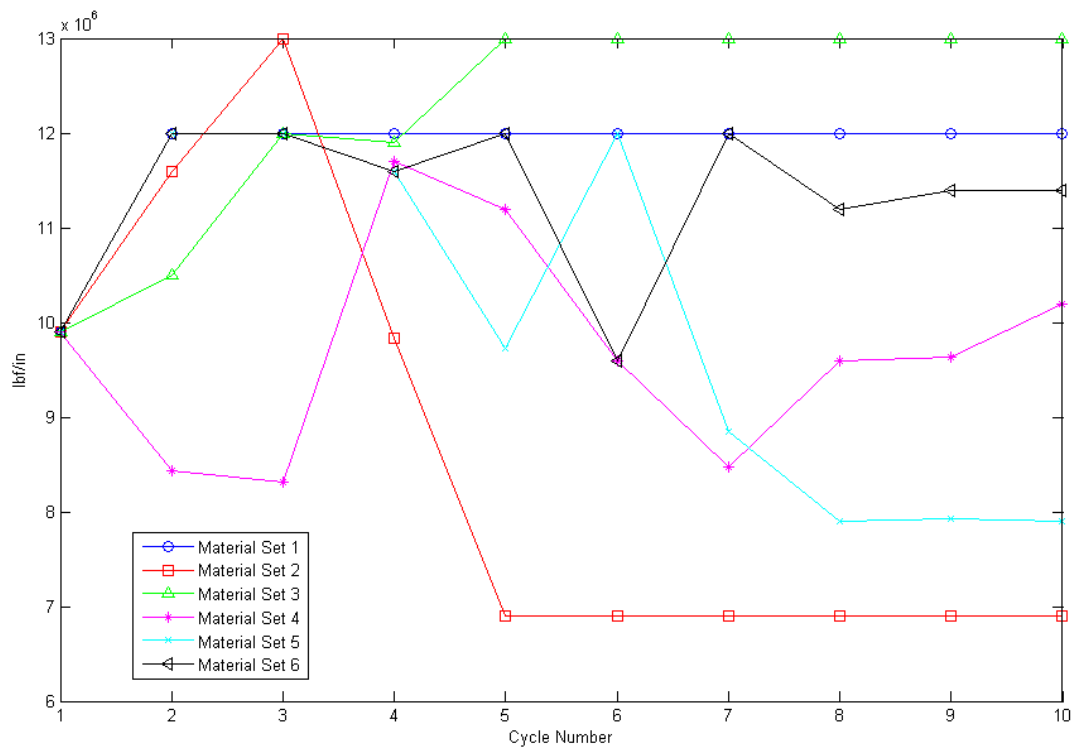
Figure 4.4: Modulii of elasticity for several material cards on the base panel FE model through ten optimization cycles.

the star patterns of plate elements simulating solid aluminum are given a larger modulus of elasticity range during the optimization. Selected modulii of elasticity from material cards in the base panel FE model optimization are shown in Figure 4.4 and the elements assigned to each material card are shown in Figure 4.5. The star pattern plate elements shown in green (Material Set 3) on Figure 4.5 are significantly stiffened at convergence
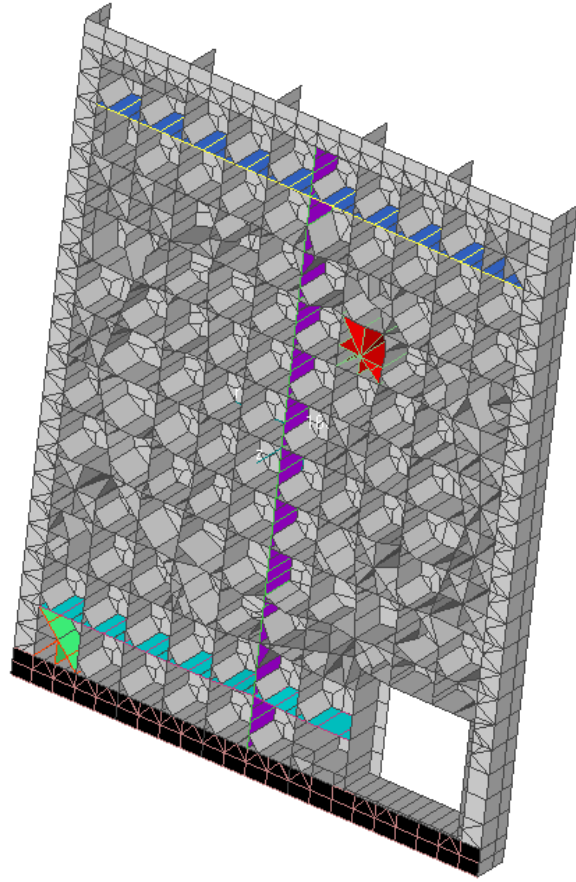
Figure 4.5:   Base panel FE model showing location of each material card from Figure
4.4. Colors on this Figure match the line colors from the graph.

while the red star pattern plate elements are loosened. Of the rib and edge elements represented in the chart, those shown in blue and black (Material Sets 1 and 6) are stiffened at convergence, teal elements (Material Set 5) are loosened, and purple elements (Material Set 4) settle close to the default value.

4.2.3 Panel Mode Shapes and Natural Frequencies. When performing optimizations for the panels, several parameters are established which control how each job runs. First are the weighting terms in Equation (2.18). For this research all weighting terms are unity meaning each value of each eigenvector and each eigenvalues are all affect the optimization equally. The second parameter the analyst must set is the range of deviation from measured natural frequencies on which the optimizer may converge. Next is the range from nominal which the optimizer may alter each design variable - modulus of elasticity for the panels. The user must consider the desired physical accuracy of the model when assigning this range. A large range in design variable trade space might improve tuning results for modal analysis but decrease the accuracy of other analyses. The stiffness deviations chosen for panel tuning in this project are plausible because they are machined from uncharacterized bulk sheets of aluminum. Finally, the number of eigenvalues and eigenvectors over which to optimize must be specified. Final panel test parameters are shown in Table 4.5

Table 4.5:   Panel Test Parameter Summary

Panel	Eigenvalue Deviation (%)	Stiffness Deviation (%)	Eigenpairs Tuned
Positive X	2	20	8
Negative X	3	25	8
Positive Y	2	20	8
Negative Y	2	20	8
Top	3	20	6
Base	3	20	5

Tuning determined that visual comparisons of the animated FE model predicted eigenvectors and animated complex-valued extracted mode shapes must be relatively close in order for the optimization to converge. Convergence occurs when the objective function cannot be minimized further by manipulation of the design variables. Nodal

lines of the tuned FE model eigenvectors differ very little from the untuned eigenvectors in the first several modes. Noticeable differences between untuned and tuned predicted eigenvectors do show for some frequencies, however. Figure 4.6 shows side-by-side comparisons of untuned, measured, and tuned mode shapes and associated natural frequencies for each of the five tuned base panel modes. Tuning clearly drove the analytical eigenvalues in the FE model closer to the squared measured natural frequencies, but a definitive assessment of eigenvector tuning is not possible from viewing nodal lines. Upon inspection, one can see that the vertical nodal line on untuned eigenvector Figure 4.6(h) shifts slightly to the left on the tuned eigenvector Figure 4.6(i). Also, the horizontal nodal line on untuned eigenvector, shown in Figure 4.6(n), shifts down slightly on the tuned eigenvector, shown in Figure 4.6(o).

Since these differences are difficult to characterize with visual inspection, a MAC is generated to determine tuning validity for the positive Y panel. Plotting the MAC as a bar graph with FE model both untuned and tuned eigenvectors versus measured mode shape produces an interesting visual as shown in Figure 4.7. However, from this figure one still cannot determine whether the tuning process improves the accuracy of the panel FE model. The positive Y panel FE model eigenvectors match quite closely with the measured data before tuning since the diagonal values on Figure 4.7 have a value near one. A calculation of percent error between vectors is not possible. Therefore a quantitative approach to determine the quality of tuning results is to use the second half of Equation (2.18). The cost for each mode of interest can be calculated with the sum of squared error between normalized untuned and measured eigenvectors and compared to the similarly calculated cost for turned versus measured eigenvectors. Table 4.6 shows these calculated costs for the positive Y panel. From this table, it is clear that the tuning process reduced the overall cost function. Most of the tuned analytical eigenvectors are closer to the measured mode shapes than the untuned eigenvectors. The exceptions are modes 2, 3, and 9. The tuning process actually reduced the accuracy of the FE model for these modes in order to improve the other six modes. Note, the mode with the largest untuned and tuned cost is mode eight which also corresponds to the lowest diagonal value on the MAC plot of Figure 4.7.

(a)   Measured Mode 1 237 Hz

(b)   Untuned Mode 1 223 Hz

(c) Tuned Mode 1 235 Hz

(d)   Measured Mode 2 460 Hz

(e)   Untuned Mode 2 448 Hz

(f) Tuned Mode 2 468 Hz

(g)   Measured Mode 3 615 Hz

(h)   Untuned Mode 3 582 Hz

(i) Tuned Mode 3 612 Hz

(j)   Measured Mode 4 691 Hz

(k)   Untuned Mode 4 669 Hz

(l) Tuned Mode 4 702 Hz

(m)   Measured Mode 5 855 Hz

(n)   Untuned Mode 5 784 Hz

(o) Tuned Mode 5 842 Hz
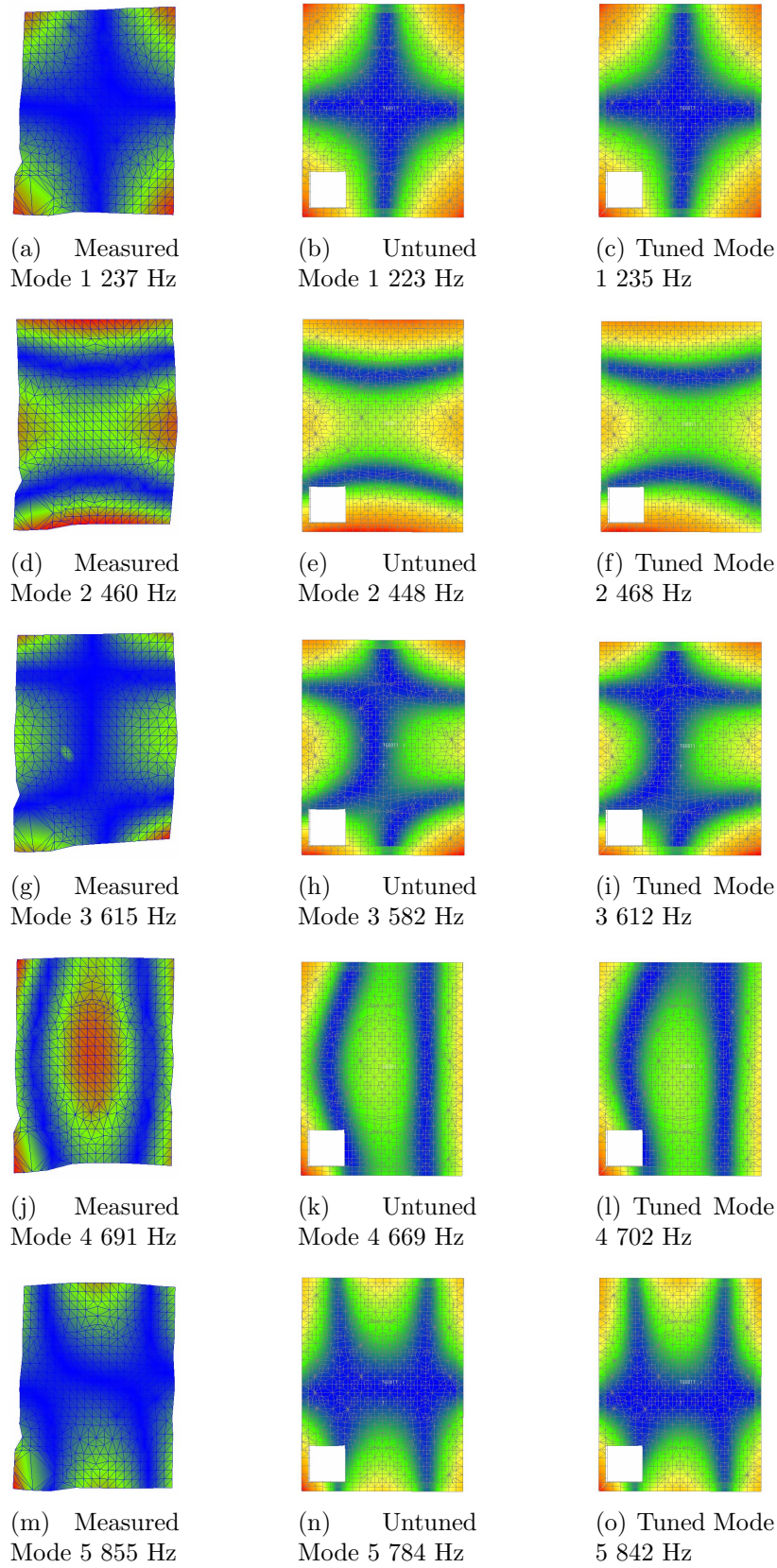
Figure 4.6:   Base Panel FE Model Tuning Results

86
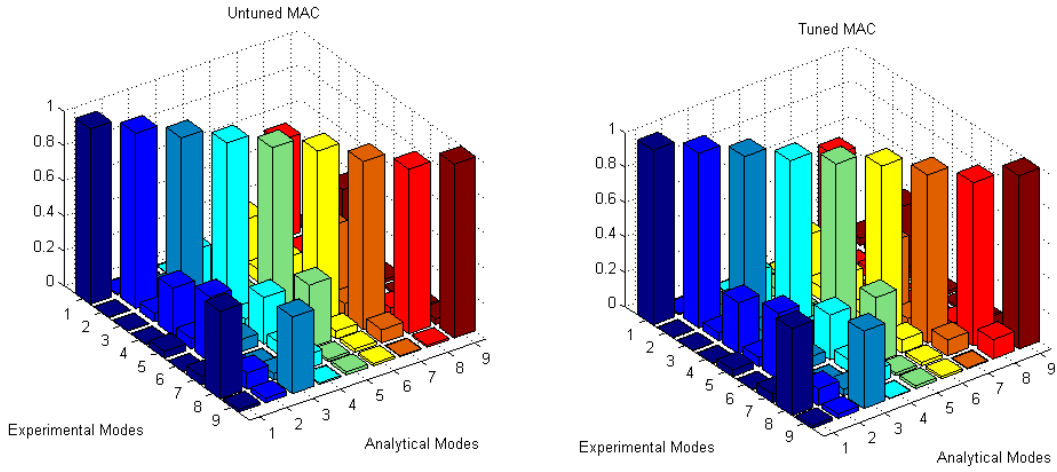
Figure 4.7:   Untuned analytical eigenvectors versus measured mode shapes MAC (left) and tuned analytical eigenvectors versus measured mode shapes MAC (right)

Table 4.6:   Positive Y Panel Tuning Results - Cost

Mode	Untuned vs Measured	Tuned vs Measured
1	25.3	23.3
2	11.1	13.2
3	93.8	449.3
4	3378.2	2207.0
5	816.0	555.7
6	9224.7	541.1
7	1041.4	818.8
8	30327.3	4439.1
9	6340.0	9753.1
Total	51257.7	18800.6

4.2.4   Panel Summary Results.   Every panel FE model tuned to match the measured data to at least 600 Hz. Panel FE model tuning results for natural frequency are given in Table 4.7. Overall, the tuned panel eigenvalues matching the squared measured natural frequencies to within 2% and the general deceases in the cost functions indicate successful panel tuning.

4.3   Full Satellite FEM Tuning Results

In this section, results of the final step in the tuning process - measuring and tuning the 6DOF connection springs and adapter ring stiffness are discussed for the entire satellite. First, the final test configurations and settings are discussed. Next, trends in selected spring constants over each design cycle of the optimization are shown. Trends in minimizing the objective functions for full satellite tuning follow. Finally, tuning results of eigenvalues and eigenvectors for the entire satellite are shown.

4.3.1   Full Satellite Test and Tuning Configuration Results.   Final excitation is via an automated ping hammer located at the positive X, negative Y, positive Z corner. The hammer strikes a flat plate surface bolted to the corner at a 45° elevation angle with respect to horizontal. One measurement set is collected on each panel separately. Evaluation of the complex-valued modes reveals that enough energy was placed into the structure to adequately excite all modes of interest.

The first two measured modes shapes - rocking motion - occurred at natural frequencies of 42.6 and 46.9 Hz. The original FE model has arbitrary initial values of 6DOF spring constants set to 1×10^6 lbf/in for translation and 1×10^6 lbf/rad for torsion. Initial adapter ring modulus of elasticity is set to 1.2×10^7 ksi. The model predicts the first two natural frequencies as 64.2 and 68.6 Hz. Therefore, the 6DOF spring constants and adapter ring stiffness are manually tuned to starting values of 3000 lbf/in, 3000 lbf/rad, and 1×10^7 ksi, respectively. Such drastic changes to the stiffness of the spring constants indicates that the initial arbitrary values made the FE model too stiff. The modified settings result in an analytical prediction of 42.7 and 48.2 Hz for the first two natural frequencies.

Table 4.7:   Panel Natural Frequency Tuning Results

Panel	Mode	FE Untuned (Hz)	Measured (Hz)	FE Tuned (Hz)	% Diff
Positive X					
	1	41.1	43.2	42.8	0.9
	2	219	218	218	0
	3	263	259	261	0.8
	4	277	285	287	0.7
	5	329	335	333	0.6
	6	508	505	510	1.0
	7	556	561	566	0.9
	8	641	639	636	0.5
Negative X					
	1	35.4	36.7	36.3	1.1
	2	225	219	223	1.8
	3	264	254	253	0.4
	4	276	286	281	1.7
	5	341	342	340	0.6
	6	519	510	515	1.0
	7	576	592	582	1.7
	8	655	642	638	0.6
Positive Y					
	1	41.1	42.5	42.4	0.2
	2	254	268	268	0
	3	298	310	313	1.0
	4	348	338	336	0.6
	5	399	388	392	1.0
	6	589	595	598	0.5
	7	629	673	667	0.9
	8	727	770	765	0.6
Negative Y					
	1	42.5	42.5	42.9	0.9
	2	261	265	263	0.8
	3	310	305	309	1.3
	4	337	338	336	0.6
	5	396	390	393	0.8
	6	603	593	588	0.8
	7	642	667	660	1.0
	8	757	764	756	1.0
Top					
	1	100	104	102	1.9
	2	283	259	264	1.9
	3	370	348	354	1.7
	4	443	471	461	2.0
	5	525	533	534	0.2
	6	760	731	722	1.2
Base					
	1	223	237	235	0.8
	2	448	460	468	1.7
	3	582	615	612	0.5
	4	669	691	702	1.6
	5	784	855	842	1.5

However, a direct result of importing the panel tuning stiffnesses and hand tuning the spring constants and adapter ring stiffnesses is that the predicted eigenvectors are skewed from the original. Figure 4.8 displays the original full satellite FE model predicted mode shapes for modes one and two as well as the corresponding shapes after the tuned panel stiffnesses and hand tuned spring constants are taken into account. The adjusted
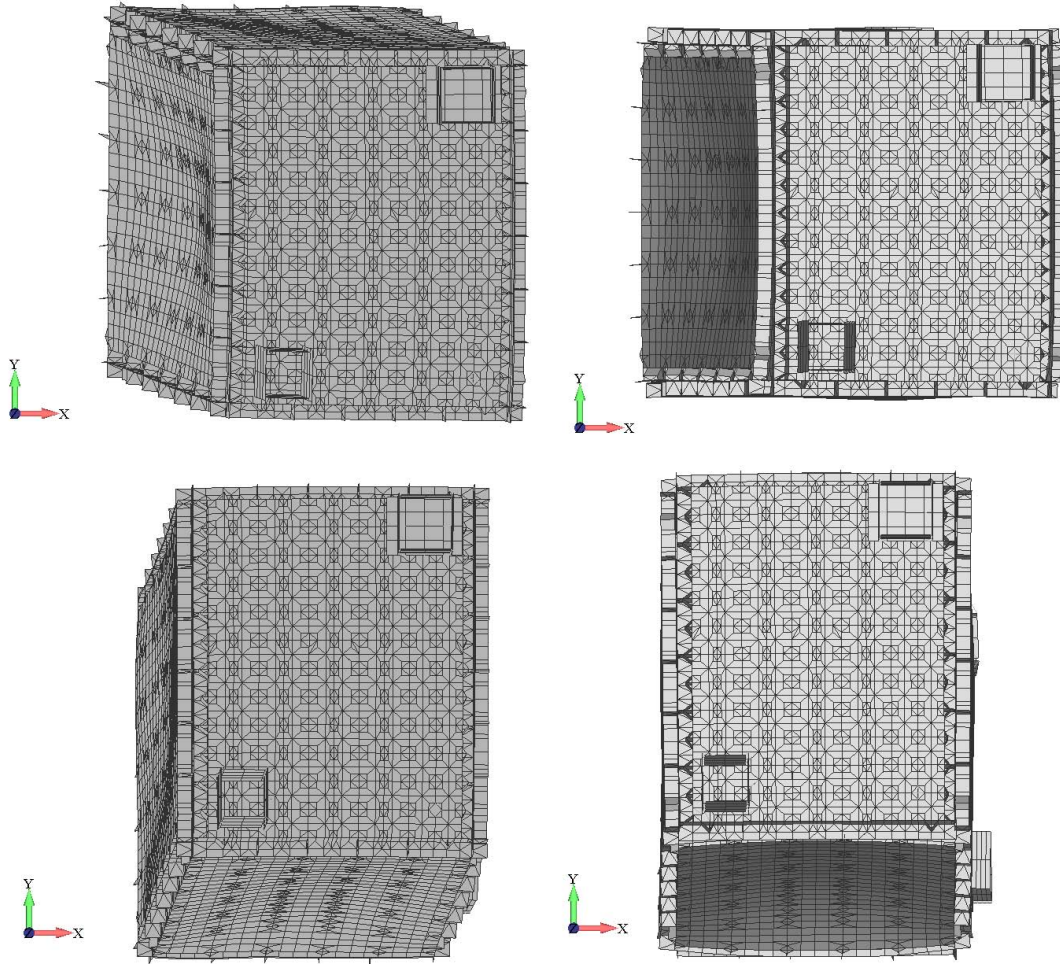
Figure 4.8:   The original FE model predicted shapes for SEM II mode 1 (top left) and mode 2 (bottom left). After importing the modulii of elasticity from the tuned panel models and hand tuning the 6DOF spring constants and adapter ring stiffness, the resulting FE model predicts mode 1 (top right) and mode 2 (bottom right) to have rocking motion in different directions than the original model.

FE model predicted mode 1 and mode 2 shapes rock almost exclusively around the Y-axis and X-axis, respectively. Theory suggests the lower frequency rocking mode should occur about the axis perpendicular to the larger panels - the X-axis - indicating the modified FE model has modes 1 and 2 are switched in order. The measured mode 1 and

90

mode 2 shapes are rocking motions about axes similar to those predicted by the original FE model of Figure 4.8. Determining if the modified FE model eigenvector for mode 1 is closer to the measured mode 1 shape or the measured mode 2 shape is impossible by visual inspection. Therefore the analyst must look at tuning results to confirm or disprove the hypothesis that modes 1 and 2 are switched in the modified untuned FE model.

Nastran optimization algorithms do not switch mode order as part of the tuning process, however. The optimization software attempts to force the FE model eigenvectors to match the measured mode shapes in the exact order of the input file regardless of how closely the modes match. Mode tracking is a function in Nastran which ensures the FE model eigenvectors do not change more than a user specified percentage from one design cycle to the next. If the FE eigenvector is not close to the associated measured mode shape Nastran will fail to converge to a solution due to mode tracking failure. Lowering the mode tracking percentage generally allows Nastran to converge on a solution for mis-matching modes, but decreases the precision of the results. Nastran optimization software attempts to match mode shapes regardless of the order of the respective modal natural frequencies, however. Since the measured modal data file from the Polytec vibrometer is exported in tabular form it is easier to manipulate than the FE model predicted modal data. Therefore, in order to make a determination on whether the modified untuned FE model has modes 1 and 2 switched, two tuning cases are run - one with the original measured data file, and one with the modes 1 and 2 switched in the measured data file.

4.3.2   Cost Function and Spring Constant Results - Full Satellite.   During the optimization of the 6DOF spring constants and adapter ring modulii of elasticity for the full satellite FE model the objective function, Equation (3.5), is minimized. Optimizations are performed for numbers of desired modes from two through five. These four optimization cases are performed using the original measured data set and also using the measured data set with mode 1 and mode 2 switched to more closely match the predicted mode shapes of the untuned FE model. Specific optimization parameters

used for these cases are summarized in Table 4.8. For all numbers of modes tuned, convergence to an optimum occurred in 28 cycles or less using the original measured data and 25 cycles or less using the switched measured data file. Objective function

Table 4.8:   Full Satellite Test Parameter Summary

Measured Data File	Eigenpairs Tuned	Eigenvalue Deviation (%)	Mode Tracking (%)
Original Measured Data	2	2	0.9
	3	2	0.9
	4	5	0.75
	5	2	0.85
Modes 1 and 2 Switched	2	3	0.9
	3	3	0.9
	4	5	0.75
	5	3	0.9

values for each analysis are shown in Figure 4.9. Several facts may be discerned from this Figure. The tuning process reduces the cost function for each analysis. Generally, the value of the cost function increases with increasing numbers of modes tuned. The initial cost function value of the untuned model is higher in the analyses using the original measured data file than in the cases using the measured data with modes 1 and 2 switched in order. For the case of tuning five modes using the switched measured data file, the cost function value is lower than that of tuning four modes. These observations are consistent with the initial assessment that the untuned FE model has modes 1 and 2 switched.

During the SEM II optimizations the 6DOF spring constants and adapter stiffnesses are being varied to minimize the cost function. Each analysis allows the 6DOF spring constants to vary from 0.01 to 100 times the initial value. Adapter ring stiffnesses are allowed to vary within 20% of the initial value. Selected spring constants are shown in Figure 4.10 and the elements these constants are assigned to are shown in Figure 4.11. Constant 1 is for a translational orientation on the indicated springs connecting the base panel with the adapter ring. The initial value of 1.00×10^6 lbf/in gradually increases to a final value of 1.92×10^6 lbf/in. Constant 2 is a torsional value for a set of springs on
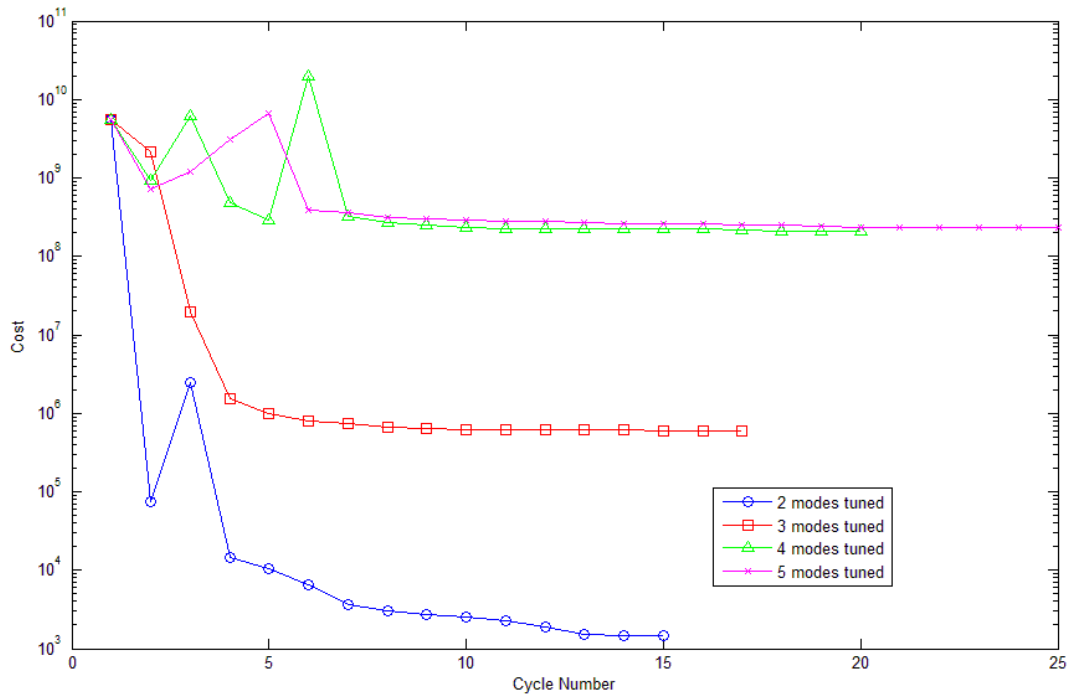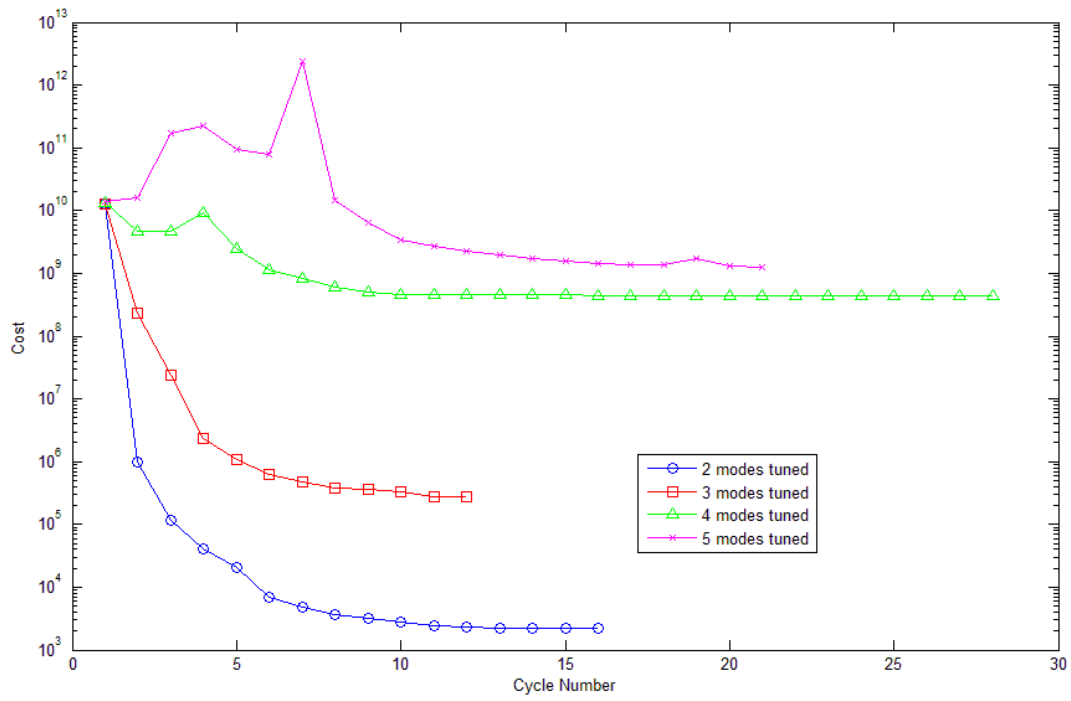
Figure 4.9: Objective function values for each analysis using the original measured data file (top) and measured data file with modes 1 and 2 switched (bottom) across their respective range of design cycles. Note: vertical axis is in log scale.

Figure 4.10: Values of 6DOF spring constants during optimization of 5 modes using the switched measured data file

Figure 4.11: FS-5 SEM II FE model showing location of 6DOF spring elements corresponding to those constants plotted in Figure 4.10. Colors on this Figure match the line colors from the graph.

the +Z, -X horizontal corner of the satellite. The initial value of 3.00 x 10^3 lbf/rad is reduced to 80 lbf/rad after tuning. This value implies that panel-to-panel connections on the model contain a relati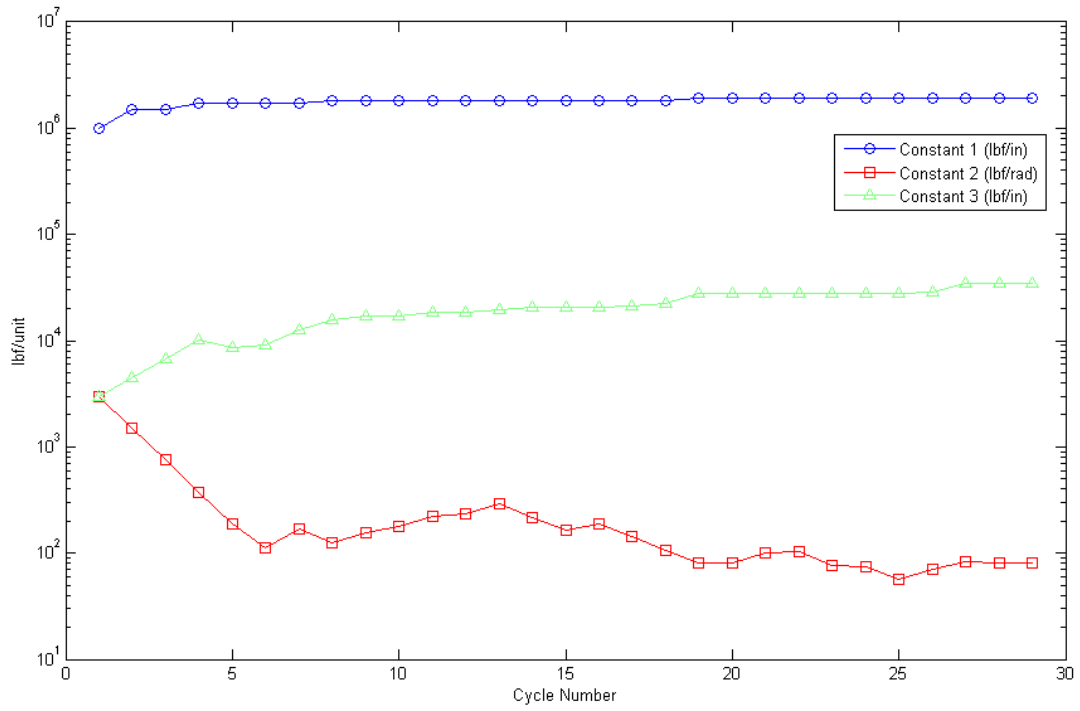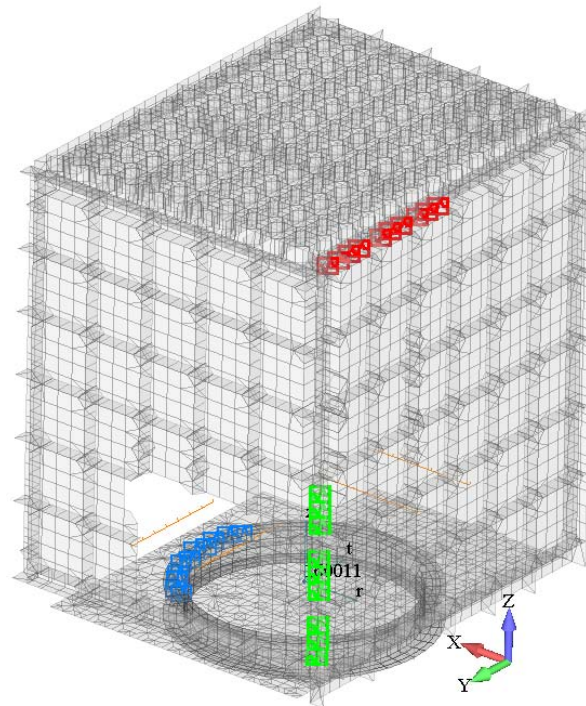vely small amount of torsional stiffness. Constant 3 is a translational value for a set of springs on the +Y, -X vertical corner and increases to a value of 3.49 x 10^4 lbf/in after tuning.

4.3.3 Full Satellite Mode Shapes and Natural Frequencies. In this section, results of tuning the full SEM II FE model eigenvalues and eigenvectors are presented. The results of tuning the FE model using the original measured data are discussed as well as results of tuning using the measured data file with modes 1 and 2 switched. Tables of measured versus untuned and tuned eigenvalues show improvements in the accuracy of the model to predict natural frequency. A study of MAC values and objective function values allow the results of eigenvector tuning to be quantified.

In order to further verify that the untuned FE model of the FS-5 SEM II has modes 1 and 2 predicted mode shapes switched the FE model is first tuned using the original measured data set. If the conclusion concerning switched mode shapes is correct, the tuning software will attempt to force the FE model mode shapes to match the measured values, but for each additional desired tuned mode shape a satisfactory solution will become less likely. Switching modes 1 and 2 in the measured data set allows the tuning software to correlate values with closer initial conditions and will produce better results. The full satellite natural frequency results are shown in Table 4.9.

A definite conclusion on whether switching modes 1 and 2 in the measured data set yields better tuning results can still not be made by examining natural frequencies. Switching the modes generally results in better natural frequency tuning than non-switched measured modes for the 5 modes case, but the same cannot be said of tuning the smaller number of modes. Therefore, the next measure of successful tuning is the MAC. The MAC plots corresponding to the tuning cases in Table 4.9 are shown in Figure 4.12. Notice in Figure 4.12(a) that analytical mode 1 has a high correlation with experimental mode 2 and analytical mode 2 has a high correlation with experimental mode 1. On MAC 4.12(b), which compares analytical to the switched experimental data

95
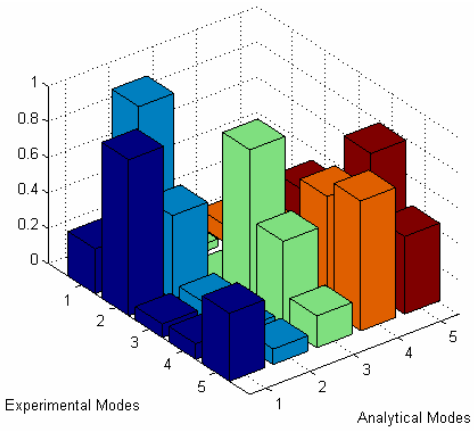
(a) Untuned Model - Original Data File
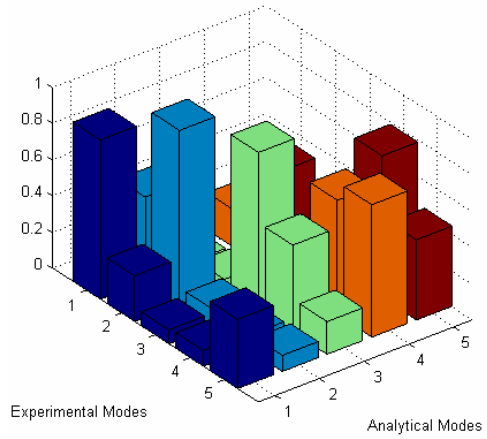
(b) Untuned Model - Switched Data File
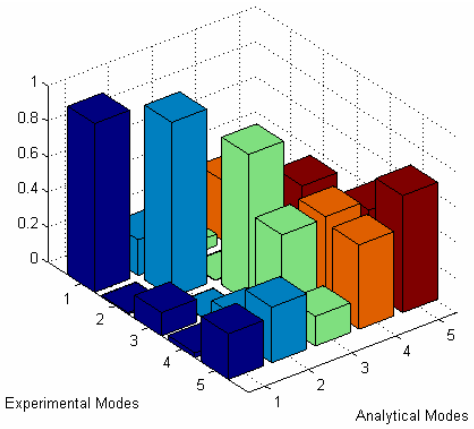
(c) 2 Modes Tuned - Original Data File
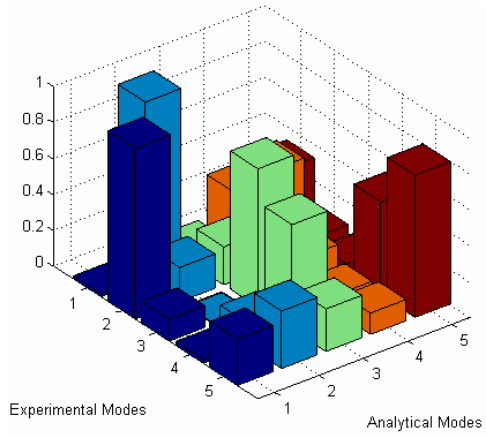
(d) 2 Modes Tuned - Switched Data File
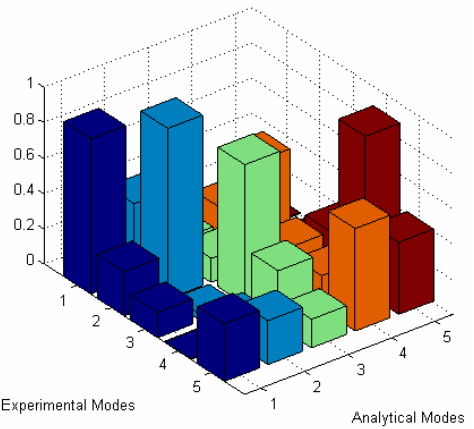
(e) 3 Modes Tuned - Original Data File
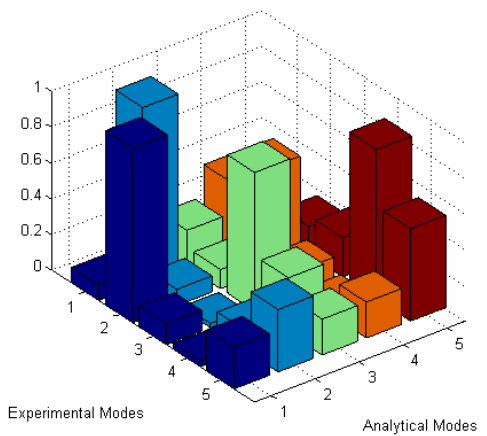
(f) 3 Modes Tuned - Switched Data File
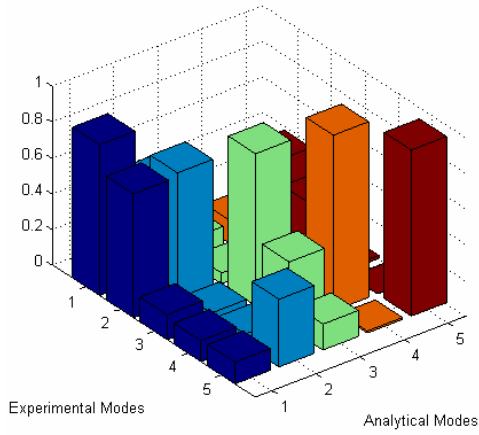
(g) 4 Modes Tuned - Original Data File
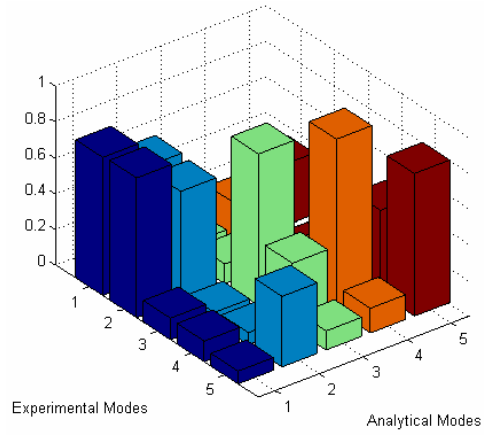
(h) 4 Modes Tuned - Switched Data File
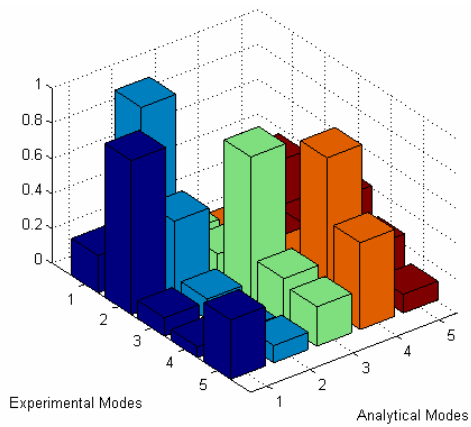
(i) 5 Modes Tuned - Original Data File
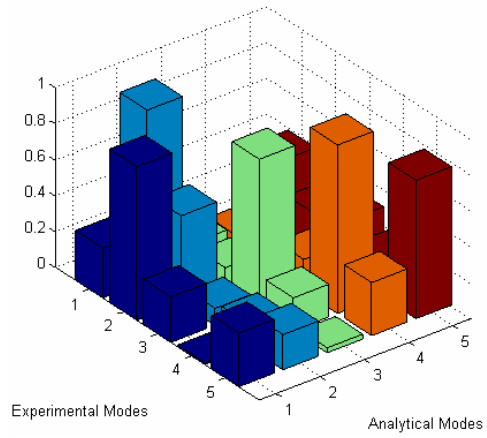
(j) 5 Modes Tuned - Switched Data File

Figure 4.12:   MAC plots of the untuned and tuned FS-5 SEM II FE models' analytical eigenvectors versus measured mode shapes. The first column of plots results from tuning using the original measured data file. The second column uses the measured data file with modes 1 and 2 switched.

Table 4.9:   Full Satellite Natural Frequency Tuning Summary

| Case	Mode 1	Mode 2	Mode 3	Mode 4	Mode 5
Untuned	42.7 (0.2)	48.2 (2.8)	107 (24.7)	130 (7.8)	143 (7.1)
2 Modes Tuned[1]	42.2 (0.9)	46.6 (0.6)			
2 Modes Tuned[2]	42.2 (0.9)	46.4 (1.1)			
3 Modes Tuned[1]	43.0 (0.9)	46.6 (0.6)	85.2 (0.7)		
3 Modes Tuned[2]	42.5 (0.2)	47.1 (0.4)	84.5 (1.5)		
4 Modes Tuned[1]	43.6 (2.3)	48.1 (2.5)	88.0 (2.6)	138 (2.1)	
4 Modes Tuned[2]	43.6 (2.3)	47.9 (2.1)	86.4 (0.7)	137 (2.8)	
5 Modes Tuned[1]	42.4 (0.5)	46.7 (0.4)	86.4 (0.7)	142 (0.7)	143 (7.1)
5 Modes Tuned[2]	43.0 (0.9)	47.6 (1.5)	86.1 (0.3)	141 (0)	145 (5.8)

Note: Error of value compared to measured in parentheses
[1] Tuned using original measured data file
[2] Tuned using measured data file with modes 1 and 2 switched

file, the corresponding modes 1 and 2 have high correlation with respect to each other. Another observation from the MAC plots is that tuning for 2 and 3 modes is possible with the original experimental file, but the tuning algorithm is no longer able to force the model to switch modes 1 and 2 in Figures 4.12(g) and 4.12(i). With the exception of tuning for 4 modes, the MAC plots in the second column of Figure 4.12 show an improvement in mode correlation. In Figure 4.12(d), the tuned analytical mode 1 correlates with the switched experimental mode 2 and tuned analytical mode 2 correlates with the switched experimental mode 1 as expected. From this data, the conclusion that the untuned FE model has the mode shapes for modes 1 and 2 switched is confirmed. The MAC diagonal values for the switched measured data file cases are shown in Table 4.10.

Overall, the tuned FE model eigenvectors for modes 4 and 5 yield MAC values which are improved by 31% and 33% over the untuned FE model respectively. These improvements in correlation to the higher order measured mode shapes require a slight decrease in correlation between the first three modes, however. The first five mode shapes

of the FS-5 SEM II as measured with the Polytec scanning laser vibrometer are shown alongside the respective tuned mode in the FE model in Figure 4.13.

Table 4.10:   MAC Mode Correlation Values - Analytical vs Measured FS-5 SEM II

Case	Mode 1	Mode 2	Mode 3	Mode 4	Mode 5
Untuned	0.8798	0.9611	0.8680	0.6327	0.4428
2 Modes Tuned	0.9494	0.9889			
3 Modes Tuned	0.9746	0.9845	0.7737		
4 Modes Tuned	0.7809	0.6262	0.8490	0.9604	
5 Modes Tuned	0.8545	0.9512	0.8303	0.9382	0.7718
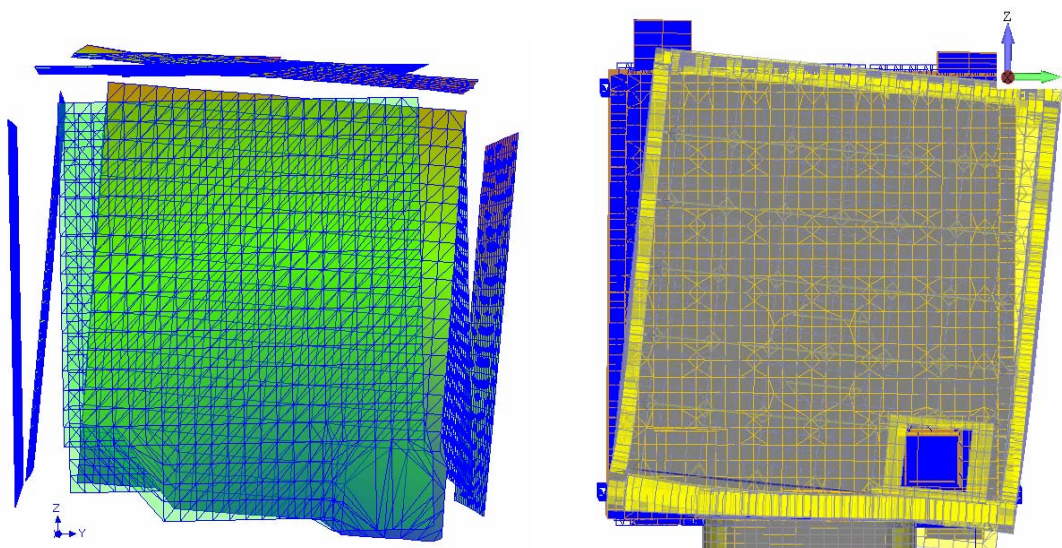
(a) Measured   (b) Tuned Analytical

Mode 1: Rocking About X-Axis
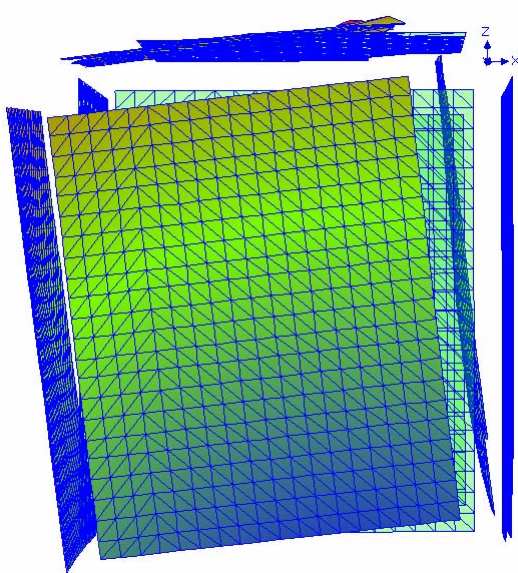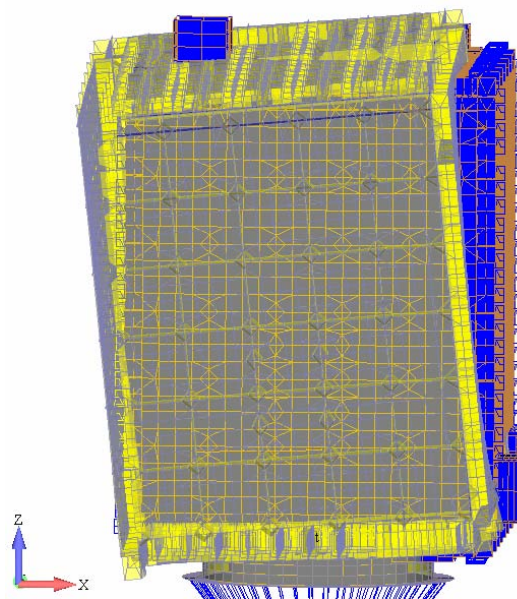
(c) Measured   (d) Tuned Analytical

Mode 2: Rocking About Y-Axis
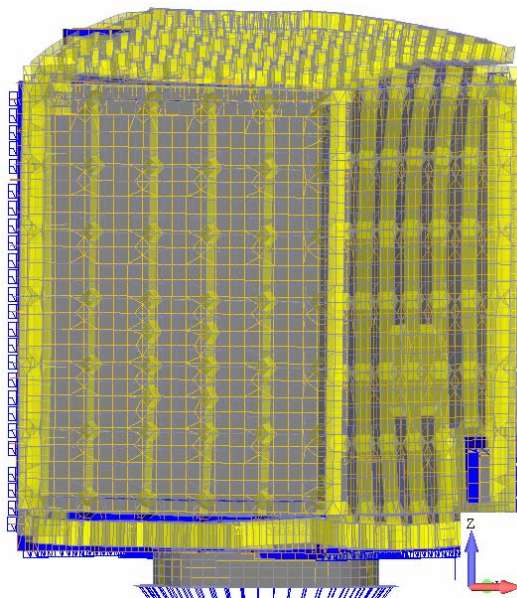
(e) Measured   (f) Tuned Analytical

Mode 3: First Axial (Pogo)

(g) Measured   (h) Tuned Analytical

Mode 4: X-Panel Symmetrical Breathing

(i) Measured   (j) Tuned Analytical

Mode 5: X-Panel Asymmetrical Breathing
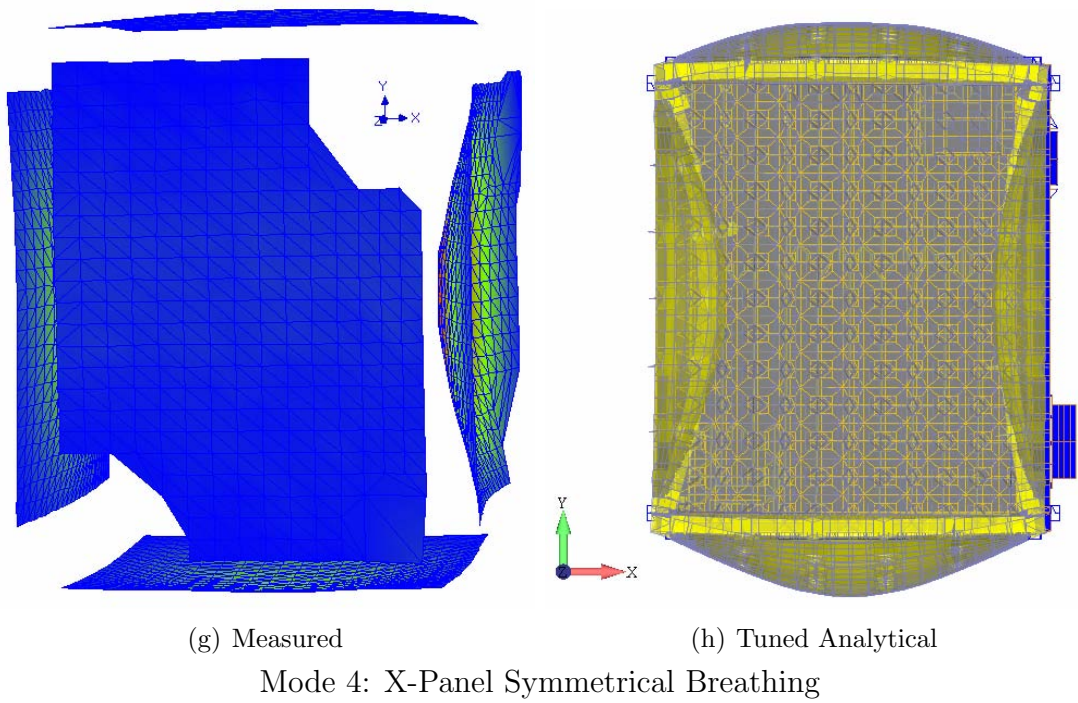
Figure 4.13:   FS-5 SEM II mode shapes with measured (left) and tuned FE model analytical (right) depictions

V.   Conclusions

S PACECRAFT designers and launch vehicle integrators require accurate dynamic models to predict vibration modes, predict frequency response, and ensure structural stability. With hundreds of parts and complicated connections between those parts, satellites pose a challenging modeling problem. Thus, finite element (FE) models of spacecraft often prove inaccurate when compared to measured data. Predictions from FE models are adjusted to match experimentally measured data by tuning the FE model. A process was developed in this research to generate an accurate FE model of the USAFA FS-5 SEM II. The mass of each component of the model was adjusted by hand and a Polytec scanning laser vibrometer is used to collect vibration data on individual panels as well as the integrated satellite model. Modal data was extracted from the measured vibration data and used to tune the FE model through the first five modes.

5.1   Research Conclusions

The FE model performs an eigenanalysis in which the first five eigenvalues and eigenvectors are computed and compared to squared measured natural frequencies and mode shapes, respectively. Natural frequencies, d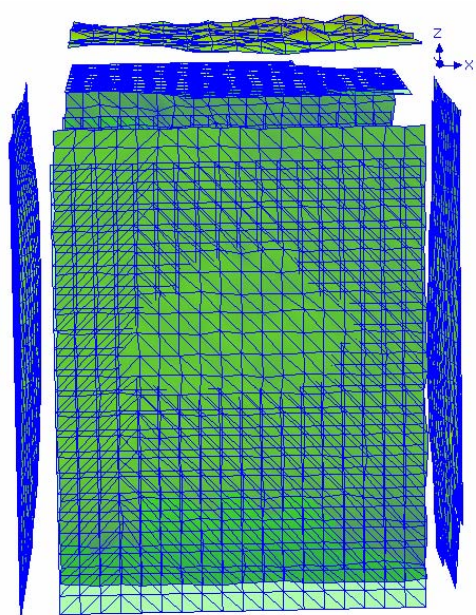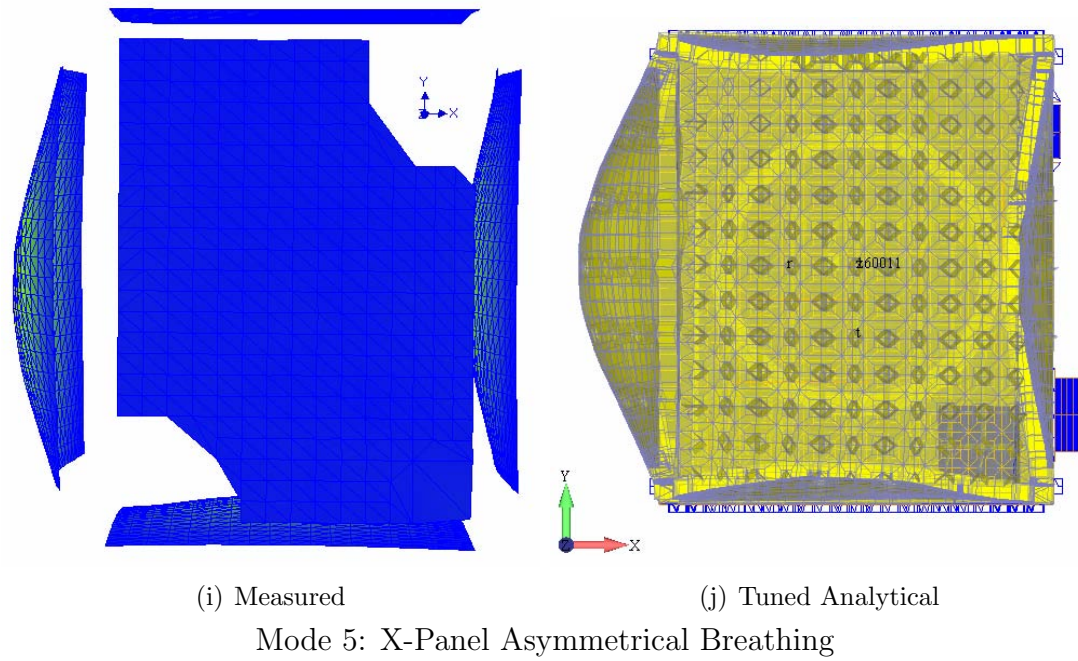amping ratios, and mode shapes are the key parameters defining a structure's dynamic response to harmonic excitations. A scanning laser vibrometer is used to measure vibration data by collecting excitation input force and corresponding output velocity of the structure over a dense grid of scan points using Doppler shift principles. Curves are fit to the measured frequency response data in order to extract the aforementioned key parameters from this data. Previous efforts in this field tuned the first three modes of a spacecraft FE model using up to ten measurement points from the laser vibrometer. The goal of this research was to develop a process which uses hundreds of measurement points to tune more natural frequencies and mode shapes on a more complex satellite structure.

The first step of the process was to generate an untuned FE model of the spacecraft structure. Next, each major component of the structure was weighed and the corresponding components in the FE model are hand tuned to ensure the overall model is within 2% of the actual mass. The third step was to collect vibration data on each satellite panel

individually. After modes and natural frequencies are extracted from this data, each panel FE model was tuned using discretized rib stiffnesses as design variables. The full satellite FE model was updated to include the tuned panel stiffnesses. Finally, frequency response data was collected from the full satellite at thousands of measurement locations using a laser vibrometer. The mode shapes and natural frequencies extracted from the measured vibration data were used in tuning the satellite FE model using 6DOF spring panel connection elements and adapter ring stiffness as the design variables. The resulting deliverable from the process was an accurately tuned FE model of the spacecraft which may be used by the launch vehicle contractor for coupled loads analysis over a large frequency range.

The starting point for the untuned FE model for this research was the FS-5 SEM I model developed by *Black et al.* [2008]. Numerous modifications to the model were required to match design changes which significantly stiffened the structure. Initial panel tests revealed that small rib connection fillets needed to be modeled in order to make the panel models accurate enough for tuning. Previous studies suggested that modeling internal components individually is more accurate than using concentrated mass elements and was the approach used in this research. Hand tuning component masses resulted in panel models within 0.5% of the measured values and the overall satellite model within 1.3% of the actual total mass. The final untuned FE model has a total of 19,733 elements and 14,521 nodes. Since the primary structure of FS SEM II is comprised of panels with relatively thin thickness, bilinear plate elements are predominantly used in the FE modeling approach. The primary material type in the model is aluminum 6061-T651 with the default mass density of 0.0975 $\text{lbf} \cdot \text{s}^2/\text{in}^4$, Poisson's ratio of 0.33, and reference temperature of 70 °F. The adapter ring of the FE model is constrained to a concentrated mass element weighing over 800,000 lbs using rigid link elements to simulate the launch vehicle interface.

An MB Dynamics Cal50 Exciter electrodynamic shaker was driven with an Agilent Technologies 33120A Arbitrary Waveform Generator programmed to generate a burst square wave function to excite the panels. This shaker and generator combination resulted in an extremely easy-to-control system able to generate impacts which yielded

very good coherence and spectral densities. A vertical test stand with springs suspending panels at the corners stiffened the structure so far as to change its dynamic properties. Therefore, a horizontal test stand was used for panel testing. Many panels required more than one test in order to properly excite all modes in the range of interest. Tuning the panel FE models based on the collected data reduced the objective function values of Equation (2.18) with the exception of the top panel. Rigid link elements were used to adjust the top panel FE model predicted mode shapes before tuning and resulted in the untuned model predictions being very close to the measured. As shown in Figure 4.6 most untuned analytical panel eigenvectors were very close to the measured shapes in the frequency range of interest. The first eight modes of each side panel, six modes of the top panel, and five modes of the base panel were tuned with eigenvalues matching measured natural frequencies within 2%.

The same shaker and waveform generator system as used for the panels was used to excite the full satellite. The stinger from the exciter struck a flat plate surface bolted to the corner of the satellite at a $45°$ elevation with respect to horizontal. The base of the SEM II was bolted to the floor to avoid external resonance sources. The untuned full satellite FE model mode order disagreed with the order of the first two measured mode shapes. A switch in order of the first two modes and natural frequencies in the measured data file allowed Nastran to avoid mode tracking failures. The objective function Equation (3.5) was reduced in tuning cases ranging from two modes to five modes. Equal weighting was assigned to each mode and between each eigenvalue and eigenvector for all tuning. The full satellite tuned FE model predicted natural frequencies were within 3% of measured values for most cases and modes. MAC values comparing tuned FE model eigenvectors and measured mode shapes decreased with increasing numbers of modes tuned, but remained above 0.75 through tuning five modes. Though the MAC mode shape correlation values are not all above the NASA 0.95 correlation criteria for fundamental bending modes, they do show significant improvement from the untuned model. Modes 4 and 5 showed the most improvement in MAC correlation. Mode 4 improved from an untuned MAC correlation of 0.63 to a tuned correlation of 0.94. Mode 5 improved from an untuned MAC correlation of 0.44 to a tuned correlation of 0.77.

These improvements to higher order modes required slight reductions in correlation for the first three modes.

Several approaches used during creation of the tuning process were critical to its success. First, creating nodes on the untuned FE model directly from the structure geometry files allows the panel models to predict modal data that closely matches the measured values before adjusting design variables. This practice allows the tuning software to minimally adjust the modulii of elasticity of panel ribs from the default values. Next, collecting vibration data using the Polytec laser vibrometer only at night is a large reason the measured FRF data has very low noise content. Tests which occurred during working hours are generally of poor quality compared to night tests. Another contributor to clean test data is the use of impact hammer excitation. The electromagnetic shaker was initially bolted to the corner of the full satellite and programmed with a white noise input. FRF data collected using this excitation technique showed that the generator does not add enough mass to change the dynamic properties of the satellite, but poor coherence values reveal an unacceptable increase in noise. During the tuning stages of the process, the the quality of the results and the ability of the software to converge are most sensitive to the desired allowable eigenvalue deviation. The user specified range of stiffness and spring constant deviation are less of a determinant in the tuning results as the eigenvalue deviation. Finally, reducing the mode tracking parameter from the default value of 0.9 allows tuning four and five modes of the full satellite. The tuning software suffers mode tracking failure and does not converge with four and five desired mode cases using the default mode tracking value. Modifications to the untuned FE model which make it closer to the measured data would be required to further improve tuning results for these modes.

5.2   Future Work

Numerous studies could follow from this research. First, the untuned full satellite FE model could be adjusted further in order to eliminate the switched modes 1 and 2. The adapter ring elements and connections of the adapter ring elements to the base panel are logical starting points for these updates. Second, analysts could further discretize

the panel rib materials, spring constants, and adapter ring materials in order to create more design variables for tuning. Next, more of the measured data could be used in the tuning approach if a separate objective function was assigned for each face of the satellite. At the conclusion of this research, the objective function was discretized by mode number and DOF and discarded approximately 2/3 of the measured data points in order to meet the 32,000 character Nastran limit. Breaking the objective function into five more components - one for each face - would allow more data points to be used and might improve overall tuning results. Another approach to achieve better tuning results may be to make use of the weighting coefficients. For example, the first three modes - generally considered the primary modes - could be given a higher weighting in the objective function in order to improve the tuned MAC values at the expense of lower MAC values for the higher modes. A study characterizing the trade space of eigenpair weighting effects on tuning results would be insightful to improving the overall process. Similarly, a study characterizing the number of measurement points used in the tuning software would be valuable. One could compare results, running cases ranging from the most points allowable with the objective function character limits to a single measurement point on one panel. Finally, in order to highly refine the 6DOF spring constant values for the full satellite, one could run an initial tuning case allowing large deviations in spring constant values.

After reviewing trends in tuned spring constant values, the tuned FE model may be used as the initial conditions for a second tuning case in which any 6DOF springs that reached the upper or lower bounds in the first tuning case are allowed to deviate further. Higher modes could be tuned using this technique as well. In order to test the validity of the material stiffness and spring constant modifications reached during tuning, the FE model can be used for various analyses. These analyses include the forced response from booster loads, the response to acoustic loads, and the shock response to fairing, payload, or stage separation. A comparison of FE model predicted behavior to any experimental data collected in these technical areas would reveal the validity of the model developed in this tuning process.

Bibliography

Agilent, T. (2000), The fundamentals of modal testing, *Tech. Rep. 5954-7957E*, Agilent Technologies, telephone 1-800 452-4844.

Black, J. T., L. George, and E. D. Swenson (2008), Measuring and modeling 3d mode shapes of falconsat-5 structural engineering model, in *49th AIAA/ASME/ASCE/AHS/ASC Structures, Structural Dynamics, and Materials Conference*, vol. 2008-1851.

Cobb, R. G., R. A. Canfield, and B. S. Liebst (1996), Finite element model tuning using automated structural optimization system software, *American Institute of Aeronautics and Astronautics, Volume 34* (No. 2).

Cook, R. D., D. S. Malkus, M. E. Plesha, and R. J. Witt (2002), *Concepts and Applications of Finite Element Analysis*, 719 pp., John Wiley and Sons, INC.

Coppotelli, G., R. Rinaldi, L. B. Crema, and V. Spadoni (2008), Structural updating of the vega-ucmec fe model using vibration test data, in *49th AIAA/ASME/ASCE/AHS/ASC Structures, Structural Dynamics, and Materials*, vol. AIAA 2008-1850.

Deal, D., J. Richmond, K. Nastasi, J. Speakman, K. Le, and K. Smaagard (2007), Falconsat-5 critical design review.

France, M., and T. Lawrence (2006), Falconsat-2 launched (and recovered), *Tech. rep.*

Friswell, M. L., and J. E. Mottershead (1995), *Finite Element Model Updating in Structural Dynamics*, 286 pp., Kluwer Academic Publishers, Boston.

Garmann, D. (), A basic guide for creating a nastran bulk data file foro modal optimization, *Tech. rep.*

Meirovitch, L. (2001), *Fundamentals of Vibrations*, 806 pp., McGraw-Hill, Boston.

MSC.Software, C. (2003), *MSC.Nastran 2004 Design Sensitivity and Optimization User's Guide*, 634 pp., MSC.Software Corporation, mSC.Software Corporation 2 MacArthur Place Santa Ana, CA 92707 USA Telephone: (800) 345-2078 Fax: (714) 784-4056.

Niedbal, N. (1984), Analytical determination of real normal modes from measured complex responses, *American Institute of Aeronautics and Astronautics*, (84-0995), 292.

O'Reilly, K. (2004), Falconsat-2 lesson plan lesson 1 - mission familiarization training charts.

Owen, R., W. Saylor, R. Adams, and D. Deal (2008), Falconsat-5 structural engineering model 2 (sem2) vibration and mass measurement test report, *Tech. Rep. Draft*, Space Systems Research Center.

Polytec (2007a), Polytec scanning vibrometer hardware manual, polytec, Inc., Midwest Office 3915 Research Park Dr., Suite A-12 Ann Arbor, MI 48108 1-734-662-4900.

Polytec (2007b), Polytec scanning laser vibrometer theory manual.

Polytec (2007c), Polytec scanning vibrometer software manual, *PSV, PSV-3D, MSA/MSV* (Software 8.51).

Rees, W. G. (2001), *The Doppler effect*, chap. 2.4, p. 18, Physical Principles of Remote Sensing, 2nd edition ed., Cambridge University Press, Cambridge.

Richardson, M., and B. Schwarz (2003), Modal parameter estimation from operating data, *Tech. rep.*

Richardson, M. H. (1997), Is it a mode shape or an operating deflection shape.

Sarafin, T. (2003), Falconsat-3 finite element model report fs3fm-2ls model, *Tech. rep.*, Instar Engineering.

Tavelli, B., and R. Holland (2006), Falconsat-3 flight model mass properties measurement, vibration, and thermal vacuum test report, *Tech. rep.*, Space Systems Research Center.

Visser, B. (2006), Falconsat-3 qualification model (qm) thermal-vacuum, vibration test, and mass properties measurement test report, *Tech. rep.*, Space Systems Research Center.

REPORT DOCUMENTATION PAGE

Form Approved
OMB No. 0704–0188

The public reporting burden for this collection of information is estimated to average 1 hour per response, including the time for reviewing instructions, searching existing data sources, gathering and maintaining the data needed, and completing and reviewing the collection of information. Send comments regarding this burden estimate or any other aspect of this collection of information, including suggestions for reducing this burden to Department of Defense, Washington Headquarters Services, Directorate for Information Operations and Reports (0704–0188), 1215 Jefferson Davis Highway, Suite 1204, Arlington, VA 22202–4302. Respondents should be aware that notwithstanding any other provision of law, no person shall be subject to any penalty for failing to comply with a collection of information if it does not display a currently valid OMB control number. PLEASE DO NOT RETURN YOUR FORM TO THE ABOVE ADDRESS.

1. REPORT DATE (DD–MM–YYYY) 26-03-2009	2. REPORT TYPE Master's Thesis	3. DATES COVERED (From — To) May 2008 – Mar 2009

4. TITLE AND SUBTITLE Finite Element Model Optimization of the FalconSAT-5 Structural Engineering Model	5a. CONTRACT NUMBER
	5b. GRANT NUMBER
	5c. PROGRAM ELEMENT NUMBER
6. AUTHOR(S) Doupe, Cole C., Capt., USAF	5d. PROJECT NUMBER
	5e. TASK NUMBER
	5f. WORK UNIT NUMBER

7. PERFORMING ORGANIZATION NAME(S) AND ADDRESS(ES) Air Force Institute of Technology Graduate School of Engineering and Management (AFIT/ENY) 2950 Hobson Way WPAFB OH 45433-7765	8. PERFORMING ORGANIZATION REPORT NUMBER AFIT/GA/ENY/09-M04

9. SPONSORING / MONITORING AGENCY NAME(S) AND ADDRESS(ES) USAFA/DFAS Attn: Lt Col Timothy Lawrence 2355 Faculty Drive US Air Force Academy, CO 80840 (719) 333-4110 (DSN: 333-4110)	10. SPONSOR/MONITOR'S ACRONYM(S) USAFA/DFAS
	11. SPONSOR/MONITOR'S REPORT NUMBER(S)

12. DISTRIBUTION / AVAILABILITY STATEMENT
APPROVED FOR PUBLIC RELEASE; DISTRIBUTION UNLIMITED

13. SUPPLEMENTARY NOTES
This material is declared a work of the U.S. Government and is not subject to copyright protection in the United States.

14. ABSTRACT

Space launch vehicles produce tremendously harsh environments for their payloads. One of the worst contributors to this harsh environment is vibration. Launch vehicle contractors require accurate dynamic models in order to perform coupled loads analyses with each payload to mitigate risks. Accurate predictions of the dynamic response of the payload are not achieved easily. The Finite Element (FE) method has proven to be the best approach in creating accurate dynamic models of complex structures. To improve the agreement between and FE model and the structure it represents, a common practice is to 'tune' or adjust parameters of the FE model to match experimentally measured data. In order to collect spatially dense and accurate dynamic responses from a satellite, a Polytec laser vibrometer is used which measures the Doppler shift to determine the frequency response from an excitation. To illustrate the benefits of employing this approach, a process is developed to measure dense modal data and tune an FE model of the US Air Force Academy's FalconSAT-5 Structural Engineering Model.

The first step in the process developed in this research involves measuring and tuning models of the satellite structure panels individually. In tuning the structural panels, material stiffness is the major design variable. The tuned FE models of the panels are integrated into the full satellite model which is then tuned based on the spring constant of the connections between the panels. The first eight modes of each side panel, six modes of the top panel, and five modes of the base panel were tuned with eigenvalues matching measured natural frequencies within 2%. Next, the first five modes ranging through 154 Hz were tuned on the full satellite FE model. Predicted natural frequencies were within 3% of measured values for most cases and modes. Modal assurance criterion values comparing tuned FE model eigenvectors and measured mode shapes decreased with increasing numbers of modes tuned, but remained above 0.75 through tuning five modes.

15. SUBJECT TERMS
FalconSAT, Finite Element Model, Optimization, Tuning, Modal Analysis, Laser Vibrometry

16. SECURITY CLASSIFICATION OF:			17. LIMITATION OF ABSTRACT	18. NUMBER OF PAGES	19a. NAME OF RESPONSIBLE PERSON Eric D. Swenson, Lt Col, USAF (ENY)
a. REPORT	b. ABSTRACT	c. THIS PAGE	UU	124	19b. TELEPHONE NUMBER (Include Area Code) (937) 255-3636, X7479 eric.swenson@afit.edu
U	U	U			

Standard Form 298 (Rev. 8–98)
Prescribed by ANSI Std. Z39.18